ANALYSIS OF THE STEADY STATE AND DYNAMIC PERFORMANCE OF VOLTAGE CONTROLLED INDUCTION MOTOR DRIVES

By

N PRABHAKARAN

DEPARTMENT OF ELECTRICAL ENGINEERING

INDIAN INSTITUTE OF TECHNOLOGY KANPUR

AUGUST, 1980

ANALYSIS OF THE STEADY STATE AND DYNAMIC PERFORMANCE OF VOLTAGE CONTROLLED INDUCTION MOTOR DRIVES

A Thesis Submitted
in Partial Fulfilment of the Requirements
for the Degree of
DOCTOR OF PHILOSOPHY

By
N PRABHAKARAN

to the
DEPARTMENT OF ELECTRICAL ENGINEERING
INDIAN INSTITUTE OF TECHNOLOGY KANPUR
AUGUST, 1980

EE-1180-D-PRA-ANA

CERTIFICATE

Certified that this work "Analysis of the Steady State and Dynamic Performance of Voltage Controlled Induction Motor Drives" by N Prabhakaran has been carried out under my supervision and that this work has not been submitted elsewhe for a degree

(Dr K R Padiyar)
Assistant Professor
Department of Electrical Engineering
Indian Institute of Technology
Kanpur, India

ACKNOWLEDGEMENTS

I express my heartfelt thanks and deep sense of gratitude to Dr K R Padiyar for his excellent guidance and encouragemen throughout the period of this thesis work His sincere interes in this work is gratefully acknowledged

I express my deep sense of gratitude to Dr V V Sastry, Department of Electrical Engineering, Indian Institute of Technology, Madras (formerly with I I T ,Kanpur) for his valuab guidance in the initial stages of this work The work reported in Chapters 2 and 3 of this thesis were completed under his supervision I thank him for his sincere interest in this work

I am thankful to M/s C Radhakrishna, C. Vijayan, Y Venkataramani, Ravi Kumar, Dr K Gomathi, Salomi Varghese and S S Bhatnagar for the valuable help rendered at different stages during the course of this work

Thanks are also due to Mr B B Srivastava for the good tracings, Mr C M Abraham for the patient and skillful typing Mr T Tiwari for the efficient cyclostyling and Mr Kalyan Da for the neat ammonia printing work

Finally, I am grateful to my wife for her constant encouragement throughout this work

Prabhakaran

TABLE OF CONTENTS

Page

Page

Page

Page

LIST OF FIGURES

LIST OF TABLES

LIST OF PRINCIPAL SYMBOLS

p	differential operator
t	time in seconds
ω	synchronous angular velocity in radians/sec
ω_r	instantaneous angular velocity of machines in radians/sec
θ_o	ωt
θ_r	$\omega_r t$
S	fractional slip
s	Laplace operator
$v_{a'n}, v_{b'n}, v_{c'n}$	source voltages per phase
v_{as}, v_{bs}, v_{cs}	motor voltages per phase
i_{1a}, i_{1b}, i_{1c}	phase currents
i_{1d}, i_{1q}	d and q axes components of stator current
ψ_{2d}, ψ_{2q}	d and q axes components of rotor flux linkages
i_{ds}, i_{qs}	stator phase currents resolved to 2-phase quantities
i_{dr}, i_{qr}	rotor phase currents resolved to 2-phase quantities
α	triggering angle
γ	hold off angle
V_m	peak value of the source voltage/phase
I_{1a}, I_{1b}, I_{1c}	dependent current sources
δ	unit impulse function
R, L	per phase resistance and self inductance of the winding
J	moment of inertia

D	frictional coefficient
L_{12}	maximum value of mutual inductance in a hybrid model
L_{11}	mutual inductance between two stator windings
l_s	source inductance
R_1, R_s	stator resistance
X_{sl}, X_{rl}	per phase stator and rotor leakage reactances
X_m	magnetizing reactances
m	X_m/ω
K	$\omega L_{12}/L_2$
T	transpose
T_e	electromagnetic torque
T_m	mechanical torque input
$\underline{x}$	vector x
$\hat{x}$	phasor x

Subscripts

d-q	direct and quadrature axes
f	final
i	initial
s,1	stator side
r,2	rotor side

SYNOPSIS

N PRABHAKARAN
Ph D
Department of Electrical Engineering
Indian Institute of Technology, Kanpur
August, 1980

ANALYSIS OF THE STEADY STATE AND DYNAMIC PERFORMANCE OF VOLTAGE CONTROLLED INDUCTION MOTOR DRIVES

This thesis is devoted to the analysis and simulation of voltage controlled induction motor drives using thyristors Both open-loop and closed-loop (with speed signal feedback) operations are considered Analytical results are backed by experimental investigations

It is a well established fact that the speed control of squirrel cage induction motors of small and medium sizes with fan-type loads is feasible, by voltage control, over reasonable ranges Although the voltage controlled induction motor (VCIM) drives are inefficient compared to inverter-fed and cycloconverter drives, the main reasons for its application are due to its reliability, simplicity and low cost Phase controlled thyristors can be effectively used for voltage control applications Although many schemes are possible, a wye-connected induction motor with a pair of back-to-back connected thyristors in each line is usually preferred for speed control applications.

The use of VCIM drive for speed control applications requires the analysis of the system response during steady state

and transient conditions In this context the main contributions of the thesis can be summarized as follows

1) The application of boundary value approach (BVA) to the steady state analysis using digital simulation
2) The development of hybrid models of induction motors suitable for transient and steady state analysis
3) Simplified, yet accurate,evaluation of the steady state performance of VCIM from the solution of nonlinear algebraic equations
4) Development of a linearized state space model of the VCIM and its application for predicting the stability of the VCIM drive from eigenvalue analysis
5) Development of transfer functions and the design and testing of closed-loop control system for the speed control

A brief description of the work reported in this thesis is given below

The BVA, which has been used earlier for the analysis of inverter-fed induction motor drives, is extended to the steady state analysis and simulation of the following cases,

1) wye-connected induction motor (isolated neutral) with a pair of back-to-back connected thyristors in each line,
2) induction motor with delta connected thyristors at the open star point,
3) wye-connected motor with a pair of back-to-back connected thyristor-diode combination in each line.

BVA makes use of boundary relationships and superposition principles for the solution The main features of this approach are

a) the machine equations are invariant while the different modes of operation are accounted for by altering the forcing voltages,
b) formulation becomes general and simple

Analytical and experimental results and a comparative performance of the drives with different thyristor configurations are presented

Two hybrid models of an induction motor, that are well suited for the digital simulation of machines with terminal constraints, are developed

The special features of the models are

a) the identity of the motor terminals either on the stator side or on the rotor side is retained
b) time dependence of the inductance matrix is eliminated
c) the models are represented by simple equivalent circuits so that formulation of the state equations for any terminal constraint is possible with direct application of network theory

The following examples are considered for the steady state and transient analysis using one of the hybrid models

1) a wye-connected induction motor with a pair of back-to-back connected thyristors in each line,

2) a delta connected induction motor with a pair of back-to-back connected thyristors in each line,

A comparative study of the performance of these drives are presented

A simplified analysis of a VCIM drive, during steady state, is described in which, the motor performance is directly related to the control variables This relationship can be effectively used for the design of speed controllers during closed-loop operation Another feature of this simplified analysis is that the steady state operating variables (phase angle ϕ, fundamental components of stator currents and rotor flux linkages and average torque) can be predicted accurately by solving three nonlinear algebraic equations for any given value of triggering angle, slip and source voltage The assumption made in the simplified analysis is that the rotor flux linkages referred to a synchronously revolving reference frame are constants during constant speed operation Validity of this assumption is confirmed analytically and justified by simulation results

Using a linearized model, the stability analysis of the VCIM drive is performed From the eigenvalue analysis, it is observed that certain category of machines may experience instability at near maximum speed

Using the linear model of the VCIM drive and its associated transfer functions, a speed controller for closed-loop operation is designed Classical control theory is used for the design of the controller Dynamic response of the closed-loop system due to perturbations in the load torque and reference input is determined both analytically and experimentally

CHAPTER 1

INTRODUCTION

1 1 GENERAL

The speed control of induction motor drives has been revolutionized with the advent of thyristors in 1957 Thyristors capable of switching several hundred amperes at quite high voltages provided a flexible and reliable method of power control. The impact of these developments was first felt in the area of power conversion - replacement of bulky and costly mercury are rectifiers, thyratrons and motor-generator sets by thyristors Until the middle of sixties, the d.c machine in spite of its disadvantages - costly and regular maintenance - occupied the dominant role in the field of variable speed drives The robust, cheap, rugged and practically maintenance free squirrel cage induction motor was mostly restricted to applications involving constant speed operation, due to its inherent constant speed characteristics Now, with large scale application of thyristors, squirrel cage induction motor drives are increasingly replacing the conventional d.c motors in speed control applications

Many thyristor controlled drives have been developed in the past two decades However, exact analysis and design of many of these systems are still being developed due to the

complexity of the problem introduced by the switching elements (thyristors) The currents and voltages are non-sinusoidal and the forcing voltages are difficult to determine in many instances In this connection, modern digital computers have come to the help of designers and researchers to a great extent Computer based analysis and design have been developed for many complex systems and this topic has been an active subject of research Although conventional models of the induction machine have been extensively used for the analysis, many attempts have been made to develop new digital models of the machine to cope with the new situation created by the application of thyristors

The two common techniques employed for the speed control of squirrel cage induction motors are

a) stator voltage control

b) stator voltage and frequency control

1.2 STATOR VOLTAGE CONTROL

Simple and most reliable method of speed control of squirrel cage induction motor with fan-type load is by the use of stator voltage control Since the torque developed in an induction motor is proportional to the square of the r.m.s voltage applied to the motor, the torque-speed characteristics of the motor (Fig 1 1) can be adjusted by varying the input voltage Conventionally variable voltage is obtained by using variacs and tap changing transformers The

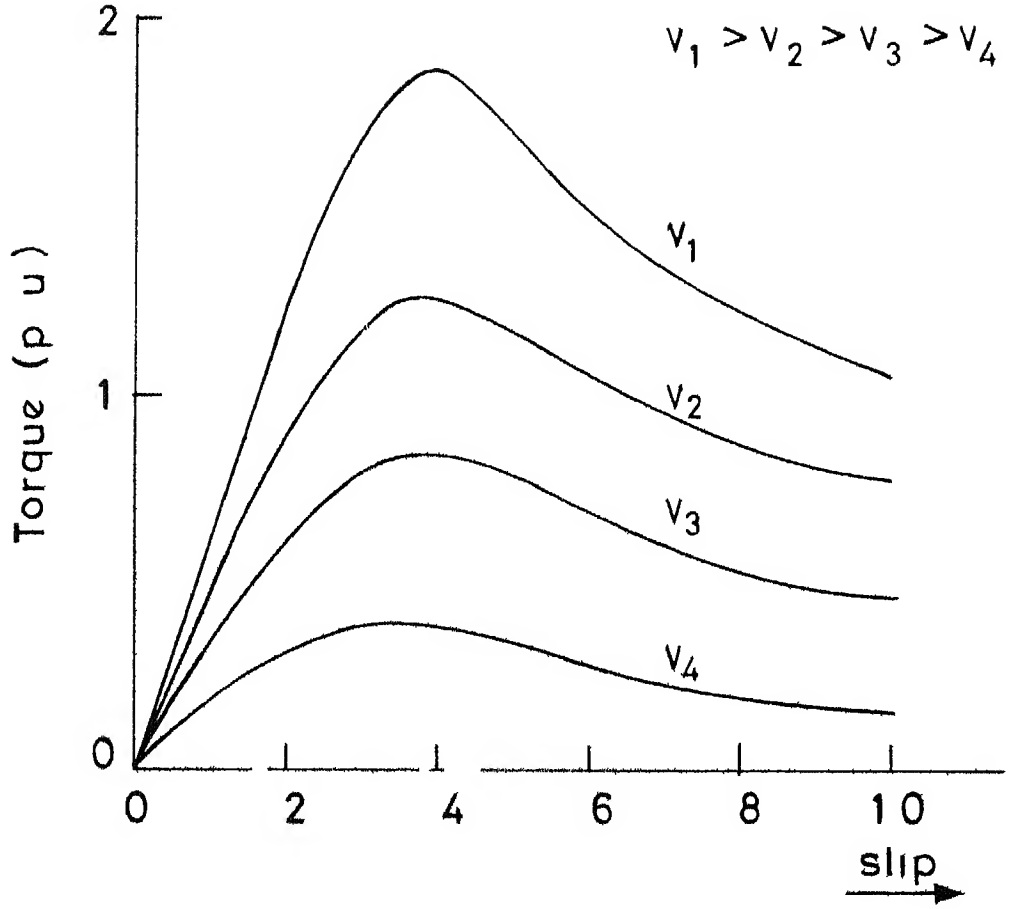

Fig 1 1 Induction motor characteristics with stator voltage control

same objective is achieved by using phase controlled thyristors [1-3] in which the triggering angle (α) is varied to obtain variable voltage The phase controlled thyristors are turned off at the natural current zero and hence no forced commutation is required Speed control of induction motors fed from a fixed frequency supply is inevitably an inefficient process The slippage power ($(\omega - \omega_r)T$) - difference between the stator input power (ωT) and the rotor output power ($\omega_r T$) - is dissipated in the rotor as heat [4] The motor may experience excessive heating at lower speeds and special care is to be taken while selecting a motor for voltage controlled applications

Although the voltage control scheme for the speed control of induction motors is an inefficient approach, this is employed for many industrial applications of small and medium type induction motors with nonlinear load characteristics The reason for its popularity is its simplicity and reliability The cost of a voltage controlled drive is very much less compared to frequency controlled drives

1 3 STATOR VOLTAGE AND FREQUENCY CONTROL

The most efficient method of speed control of squirrel cage induction motors is by means of variable frequency control A variable frequency control is normally accompanied by voltage control as well so that the air-gap flux remains constant throughout the operating range Thyristor inverters [5]

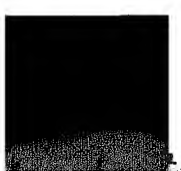

are now commonly used for the variable frequency, variable voltage control A variable d c voltage, obtained by means of a controlled rectifier, is fed to an inverter to produce variable frequency and variable magnitude a c voltages The static inverters are designed with a variety of circuit conf-- gurations [6,7] and employ forced commutation methods for turning off of the thyristors Basically there are two types of inverters - voltage source inverter and current source inverter [8,9]

Variable frequency can also be obtained using cyclo-converters [10] A cycloconverter, which converts alternating current at one frequency to alternating current at another frequency, employs line or load commutation for turning off of thyristors Since, there is no d c link in cycloconverters, these are more efficient than inverter-fed systems

Although cycloconverter and inverter-fed drives are more efficient, they are very expensive and hence applicable mainly for large machines

1 4 REVIEW

Before discussing the work reported in the thesis a brief literature survey, pertaining to the analysis of voltage controlled induction motor drive, is undertaken

are now commonly used for the variable frequency, variable voltage control A variable d c voltage, obtained by means of a controlled rectifier, is fed to an inverter to produce variable frequency and variable magnitude a c voltages The static inverters are designed with a variety of circuit conf-- gurations [6,7] and employ forced commutation methods for turning off of the thyristors Basically there are two types of inverters - voltage source inverter and current source inverter [8,9]

Variable frequency can also be obtained using cyclo-converters [10] A cycloconverter, which converts alternating current at one frequency to alternating current at another frequency, employs line or load commutation for turning off of thyristors Since, there is no d c link in cycloconverters, these are more efficient than inverter-fed systems

Although cycloconverter and inverter-fed drives are more efficient, they are very expensive and hence applicable mainly for large machines

1.4 REVIEW

Before discussing the work reported in the thesis a brief literature survey, pertaining to the analysis of voltage controlled induction motor drive, is undertaken

1 4 1 Steady State Analysis

Shepherd and Stanway [11] reported an approximate solution for a delta connected machine with back-to-back connected thyristors, in series with each phase winding An exact solution was attempted by Shepherd [12] in which the motor was represented by five nonlinear differential equations in terms of winding currents and time dependent inductance coefficients Possible approaches to the solution are discussed but no solution is attempted

Takeuchi [13] proposed a ϕ -function method to analyse a wye-connected induction motor with three pairs of back-to-back thyristors, connected in delta, at the open neutral point The average torque, voltages and currents are approximated as an infinite series of Fourier components and the computation of the resulting equations is tedious Since the back-emf across the open circuited phase is neglected, accuracy of the results will be poor for large delay angles, when the motor is near maximum speed

Lipo [14] presented a steady state analysis, using state variable technique, of a wye-connected induction motor with thyristor voltage control Closed form expressions for the steady state initial vector are derived which lead to the steady state solution The different modes of operation during voltage control are taken into account by changing the machine equations Analysis of a similar scheme has been

presented by Ramamoorty and Samek [15] and results obtained by state variable method and harmonic equivalent circuit are compared The basic idea behind harmonic equivalent circuit method is to determine the Fourier components of the stator voltage and the resulting current components using steady state harmonic equivalent circuits The back-emf and phase angle ϕ were obtained by an iterative procedure

Bedford and Nene [16] described a time domain analysis of a wye-connected motor using α-β-o transformation Ilango and Ramamoorty [17] presented the analysis of a wye-connected four wire induction motor The mathematical model used for the analysis retains the identity of the stator currents for motors, with neutral connected or unconnected

Lipo's [14] work has been extended to the analysis of an induction motor with voltage control using thyristor-diode combination (thyrode) by Rahman and Shepherd [18] Arunachalam [19] presented the analysis of the same scheme in which state variable technique was used to obtain the initial vector and the final solution was obtained by the application of harmonic equivalent circuits Experimental observations of efficiency and power output of an induction motor controlled by delta connected thyristors at the open neutral of the stator winding was reported by Spooner [20] Hayashi [21] has performed the analysis of the same scheme using state variable approach

Paice [4] has established the fundamental laws relating the speed control of induction motors by voltage control schemes He also presented test results of eight different thyristor voltage control schemes to enable a comparative study A comparative study of circuits using six thyristors in different configurations has been reported by McMurray [22]

1 4 2 Modelling of Induction Motors

Two-axis models of induction motors described by Stanley equations [23] are commonly used for digital simulation [24,25] Krause [26] has described the machine equations in an arbitrary reference frame One of the advantages of using the two-axis models is that the time dependence of the inductance coefficients is eliminated Saito and Miyazawa [27] described digital simulation of polyphase induction motors using a three phase model in which the machine equations are directly solved by finite difference methods for balanced and unbalanced conditions Using a three phase model, the digital simulation of an induction motor with non-sinusoidal excitation was presented by Sarkar and Berg [28]. The main disadvantage of the three phase models [27,28] is that inverse of a time dependent matrix is to be computed at each step of integration Robertson and Hebbar [29] presented a digital model of an induction motor in which the machine behaviour is described directly in terms of the stator phase variables The variable stator-to-rotor mutual inductance is made constant by describing

the rotor variables in a stationary reference frame

Ramshaw and Padiyar [30] described a generalized system model for all types of slip-ring machines including synchronous and induction motors A current source equivalent circuit for an induction motor and its dynamical equations were presented by Padiyar and Ramshaw [31]

1 4 3 Transient Analysis

Numerous studies of the transient performance of induction machines with constant applied voltage have been reported [32-36] and a wide range of performance aspects including starting, overspeeding, plugging and switching have been covered Performance of the induction motor with variable-frequency supply has been described in [37] Dynamic behaviour of the induction motor during balanced and unbalanced supply conditions were presented in [38] using analog computers Transfer functions and dynamic response of induction motors with constant voltage have been presented [39,40] on the basis of non-dimensional parameters

Transient analysis of a voltage controlled induction motor drive with thyristor and thyrode controllers was presented by Rahman and Shepherd [18], using state space techniques The start up transient currents, torques and speed are obtained from digital simulation

In the design of a speed controller for an induction motor with phase controlled triacs, Kenly and Bose [41] used

a very approximate first order model of an induction motor An experimental closed loop induction motor drive incorporating phase controlled thyristors has been reported by Shepherd and Stanway [42]

1 5 OBJECTIVES AND SUMMARY OF THE WORK

The objectives of this thesis are to apply and develop new techniques for the analysis and simulation of the steady state and dynamic performance of voltage controlled induction motor drives Both open-loop and closed-loop operations for speed control are considered and analytical results are supplemented by experimental investigations A novel hybrid model of an induction motor is developed which is simple in structure, yet general enough to consider any set of stator terminal constraints introduced by thyristor switching This model is then used for the development of model for the dynamic analysis of the drive

A chapterwise summary of the work reported in this thesis is given below

In Chapter 2, the steady state analysis of a voltage controlled 3-phase induction motor using back-to-back connected thyristors is described Boundary value approach [43-46] is used for the analysis by which the steady state initial vector is obtained without an iterative procedure The machine equations are unaltered while forcing voltages are defined for each mode of operation Computed results are

compared with experimental and other published results An equidistant pulse firing circuit [47] developed for the experimentation is briefly discussed

In Chapter 3, BVA is applied to the steady state analysis of delta controlled and thyrode controlled induction motor drives A comparative study of the performance of these drives is presented Digital simulation results showing the steady state performance are given

In Chapter 4, two novel hybrid models are developed which are well suited for the steady state and transient analysis of induction motors under wide range of terminal constraints In the first model, rotor flux linkages on a synchronously rotating reference frame, are used and the stator is represented by a 3-phase circuit model with constant parameters The time varying mutual coupling between the stator and rotor windings is replaced by a dependent current source along the lines of [31] This enables the simulation of stator controlled drives by direct application of the network equations. In the second model, the stator variables are transformed into two phase variables on synchronously rotating reference frame and rotor variables are undisturbed so that any rotor terminal constraints can be directly incorporated Two examples are given to illustrate the applicability of the model for the digital simulation of thyristor controlled drives

Utilizing the circuit model developed in Chapter 4, a simplified analysis of steady state performance of a voltage controlled induction motor is described in Chapter 5. The analysis is based on the assumption that rotor flux linkages referred to a synchronously revolving frame are constants during steady state operation Analytical expressions for the stator current and voltage, during steady state operation, are derived From this, nonlinear algebraic equations for phase angle ϕ and fundamental Fourier components of stator current are obtained as functions of triggering angle, supply voltage and rotor flux linkages By solving the set of nonlinear equations by Newton-Raphson method, the steady state operating variables such as constant component of torque, rotor flux linkages, fundamental components of stator voltage and current and phase angle ϕ are obtained for any given value of slip, triggering angle and supply voltage. The predicted results match excellently with the simulation results of Chapter 4.

In Chapter 6, a third order linearized model of the drive about an operating point is developed to study the dynamic response due to perturbations in triggering angle, load torque and source voltage Stability of the drive based on eigenvalue analysis is presented Utilizing the transfer

functions of the drive, a closed loop control scheme is designed and developed to regulate speed An example illustrating the design of the speed controller is given Analytical and experimental results for the system response due to perturbations in load torque and reference voltage are furnished

Chapter 7 summarizes the main contributions of the thesis and indicates the scope for further work in the area

CHAPTER 2

STEADY STATE ANALYSIS AND SIMULATION OF 3-PHASE INDUCTION MOTORS WITH VOLTAGE CONTROL BY SYMMETRICALLY TRIGGERED THYRISTORS

2 1 INTRODUCTION

One of the methods of speed control of induction motors is to vary the terminal voltage of the motor using thyristor switching circuits [11] This type of speed control is inexpensive and reliable and is well suited for induction motors with fan-type loads or with high rotor resistance Different thyristor combinations can be suitably employed for the speed control of 3-phase induction motors but a pair of back-to-back connected thyristors in each line is superior in many respects [4]. Although voltage control schemes are easy to realize in practice, the analysis of such systems is considered to be difficult

Steady-state analysis of a wye connected induction motor with voltage control using a pair of back-to-back connected thyristors in each line is described in this chapter. Boundary value approach (BVA) - an approach earlier found to be versatile in relation to the analysis of inverter-fed induction motors and h v d c systems [43-46] - is used for the analysis The steady state solution is obtained without altering the matrix differential equation describing the motor for different modes of operation Change of mode only alters the excitation Open

circuit is simulated by applying a voltage, equal to the back-emf, across the open circuited phase The initial vector which will yield steady state solution is obtained without any iteration

The basic assumptions made in the analysis are as follows

a) The 3-phase voltage source is balanced and has zero source impedance
b) All the thyristors are ideal
c) All parameters of the machines are constant and magnetic saturation is neglected
d) Rotor speed of the motor is constant during steady state operation
e) MMF in the air-gap is assumed to be sinusoidal
f) Hysteris and eddy current losses are neglected

2.2 DESCRIPTION OF THE SYSTEM

Schematic diagram of an induction motor with voltage control is given in Fig 2 1 in which a pair of thyristors connected back-to-back is included in each line These six thyristors (T_1-T_6) are triggered symmetrically at intervals of $\pi/3$ to obtain a balanced voltage across the terminals of the machine By varying the triggering angle (α) (which is measured from the zero crossing of the source voltage per phase), the effective voltage applied to the machine terminals can be varied to effect speed control

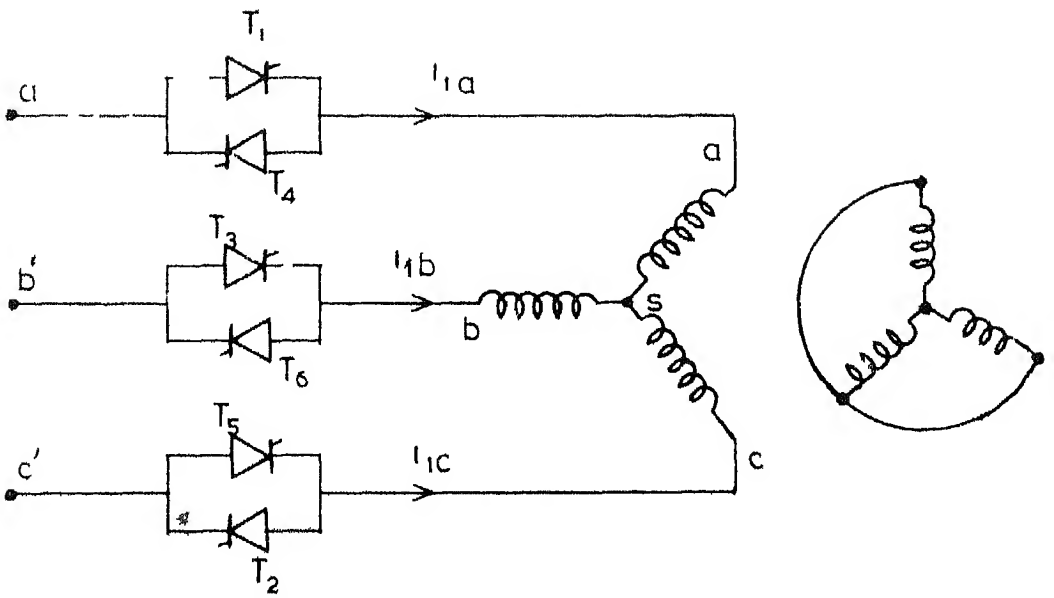

Fig 2.1 Schematic diagram of a voltage controlled induction motor

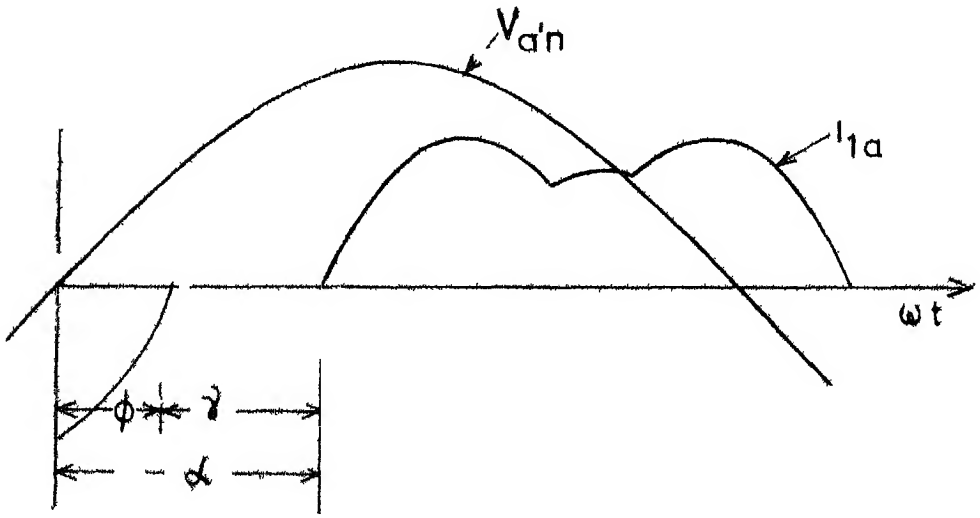

Fig 2.2 Typical current waveform

There are three distinct modes of operation for a voltage controlled wye connected induction motor with isolated neutral These modes are identified in terms of the hold off angle γ (see Fig 2 2), as follows

1) Mode-1 $0 < \gamma < \pi/3$

During this mode of operation either two or three thyristors will be conducting at any instant of time The sequence of thyristor conduction is $T_5\ T_6$, $T_5\ T_6\ T_1$, $T_6\ T_1$, $T_6\ T_1\ T_2$, $T_1\ T_2$, $T_1\ T_2\ T_3$, $T_2\ T_3$, $T_2\ T_3\ T_4$, $T_3\ T_4$, $T_3\ T_4\ T_5$, $T_4\ T_5$, $T_4\ T_5\ T_6$, $T_5\ T_6$ and so on During the period when three thyristors are conducting all the three windings of the motor are connected to the power source while single phasing of the motor takes place when only two thyristors are conducting

2) Mode-2 $\pi/3 < \gamma < 2\pi/3$

During this mode of operation, either one or two thyristors will be in conducting state When one thyristor alone is in conducting state, all phase currents will be identically zero because of the isolated neutral connection The sequence of thyristor conduction is $T_5\ T_6$, T_6, $T_6\ T_1$, T_1, $T_1\ T_2$, T_2, $T_2\ T_3$, T_3, $T_3\ T_4$, T_4, $T_4\ T_5$, T_5, $T_5\ T_6$ and so on

3) Mode-3 $2\pi/3 < \gamma < \pi$

During this mode of operation, all the stator currents will be identically zero and hence this mode is of no practical importance

2 3 MACHINE EQUATIONS

The differential equations describing the 3-phase induction motor expressed in per unit, wherein the stator and rotor variables are refeired to a stationary d-q axis, are given in matrix form [23,48,49] by

$$\begin{bmatrix} v_{ds} \\ v_{qs} \\ v_{dr} \\ v_{qr} \end{bmatrix} = \begin{bmatrix} R_s+X_sD & 0 & DX_m & 0 \\ 0 & R_s+X_sD & 0 & DX_m \\ X_mD & (1-S)X_m & (R_r+X_rD) & (1-S)X_r \\ -(1-S)X_m & X_mD & -(1-S)X_r & R_r+X_rD \end{bmatrix} \begin{bmatrix} i_{ds} \\ i_{qs} \\ i_{dr} \\ i_{qr} \end{bmatrix} \quad (2\ 1)$$

where

$$D = d/d(\omega t)$$

The relationship between d-q and phase voltages are

$$v_{ds} = \sqrt{3/2}\, v_{as} \quad (2\ 2)$$

$$v_{qs} = 1/\sqrt{2}\, (v_{cs} - v_{bs}) \quad (2\ 3)$$

The inverse relationships are

$$v_{as} = \sqrt{2/3}\, v_{ds} \quad (2\ 4)$$

$$v_{bs} = -1/\sqrt{6}\, v_{ds} - 1/\sqrt{2}\, v_{qs} \quad (2\ 5)$$

$$v_{cs} = -1/\sqrt{6}\, v_{ds} + 1/\sqrt{2}\, v_{qs} \quad (2\ 6)$$

Similar relationships hold good for the currents

The matrix differential equation (2 1) is rewritten as

$$D \begin{bmatrix} V_{s1} \\ V_{s2} \\ V_{r1} \\ V_{r2} \end{bmatrix} = \begin{bmatrix} v_{ds} \\ v_{qs} \\ 0 \\ 0 \end{bmatrix} - [A] \begin{bmatrix} V_{s1} \\ V_{s2} \\ V_{r1} \\ V_{r2} \end{bmatrix} \qquad (2\ 7)$$

where

$$\begin{aligned} V_{s1} &= X_s\, i_{ds} + X_m\, i_{dr} \\ V_{s2} &= X_s\, i_{qs} + X_m\, i_{qr} \\ V_{r1} &= X_m\, i_{ds} + X_r\, i_{dr} \\ V_{r2} &= X_m\, i_{qs} + X_r\, i_{qr} \end{aligned} \qquad (2\ 8)$$

$$[A] = \frac{1}{(X_s X_r - X_m^2)} \begin{bmatrix} R_s X_r & 0 & -R_s X_m & 0 \\ 0 & R_s X_r & 0 & -R_s X_m \\ -R_r X_m & 0 & R_r X_s & (1-S)(X_s X_r - X_m^2) \\ 0 & -R_r X_m & -(1-S)(X_s X_r - X_m^2) & R_r X_s \end{bmatrix} \qquad (2\ 9$$

The expression for the d-q currents in terms of the new variables are

$$
\begin{aligned}
i_{ds} &= (X_r V_{s1} - X_m V_{r1})/(X_s X_r - X_m^2) \\
i_{qs} &= (X_r V_{s2} - X_m V_{r2})/(X_s X_r - X_m^2) \\
i_{dr} &= (X_s V_{r1} - X_m V_{s1})/(X_s X_r - X_m^2) \\
i_{qr} &= (X_s V_{r2} - X_m V_{s2})/(X_s X_r - X_m^2)
\end{aligned}
\qquad (2.10)
$$

Equation (2 7) represents a linear, first order vector differential equation of the form

$$D\,\underline{x} = \underline{v} - [A]\,\underline{x} \qquad (2\ 11)$$

where

$$\underline{x}^T = [V_{s1}\ V_{s2}\ V_{r1}\ V_{r2}]\ , \quad \underline{v}^T = [v_{ds}\ v_{qs}\ 0\ 0]$$

Since the thyristors are triggered symmetrically, the voltage and current waveforms have half-wave and 3-phase symmetry and hence there exists a boundary relationship between the variables at $\omega t = 0$ and $\omega t = \pi/3$ during steady state The boundary relationship as given in Appendix A is

$$\underline{x}\,|\,\omega t = \pi/3 \;=\; T\,\underline{x}\,|\,\omega t = 0 \qquad (2\ 12)$$

where

$$T = \begin{bmatrix} 1/2 & \sqrt{3}/2 & 0 & 0 \\ -\sqrt{3}/2 & 1/2 & 0 & 0 \\ 0 & 0 & 1/2 & \sqrt{3}/2 \\ 0 & 0 & -\sqrt{3}/2 & 1/2 \end{bmatrix}$$

The expression for the electromagnetic torque in per unit is

$$T_e = 2/3\ X_m\ (i_{ds}\ i_{qr} - i_{dr}\ i_{qs}) \qquad (2.13)$$

In the above expression for electromagnetic torque all the variables are to be in per unit The peak values of rated line to neutral voltage and rated line current are chosen as base quantities

2 4 STEADY STATE SOLUTION BY BVA

Equations (2.11) and (2 12) constitute a two-point boundary value problem for which the steady state solution can be obtained as follows

Referring to equation (2 11), one can rewrite this to include the unknown initial vector as

$$D\ \underline{x} + A\ \underline{x} = \underline{v} + \delta(\omega t)\ \underline{x}_1 \qquad (2\ 14)$$

where, δ is the unit impulse function and the initial vector $\underline{x}_1^T = [\ x_{1i}\ \ x_{2i}\ \ x_{3i}\ \ x_{4i}]$

The equation (2 14) is split up into a number of component equations for convenience of numerical integration Superposition of the solution of these component equations, with all initial conditions set to zero, helps to evaluate the unknown initial vector $\underline{x}_i$ The component equations are ·

$$D\,\underline{x}^{0} + A\,\underline{x}^{0} = \underline{v} \qquad (2\ 15a)$$

$$D\,\underline{x}^{1} + A\,\underline{x}^{1} = \delta(\omega t)\,\underline{e}_1 \qquad (2\ 15b)$$

$$D\,\underline{x}^{2} + A\,\underline{x}^{2} = \delta(\omega t)\,\underline{e}_2 \qquad (2\ 15c)$$

$$D\,\underline{x}^{3} + A\,\underline{x}^{3} = \delta(\omega t)\,\underline{e}_3 \qquad (2\ 15d)$$

$$D\,\underline{x}^{4} + A\,\underline{x}^{4} = \delta(\omega t)\,\underline{e}_4 \qquad (2\ 15e)$$

where

$\underline{e}_1^T = [1\ 0\ 0\ 0]$, $\underline{e}_2^T = [0\ 1\ 0\ 0]$, $\underline{e}_3^T = [0\ 0\ 1\ 0]$,

$\underline{e}_4^T = [0\ 0\ 0\ 1]$ and $\underline{x}^0$, $\underline{x}^1$, $\underline{x}^2$, $\underline{x}^3$ and $\underline{x}^4$ are the components of $\underline{x}$

Equations (2 15a) to (2 15e) are numerically solved using fourth order Runge-Kutta method over an interval of $\pi/3$. The origin is chosen as the current zero point of a-phase so that the forcing voltages for different operating modes can be easily defined Applying the principle of superposition, the final values of the solution at ($\omega t = \pi/3$) can be written as

$$\underline{x}_f = \underline{x}_f^0 + x_{1i}\,\underline{x}_f^1 + x_{2i}\,\underline{x}_f^2 + x_{3i}\,\underline{x}_f^3 + x_{4i}\,\underline{x}_f^4 \qquad (2\ 16)$$

The subscript f stands for the final value at $\omega t = \pi/3$

After rearranging the terms and making use of the boundary condition as given in equation (2 12), the initial vector becomes

$$\underline{x}_i = C^{-1}\,\underline{x}_f^0 \qquad (2.17)$$

where

$$[C]=[T - X_f] \text{ and } [X_f] = [\underline{x}_f^1 \mid \underline{x}_f^2 \mid \underline{x}_f^3 \mid \underline{x}_f^4]$$

The initial vector obtained in (2 17) will lead to the steady state solution of (2 11) provided the forcing voltage vector $\underline{v}$ is defined for the period of integration

2 5 DEFINITION OF FORCING VOLTAGES

Typical waveforms of d-q forcing voltages for mode-1 and mode-2 operation of a voltage controlled motor during standstill, developed on the basis of equations (2 2 and 2 3) are given in Figs 2 3 and 2 4 For the solution of equation (2 15a), we should know the voltages v_{qs} and v_{ds} for a period of $\pi/3$ radians Starting from the current zero instant of a-phase the d-q voltages for various modes of operation are defined as follows

2 5 1 Mode - 1 hold off angle (γ) < $\pi/3$

During the interval 0 - $\pi/3$, two distinct time periods exist , namely

a) Time period I, $0 < \omega t < \gamma$

b) Time period II, $\gamma < \omega t < \pi/3$

Time Period - I, $0 < \omega t < \gamma$

During this period, current through a-phase is zero and a back-emf due to mutual coupling appears across a-phase winding Referring to Fig 2 5, the d-q voltages are

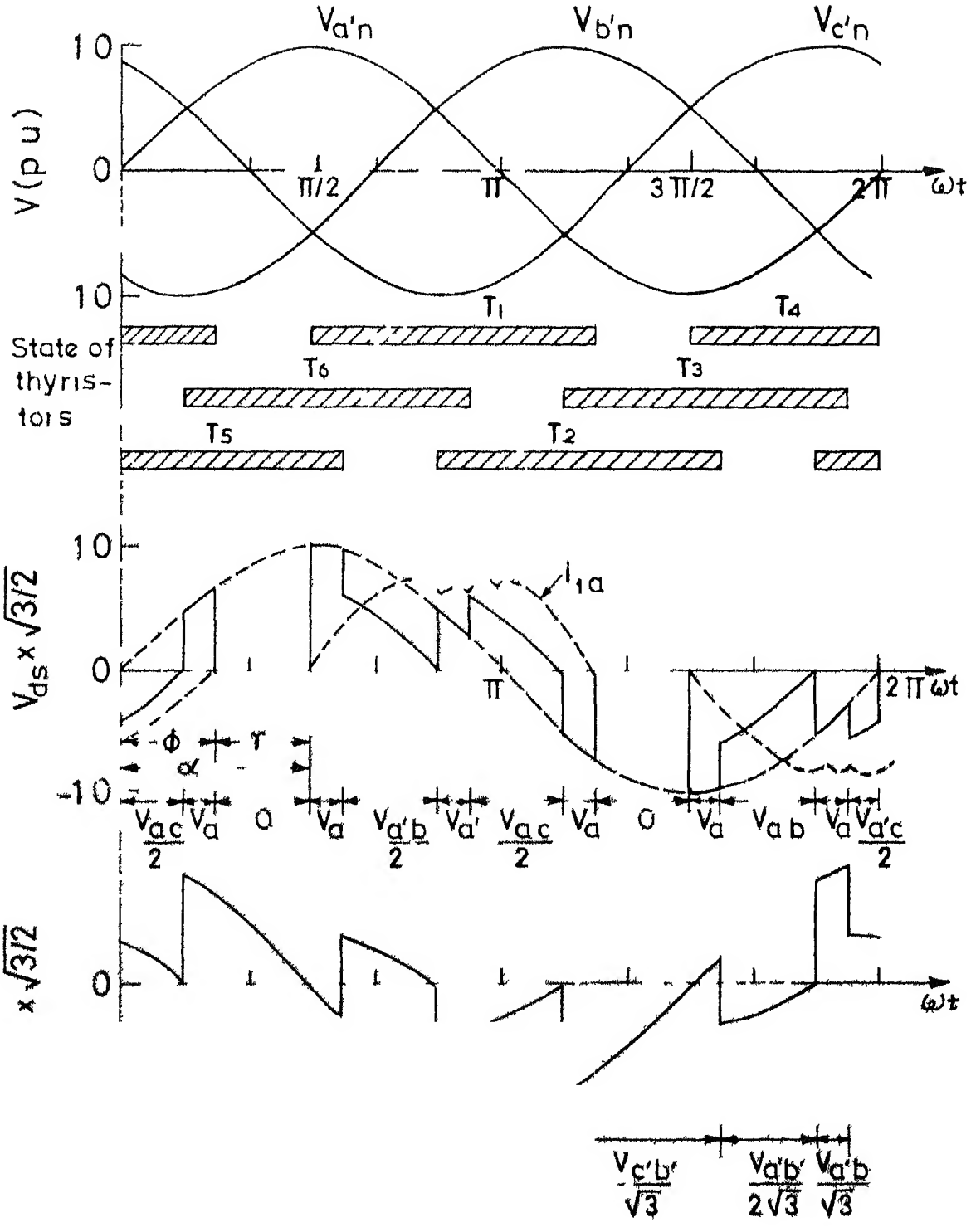

aveforms during

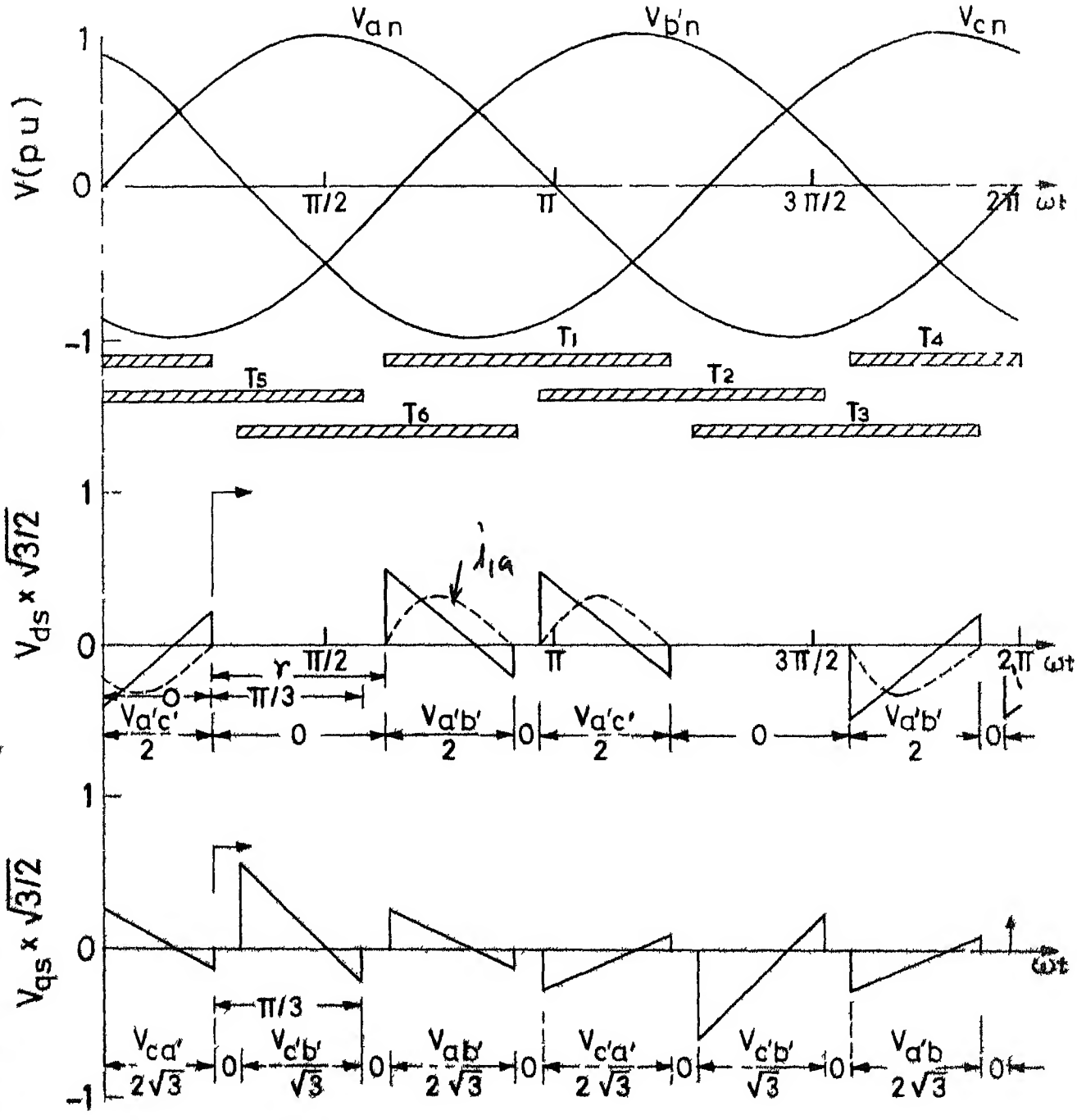

Fig 2 4 Typical d-q voltages during mode-2 (slip=1)

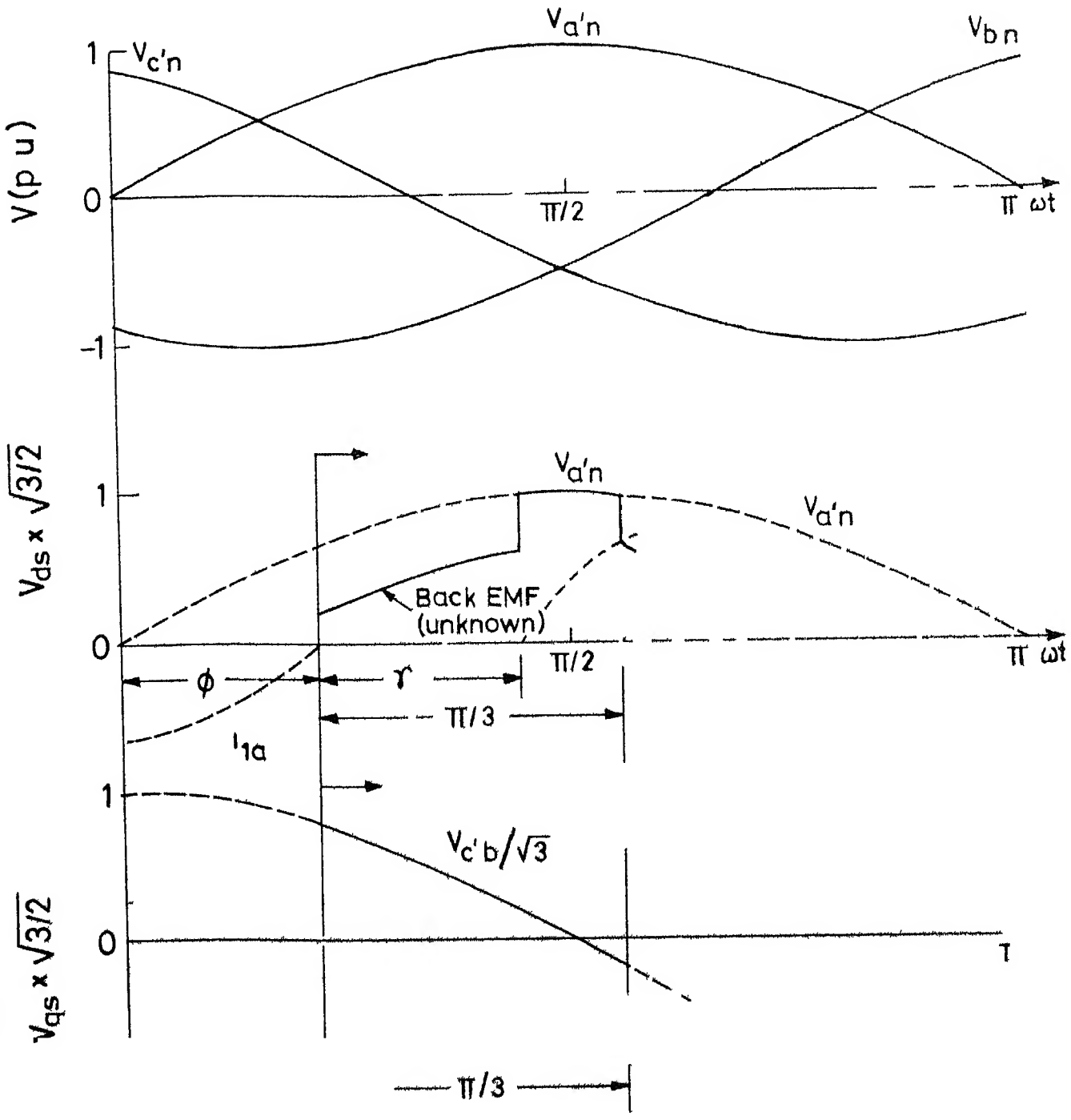

tages for a 3-phase motor during

$$v_{ds} = \sqrt{3/2}\ (\text{back-emf}) \qquad (2\ 18)$$

$$v_{qs} = \sqrt{3/2}\ V_m \cos(\omega t + \phi) \qquad (2\ 19)$$

Time Period - II, $\gamma < \omega t < \pi/3$

All the phase windings are conducting during this period and the voltage across each phase winding will be same as the source voltage Hence,

$$v_{ds} = \sqrt{3/2}\ V_m \sin(\omega t + \phi) \qquad (2\ 20)$$

$$v_{qs} = \sqrt{3/2}\ V_m \cos(\omega t + \phi) \qquad (2\ 21)$$

2 5 2 Mode - 2 $\gamma > \pi/3$ but $< 2\pi/3$

Time period I, $0 < \omega t < (\gamma - \pi/3)$

Referring to Fig 2 6, the d-q voltages during this interval are given by

$$v_{ds} = \sqrt{3/2}\ (\text{back-emf}_1) \qquad (2\ 22)$$

$$v_{qs} = \sqrt{3/2}\ (\text{back-emf}_2) \qquad (2.23)$$

Time period II, $(\gamma - \pi/3) < \omega t < \pi/3$

$$v_{ds} = \sqrt{3/2}\ (\text{back-emf}_1) \qquad (2\ 24)$$

$$v_{qs} = \sqrt{3/2}\ V_m \cos(\omega t + \phi) \qquad (2\ 25)$$

It may be noted that the voltages defined above are not explicitly known since ϕ and back-emf are still unknown These are obtained by an iterative procedure

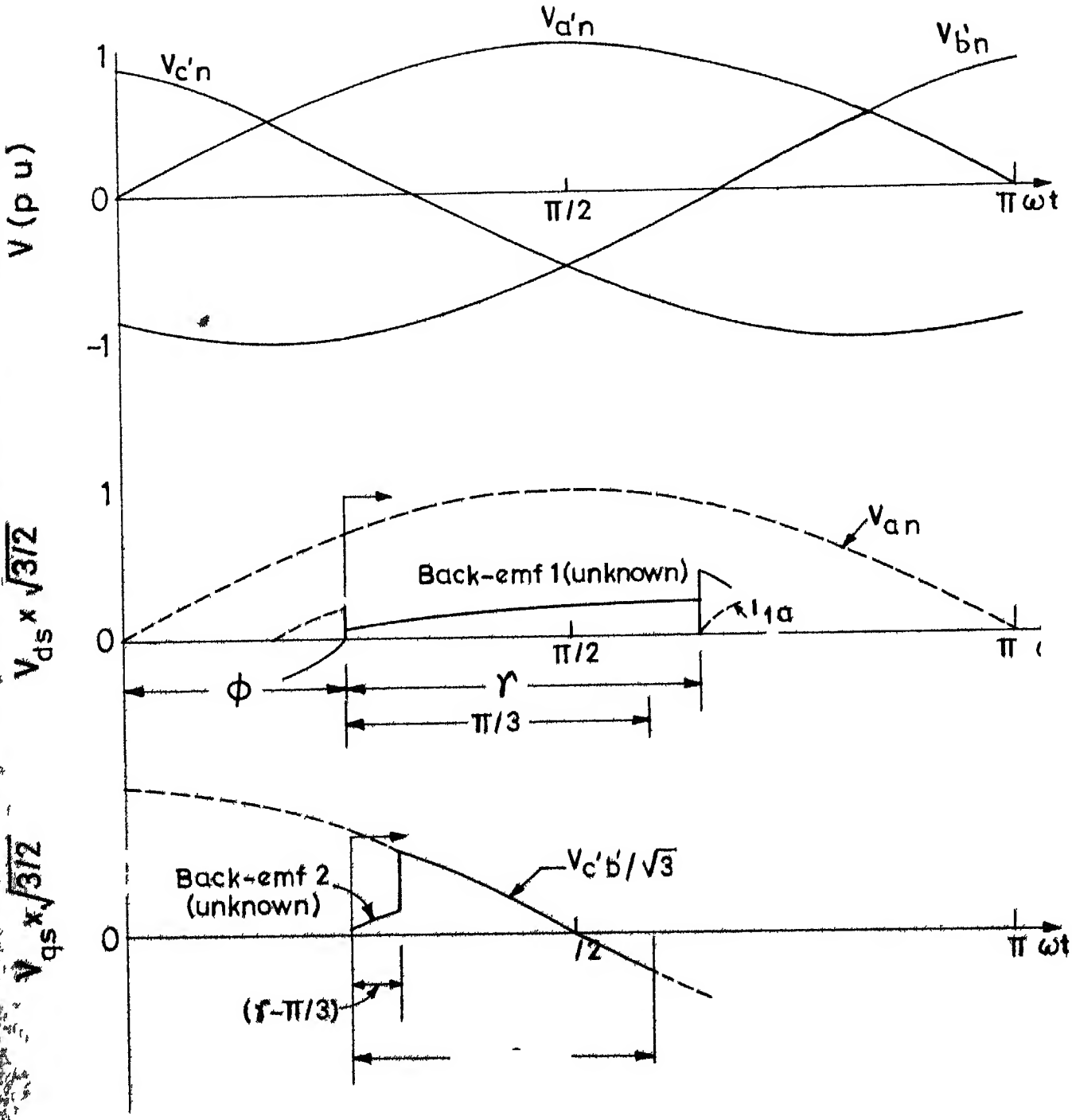
V (p u)
1
0
-1
$V_{c'n}$
$V_{a'n}$
$V_{b'n}$
π/2
π ωt
$V_{ds} \times \sqrt{3/2}$
V_{an}
Back-emf 1(unknown)
I_{1a}
ϕ
γ
π/3
$V_{qs} \times \sqrt{3/2}$
$V_{c'b'}/\sqrt{3}$
Back-emf 2
(unknown)
(γ-π/3)

mode - 2

2 6 STEADY STATE SIMULATION

2 6 1 Algorithm for Simulation

The step by step procedure for the steady state analysis of a voltage controlled induction motor through digital simulation for a given slip and γ is described below A simplified flow chart is shown in Fig 2 7(a & b)

Step-1 A suitable value of ϕ and back-emf are chosen A good approximation for ϕ is the impedance angle of the passive equivalent circuit

Step-2 The mode of operation and accordingly the forcing voltages are identified With these values of forcing voltages and with zero initial vector, the system differential equation (2 15a) is numerically integrated over one-sixth of a cycle In each step of integration during the period of current discontinuity, the back-emf is suitably modified so that the resulting phase current is very near to zero It is assumed that the back-emf remains constant in each integration step

Step-3 The solution of equations (2 15b to 2 15e) are obtained numerically over one-sixth of a cycle

Step-4 The initial vector and the a-phase stator current for the initially assumed ϕ are calculated using the equations (2 17 & 2 10)

Step-5 If the initial value of a-phase current is non-zero,

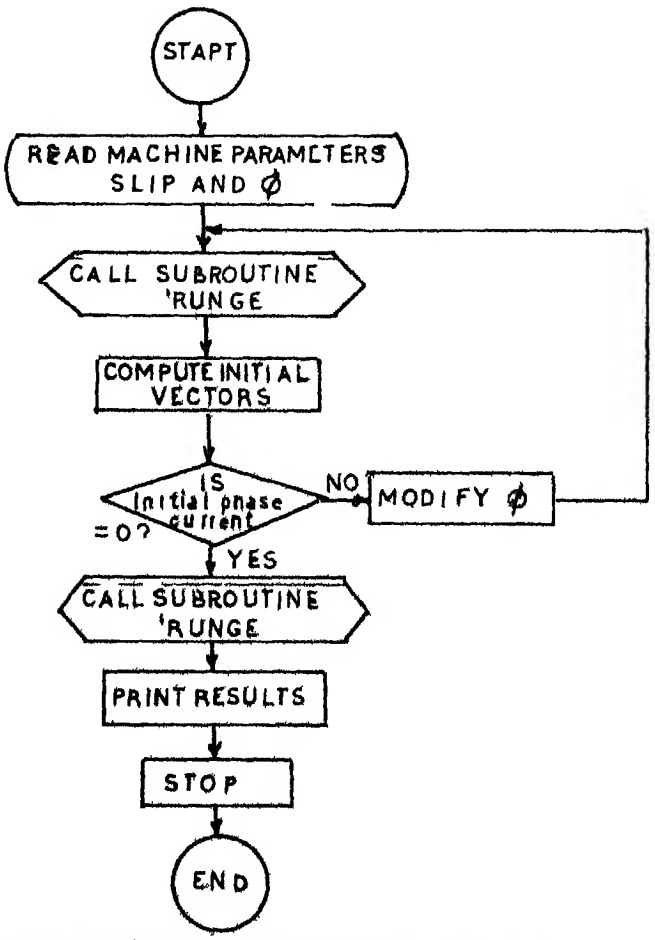

FIG 27(a) Flow chart of the computer programme

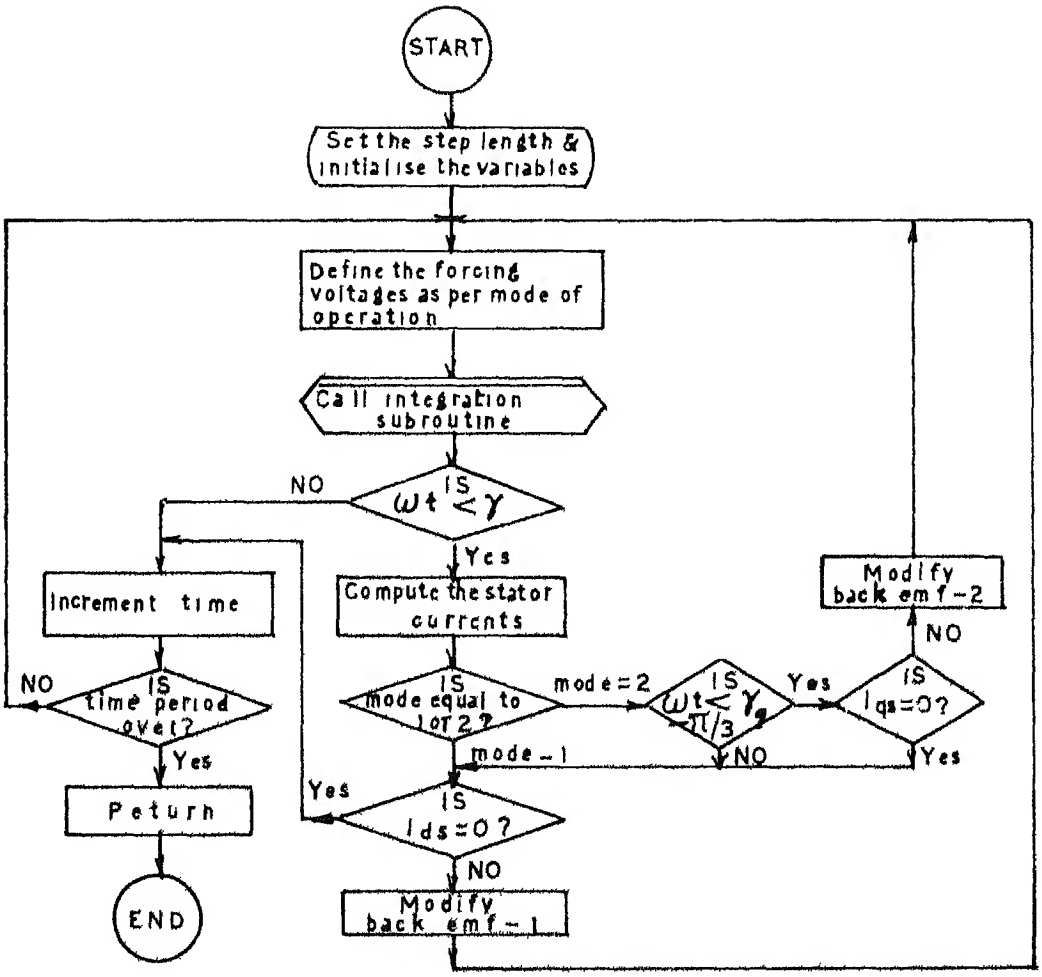

Fig 2.7(b) Flow diagram of the subroutine 'Runge' – Simulation of a 3 phase induction motor

ϕ is suitably modified and steps 2 and 4 are repeated until a-phase current becomes zero

Step-6 One more integration of equation (2 11) with the computed initial vector produces the steady state solution of the variables over the specified period The phase variables are calculated using the transformation equations

The value of ϕ and initial value of back-emf are obtained by linear interpolation The initial vector and corresponding a-phase current are computed for two different values of ϕ and hence the correct value of ϕ for which i_{1a} is zero is calculated by linear interpolation The initial guess value of ϕ is taken as the impedance angle of the conventional passive equivalent circuit The initial value of back-emf is obtained in two steps In the first step, a back-emf of 0 5 p u is assumed and resulting a-phase current is obtained after one integration step. In the second step, -0 5 p u voltage is chosen and current in a-phase is computed for the same interval By linear interpolation, the back-emf corresponding to zero current is calculated and used for the computation

During the period of current discontinuity (γ), the back-emf is to be modified, in each step of integration, such that the resulting phase current becomes practically zero In the beginning of each step of integration, the back-emf is updated from its previous value by adding a small

increment and the integration is performed If the resultant phase current is not less than the preset accuracy level, the back-emf is further modified and integration is repeated The magnitude and sign of the phase current will give an indication of the error in the chosen value of back-emf and accordingly the back-emf is modified

2 6 2 Time Varying Solution of Phase Variables Over One Complete Cycle

Since the thyristors are triggered symmetrically, it is clear that the stator currents and voltages are similar but displaced by 120° The current and voltage waveforms also have half-wave symmetry Because of these properties, the following relationships exist (see Appendix A)

$$i_{1a}(\omega t + \pi/3) = - i_{1b}(\omega t) \qquad (2\ 26)$$

$$i_{1a}(\omega t + 2\pi/3) = i_{1c}(\omega t) \qquad (2\ 27)$$

$$i_{1a}(\omega t + \pi) = - i_{1a}(\omega t) \qquad (2\ 28)$$

Similar relationships exist for the voltage waveforms. Using equations (2 26 to 2 28), the current and voltage waveforms of a-phase can be constructed over one full cycle

The instantaneous electromagnetic torque developed over one-sixth of a cycle is obtained by substituting the time solution of d-q currents in equation (2 13) For the complete cycle, the waveform gets repeated six times The average value of the torque is obtained numerically

2 7 EXAMPLE 1

In this example, a laboratory test machine whose parameters are given in Table 2 1 is considered The steady state analysis is carried out by digital simulation outlined in the previous section and the results are experimentally verified

2 7 1 Digital Simulation Results

Computed waveforms of phase current, phase voltage and electromagnetic torque of the test machine over one cycle period are shown in Figs 2 8 and 2 9 Fig 2 8 pertains to mode-1 operation in which a slip = 0 106 and γ = 35° are chosen for the computation Steady state waveforms during mode-2 operation are shown in Fig 2 9 for step = 1 and γ = 75° In Fig 2 10, the average value of electromagnetic torque is plotted against slip for constant values of γ.

2 7 2 Experimental Verification

2 7 2 1 Description

Experiments are conducted on a 1 1 kW, 4 pole laboratory test machine subjected to voltage control A separately excited d c generator with a resistive load coupled to the induction motor is used for loading the drive From the output power of the d c generator, the torque developed by the induction motor is calculated, taking into account the losses in the d c machine Since the motor torque is a

Table 2 1

DETAILS OF THE TEST MACHINES

1 1 KW, 400 V, 50 Hz, 4 pole, 3 phase, wye-connected, squirrel case induction motor

The measured parameters of the machine are

R_1 = 9 15 Ohms

R_2 = 3 268 Ohms

X_{sl} = 8 526 Ohms

X_{rl} = 8 526 Ohms

X_m = 126 432 Ohms

J = 0 016 kg-m^2

D = 0 0053 N-m-sec/rad

R_1, R_2, X_{sl}, X_{rl} and X_m are the parameters of the passive equivalent circuit

TABLE 2 2

DETAILS OF THE MACHINE GIVEN IN REF [14]

1/3 hp, 220 V, 50 Hz, 4 pole wound-rotor machine

The parameters of the machine expressed in per-unit using rated voltage as base volts and 375 W as base power are

R_1 = 0 0566

R_2 = 0 1252

X_s = 1 0318

X_r = 1 0318

X_m = 0 9690

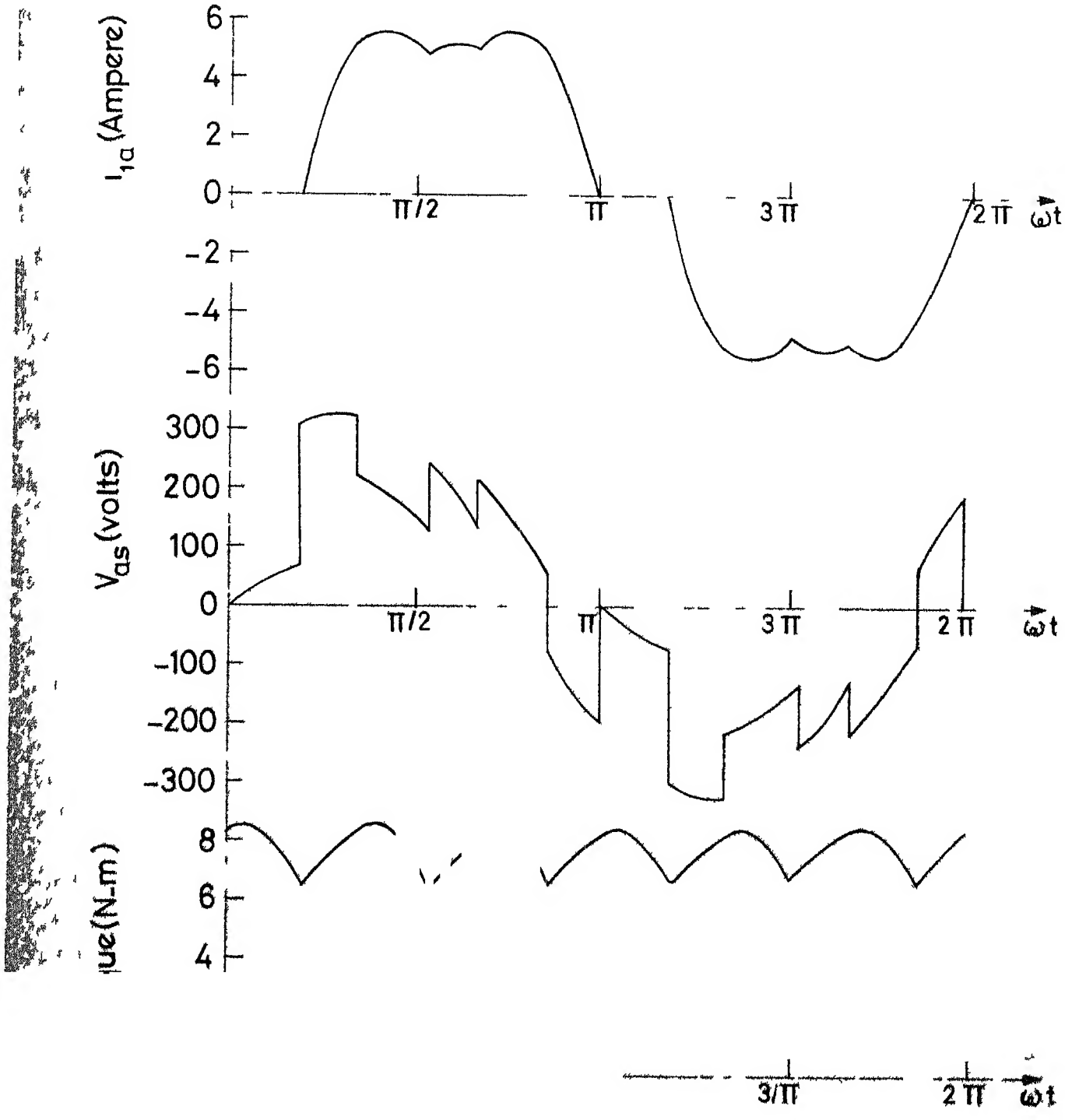

current, voltage and
$\gamma = 35°$, $\Phi = 35.5°$

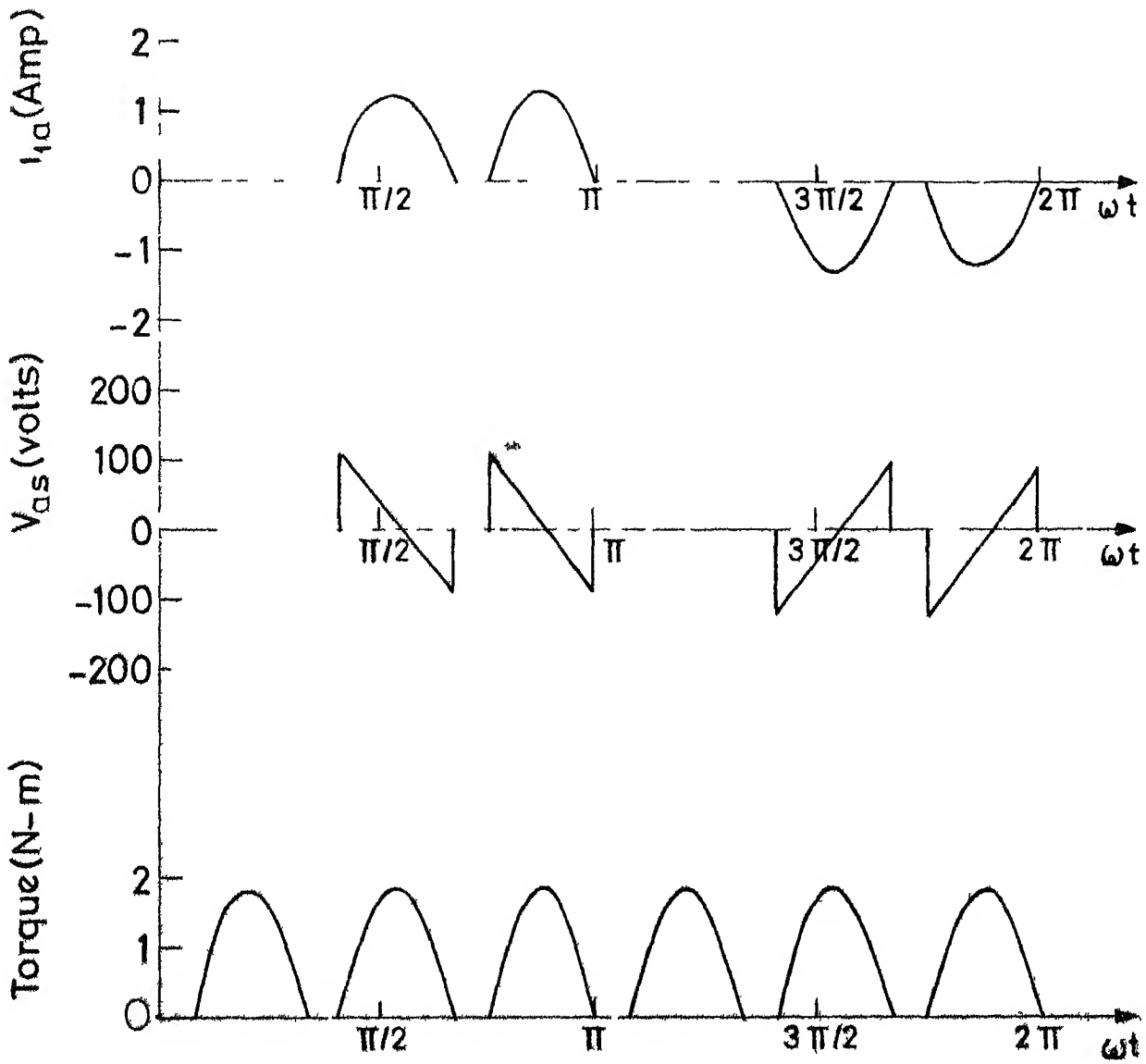

Fig 2 9 Computed results - Mode-2 operation $\gamma = 75^{\circ}$ slip = 1

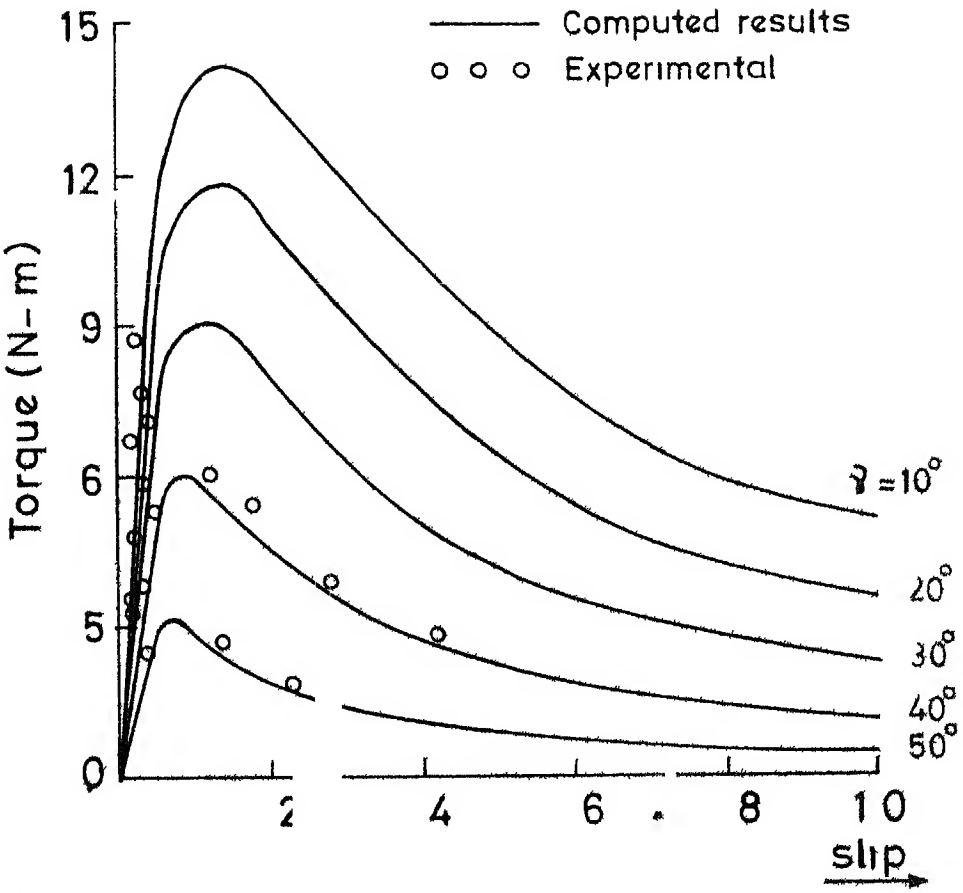

...ter...stics
...ine

function of speed, the motor could be run stably at lower ranges of speeds where the torque-slip curve of the motor has negative slope The operation at these points were limited to short duration since the motor currents were excessive The triggering angle α and hold off angle γ are measured from the actual voltage and current waveforms A description,of the triggering circuit for the control follows

2 7 2 2 Triggering circuit

An electronic triggering circuit (Fig 2 11) suitable for triggering six thyristors of a 3-phase voltage controlled system is developed The output waveforms at different stages are given in Fig 2 12 and a brief description of the circuit is given below

The input signal to the circuit is obtained from one of the phases of the 3-phase source voltage An open loop comparator is used for obtaining the zero crossing of the input signal The square wave output of the zero-crossing detector is applied to a ramp generator The output of the ramp generator is compared with a reference voltage or an error signal for controlling the triggering angle α of the thyristors. The α can be adjusted over the full range by varying the reference voltage The pulse width of the comporator output is different for different α's With the help of a monostable M_1, pulses of constant width for all

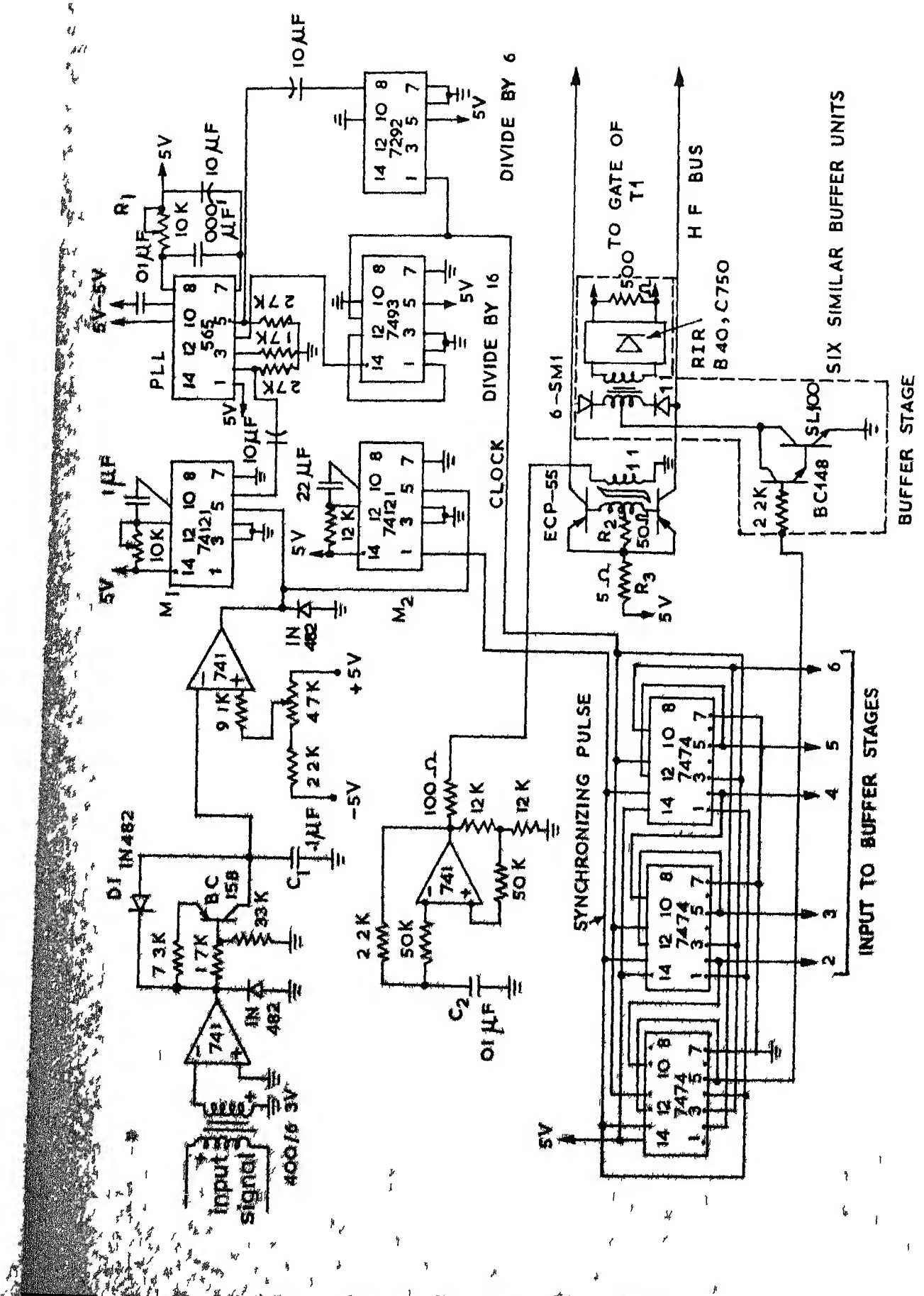

Fig 2.11 Triggering circuit

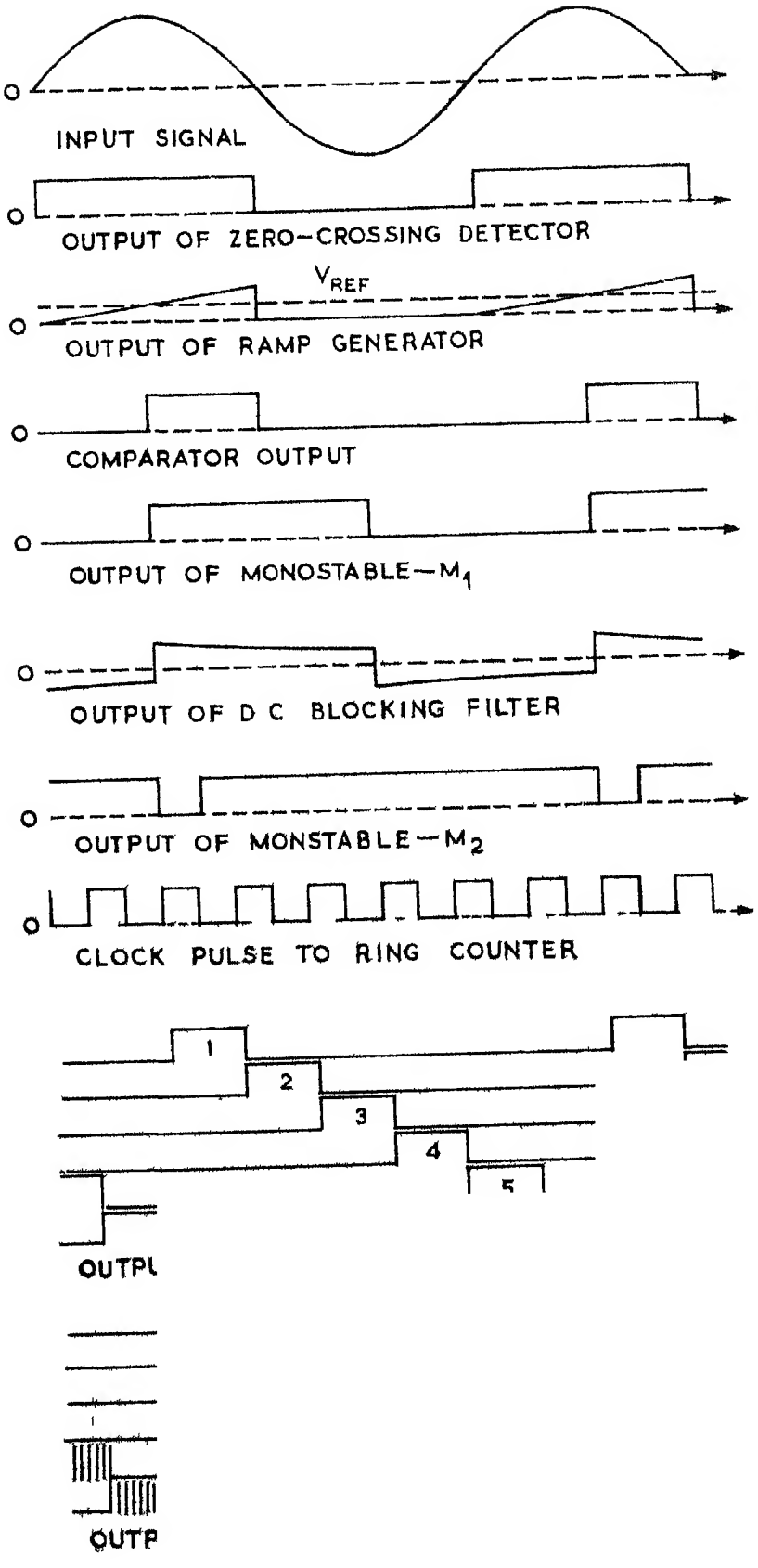
INPUT SIGNAL
OUTPUT OF ZERO-CROSSING DETECTOR
V_{REF}
OUTPUT OF RAMP GENERATOR
COMPARATOR OUTPUT
OUTPUT OF MONOSTABLE—M_1
OUTPUT OF D C BLOCKING FILTER
OUTPUT OF MONSTABLE—M_2
CLOCK PULSE TO RING COUNTER
1
2
3
4
5
OUTPU
OUTP

values of α are obtained By using a d c voltage blocking circuit, the d c component of monostable output is removed before it is applied to the phase locked loop (PLL) The PLL will provide necessary frequency multiplication and synchronization The clock pulses (six times the input signal frequency) obtained from the PLL, are applied to a ring counter consisting of six D flip-flops in cascade By means of a synchronizing pulse obtained from the monostable M_2 (Fig 2 11), the ring counter is initially set to 100000 state There is provision for feedback input for automatic control of α The triggering angle correction, if any, is made in each cycle The circuit employs digital and linear [50,51] integrated circuits The gate pulses are modulated and amplified before it is applied to the thyristor gates through pulse transformers The gate current can be set between to 10 mA and 300 mA to suit the gate characteristics of any type of thyristor The main features of the triggering circuit are

1) suitable for 3-phase voltage controlled and bridge converter systems using thyristors
2) self starting and self synchronizing capability
3) suitable for various types of thyristors with different gate characteristics
4) precise and wide range of α control
5) inhibition of the gate pulse can be easily achieved

6) only single phase input is required

7) due to the presence of synchronizing pulse throughout the operation, mal-operation of triggering sequence due to external electrical disturbances is corrected in every cycle

8) minimum number of integrated circuit components are used

2 7 2 3 Experimental results

Figure 2 10 shows, along with the computed results, the measured values of torque as a function of slip The actual voltage and current waveforms during mode-1 operation are given in Fig 2 13 When the triggering angle is adjusted for mode-2 operation, the motor was practically stalling and the voltage and current waveforms during this mode of operation are shown in Fig 2 14

2 8 Example-2

This example is used to have a comparison of the results obtained by BVA with the results given in [14] where state space technique is used for the analysis The average torque computed by BVA for various values of γ is given in Fig 2 15 The results from Lipo [14] are also shown in the same figure The details of the machine are given in Table 2 2

2 9 Discussion

The current, voltage and torque waveforms shown in Figs 2 8 and 2 9 conform well with other published results in the

Fig 2 13 Actual waveform of voltage and current during mode-1

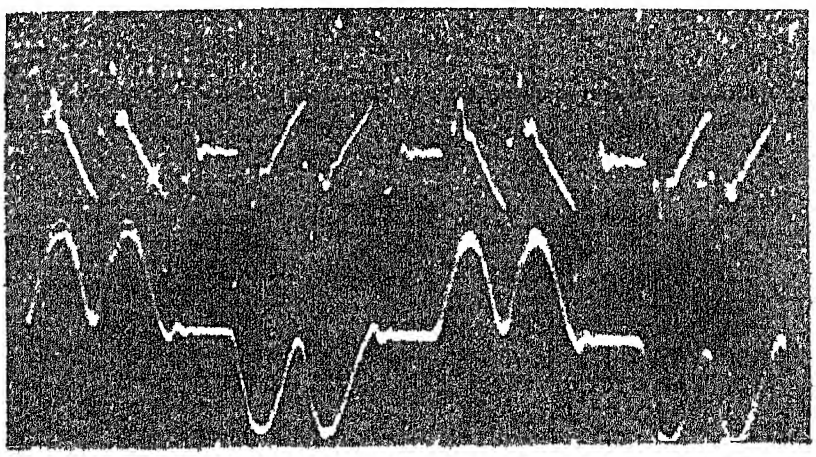

Fig 2 14 Actual waveform of voltage and current during mode-2

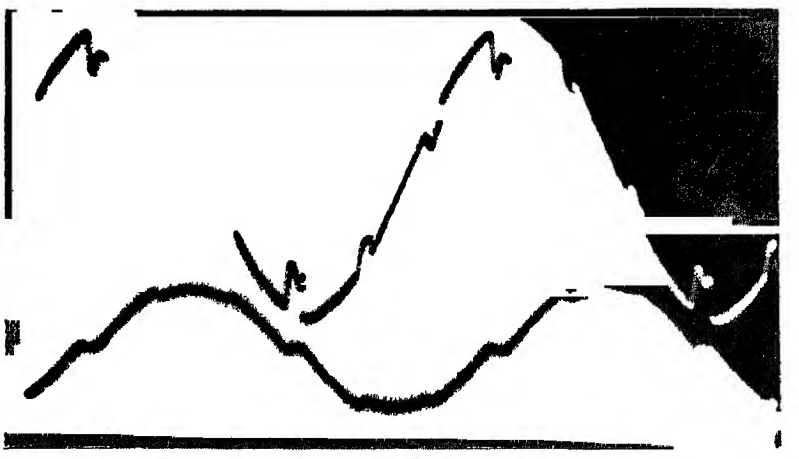

Fig 2 13 Actual waveform of voltage and current during mode-1

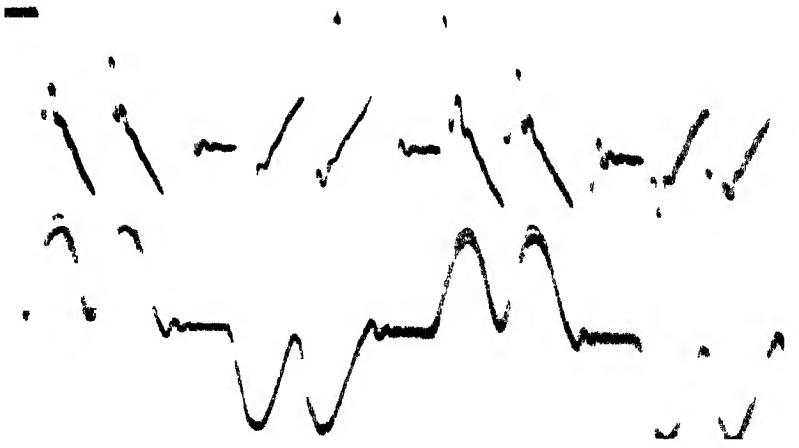

Fig 2 14 Actual waveform of voltage and current during mode-2

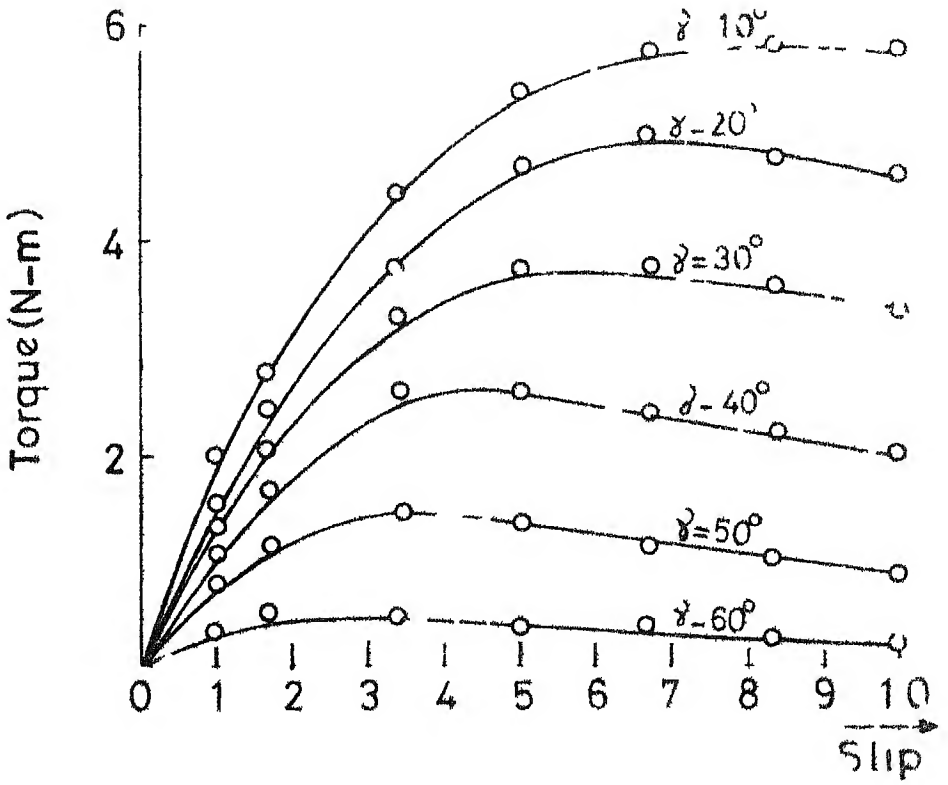

Fig 2 15 Torque-speed characteristics

literature The voltage waveform is piecewise continuous and half-wave symmetric The electromagnetic torque contains a constant component with a predominent sixth harmonic The sixth harmonic torque is produced by the fifth and seventh harmonics in the stator current Harmonic contents of the stator current increase with increase in γ When γ becomes greater than $\pi/3$, the stator current becomes discontinuous in each half cycle with two current pulses Torque waveform also becomes discontinuous with six pulses in each cycle The average torque plotted against slip for constant values of γ (Fig 2 10) has good agreement with the experimentally measured results The actual voltage and current waveform (Figs 2 13 and 2 14) also tally with the computed results

Figure 2 15 shows the torque speed characteristics computed by BVA for a motor given in [14] The results given in [14] are also shown in Fig 2 15 to facilitate comparison It is observed that there is good agreement between the results obtained by BVA and those by state space technique

Per unit quantities are used in the computation Peak value of the rated phase voltage and peak rated line current are taken as base quantities

2 10 CONCLUSION

Steady state analysis and simulation of a voltage controlled 3-phase induction motor, have been presented using the boundary

value approach The main feature of this method is that the machine equations are unaltered for different terminal constraints while excitation functions are defined according to the mode of operation Hence, the mathematical formulation becomes simple and general

CHAPTER 3

STEADY STATE ANALYSIS OF DELTA AND THYRODE CONTROLLED INDUCTION MOTORS BY BOUNDARY VALUE APPROACH

3 1 INTRODUCTION

Using BVA, the steady state analysis of a voltage controlled induction motor with a pair of thyristors connected back-to-back in each phase was described in the previous chapter. In order to demonstrate the generality of BVA, two more examples of voltage control schemes are considered in this chapter with, a) delta connected thyristors at the open star point of the stator winding, b) thyristor and diode (thyrode) combination in the stator phases

Although voltage control scheme with back-to-back connected thyristor pairs is more efficient, other types of thyristor connections [4], are sometimes used in practice when the prime consideration is not of efficiency but of economy. In a thyrode controlled scheme, three thyristors are replaced by three diodes (Fig 3 1) In a 'delta controller' three symmetrically triggered, delta connected thyristors are included at the open star point of the induction motor (Fig. 3.2) The main disadvantage of delta and thyrode controllers over back-to-back connected thyristor pairs is the presence of predominant second harmonics in the stator currents These harmonics produce braking torque and also result in increased

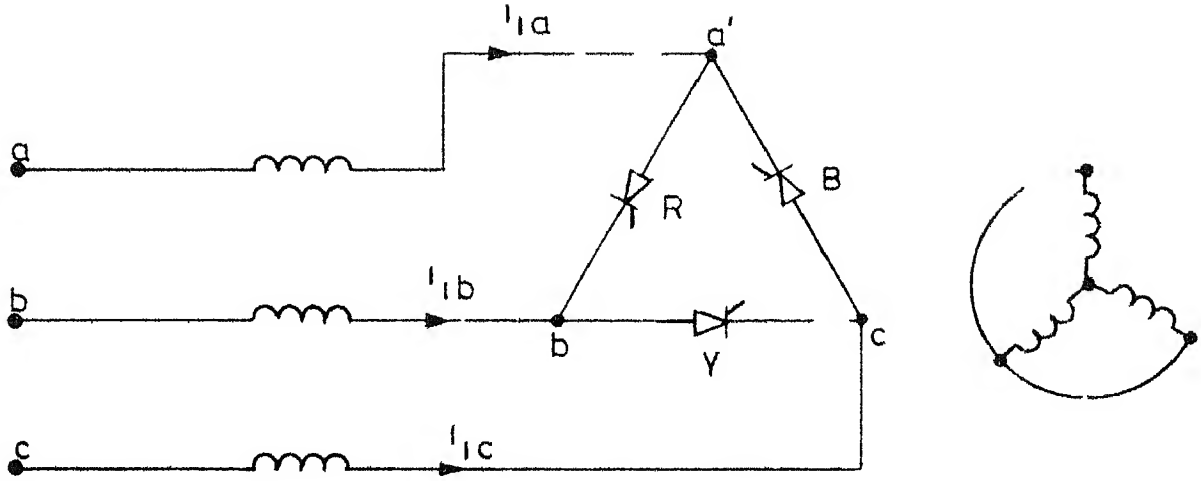

Fig 3 2 Schematic diagram of a delta controller

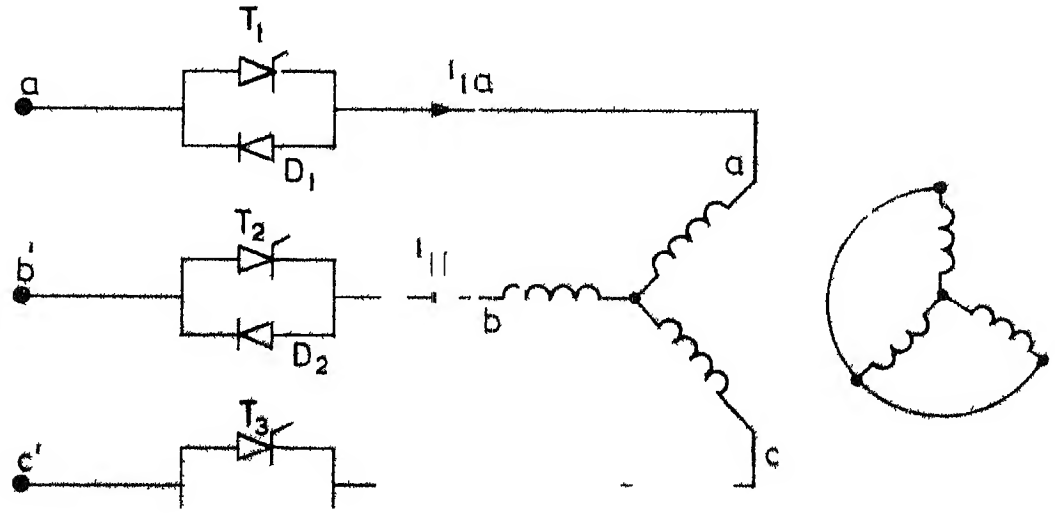

ller

iron and copper losses, which leads to a loss in the efficiency at low conduction angles

3 2 SYMMETRICALLY TRIGGERED DELTA CONNECTED THYRISTOR CONTROLLER

Three thyristors connected in delta are included at the open neutral of the stator winding The thyristors are triggered symmetrically at intervals of 2 $\pi/3$ radians By controlling the triggering angle (α), the voltage applied to the motor terminals can be fully controlled Since the thyristors are connected in delta configuration, not more than two thyristors can conduct at any instant of time This is because of the fact that when two thyristors are conducting, the third one is reverse biased When two thyristors are conducting,all the three stator windings carry current and voltage across each phase winding will be equal to the respective source voltage On the otherhand single phasing takes place when only one thyristor is conducting During this state of operation one of the stator phases is open circuited

3 2 1 Modes of Operation

Maximum period of conduction of each thyristor in a delta connected system is 4 $\pi/3$ radians If the delay angle or triggering angle (α) is zero, the thyristor R (Fig 3 2) starts conducting from a point 60° behind the positive zero

crossing of a-phase voltage The conduction period (β) of each thyristor will be a function of α, slip and the machine parameters If the value of β ranges between $2\pi/3$ and $4\pi/3$, either three or two windings of the induction motor are connected to the power source This mode of operation is denoted as either 2/1 mode or mode-1 operation The conduction period of each thyristor and typical current and voltage waveforms are shown in Fig 3 3 for 2/1 mode of operation in which α, γ and ϕ are indicated The thyristors R,Y and B are triggered at α, $2\pi/3 + \alpha$ and $4\pi/3 + \alpha$ respectively The conducting thyristors go into the blocking state at the natural current zero The sequence of thyristor conduction in this mode is B-R, R, R-Y, Y, Y-B, B, B-R and so on

When the value of β lies between 0 and $2\pi/3$ either one thyristor or none will be in conducting state Single phasing takes place when only one thyristor is conducting When none of the thyristors is conducting, all the stator currents will be identically zero but voltages may be present across the windings (induced by the rotor currents) This mode of operation is denoted as either 1/0 mode or mode-2 operation Typical voltage and current waveforms are given in Fig 3.4 Two current pulses per cycle appear in each phase winding and this mode of operation is not having any practical importance because the electromagnetic torque produced will be quite small

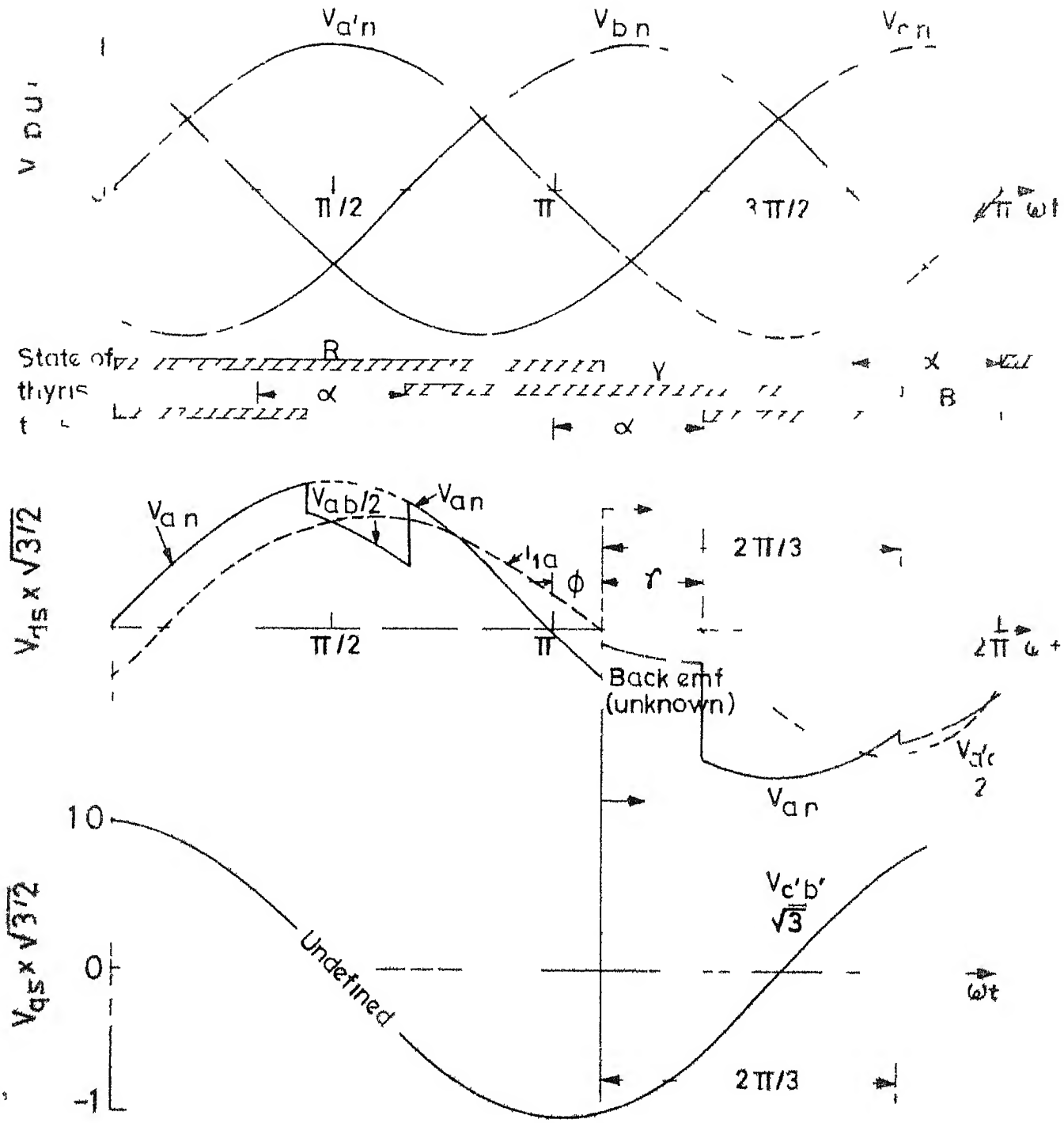

Fig 3 3 d-q Voltages of a delta controlled induction motor during mode-2/1

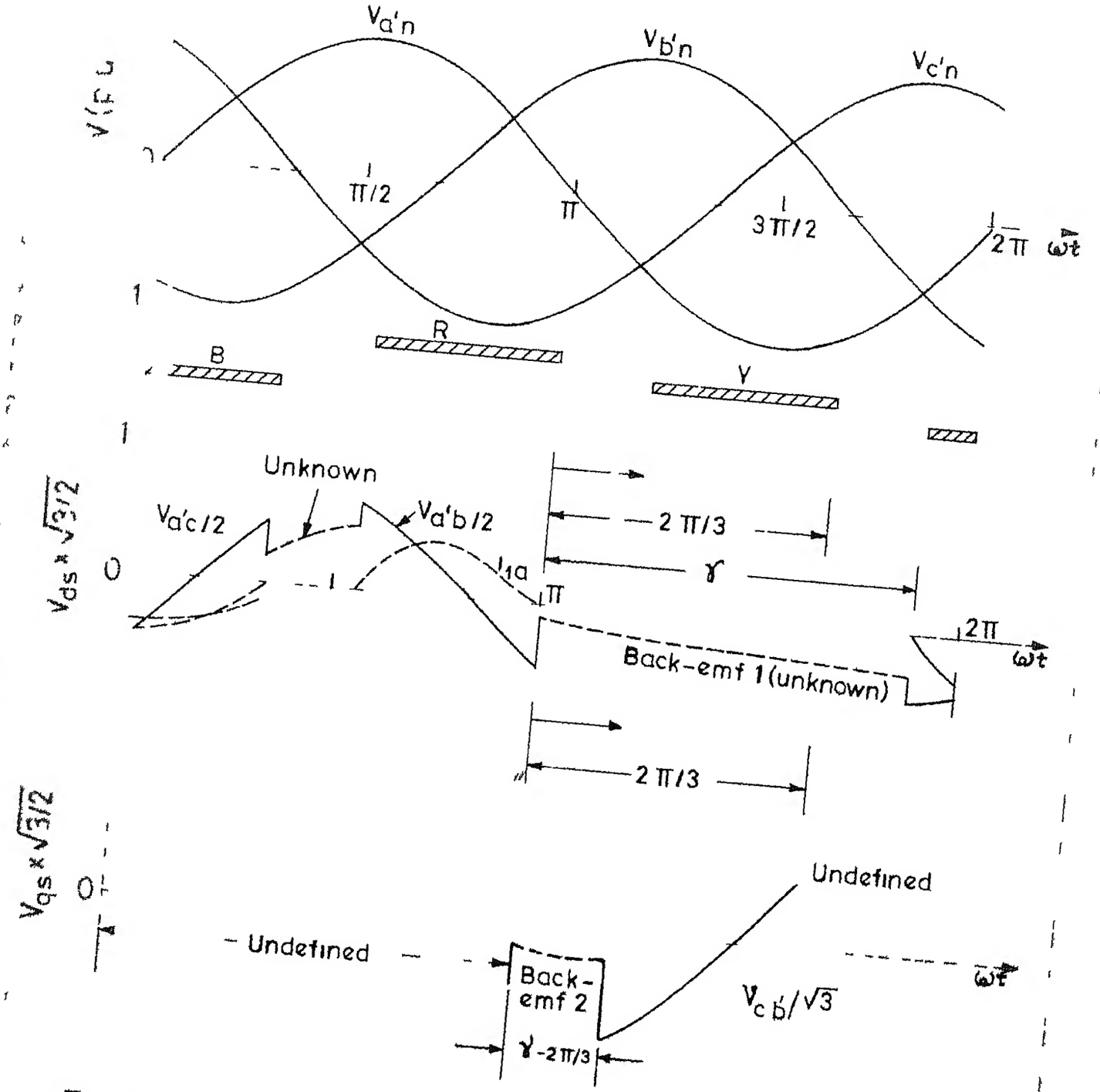

Fig 3 4 d-q voltages of delta controlled induction motor during 1/0 mode

3 2 2 Symmetry of the System

Since the three thyristors are symmetrically triggered at an interval of $2\pi/3$, the currents and voltages have 3-phase symmetry However, unlike the case of six thyristor connection, here half wave symmetry does not exist Because of the 3-phase symmetry, hold off angle γ, phase angle ϕ, delay angle α associated with the turn off of each thyristor are identical Accordingly a solution for any $2\pi/3$ interval is sufficient to uniquely define all steady state variables over the entire period A boundary relationship between the steady state variables at an interval of $2\pi/3$ is given in Appendix B

3 2 3 Machine Equations

The equations (2 1) to (2 17) derived in Chapter 2 are directly applicable to the present case except (2 12) defining the boundary condition In the present case a boundary relationship exists during steady state for an interval of $2\pi/3$ radians The boundary relationship (see Appendix B) is given by

$$\underline{Y}|_{\omega t = 2\pi/3} = T_1 \underline{X}|_{\omega t = 0} \qquad (3\ 1)$$

where

$$T_1 = \begin{bmatrix} -1/2 & \sqrt{3}/2 & 0 & 0 \\ -\sqrt{3}/2 & -1/2 & 0 & 0 \\ 0 & 0 & -1/2 & \sqrt{3}/2 \\ 0 & 0 & -\sqrt{3}/2 & -1/2 \end{bmatrix}$$

The component equations of the machine differential equation (2 15a - 2 15e) are solved numerically over a period of $2\pi/3$ The forcing function needed for the solution of (2 15a) are described in Section 3 2 4 The final value of the variables over an interval of $2\pi/3$ is

$$\underline{x}_f = \underline{x}_f^0 + x_{11}\,\underline{x}_f^1 + x_{21}\,\underline{x}_f^2 + x_{31}\,\underline{x}_f^3 + x_{41}\,\underline{x}_f^4 \qquad (3\ 2)$$

Combining equations(3 1) and (3 2), the initial vector can be obtained as

$$\underline{x}_1 = C_2^{-1}\,\underline{x}_f^0 \qquad (3.3)$$

where

$C_2 = T_1 - X_f$ and X_f is a 4x4 matrix given by

$$X_f = [\,\underline{x}_f^1 \,,\, \underline{x}_f^2 \,;\, \underline{x}_f^3 \,;\, \underline{x}_f^4\,]$$

One more integration of the system differential equation (2 15a) over an interval of $2\pi/3$ with the initial vector as computed in (3 3) provides the steady state solution

3 2 4 Definition of Forcing Voltages

Forcing voltages v_{ds} and v_{qs} are to be defined over a period of $2\pi/3$ for the solution of system differential equation (2 15a) For the purpose of analysis, the reference point for defining the forcing voltages is chosen as the instant at which the thyristor R extinguishes (Figs 3 3 and 3 4) As explained in Section 3 2 1, there are two modes of operation depending upon the conduction period of the thyristors

3 2 4 1 2/1 mode of operation

The d-q voltages as defined in equations (2 2 and 2 3) are plotted in Fig 3 3 for 2/1 mode of operation There are two distinct time periods during the interval $2\pi/3$

a) Time period I, $0 < \omega t < \gamma$

b) Time period II, $\gamma < \omega t < 2\pi/3$

Time Period I, $0 < \omega t < \gamma$

At the beginning of the interval the thyristor R goes to blocking mode resulting in zero current in phase-a A back-emf of unknown magnitude appears across the winding. Thyristor Y continues to conduct resulting in single phasing of the motor Referring to Fig 3 3, the d-q voltages are

$$v_{ds} = \sqrt{3/2}\,(\text{back-emf}) \qquad (3\ 4)$$

$$v_{qs} = -\sqrt{3/2}\, V_m \cos(\omega t + \phi) \qquad (3\ 5)$$

Time Period II, $\gamma < \omega t < 2\pi/3$

At $\omega t = \gamma$ the thyristor B is turned on resulting in 3 phase conduction The voltage across each stator winding will be same as the respective source voltages The d-q voltages are

$$v_{ds} = -\sqrt{3/2}\, V_m \sin(\omega t + \phi) \qquad (3\ 6)$$

$$v_{qs} = -\sqrt{3/2}\, V_m \cos(\omega t + \phi) \qquad (3\ 7)$$

3 2 4 2 1/0 mode of operation

The conduction period of each thyristor during this mode of operation is less than $2\pi/3$ radians The machine will be subjected to single phasing and off state alternately Two time periods can be identified (Fig 3 4) for the purpose of defining the forcing voltages

a) Time Period I, $0 < \omega t < (\gamma - 2\pi/3)$

At the beginning of this interval, the thyristor R goes to off state Currents in all the phases will be zero as no thyristor is conducting Back-emf may appear across the phase windings due to the coupling with the rotor currents The forcing voltages during this period is

$$v_{ds} = \sqrt{3/2}\ (\text{back-emf}_1) \qquad (3\ 8)$$

$$v_{qs} = \sqrt{3/2}\ (\text{back-emf}_2) \qquad (3\ 9)$$

b) Time Period II, $(\gamma - 2\pi/3) < \omega t < 2\pi/3$

At $\omega t = \gamma$, thyristor f is turned on resulting in currents in b and c phases The d-q voltages are (Fig 3 4)

$$v_{ds} = \sqrt{3/2}\ (\text{back-emf}_1) \qquad (3\ 10)$$

$$v_{qs} = -\sqrt{3/2}\ V_m \cos(\omega t + \phi) \qquad (3\ 11)$$

3 2 5 Steady State Simulation

After having defined the forcing voltages over a period of $2\pi/3$, the solution of system differential equations

(2 15a - 2.15e) can be obtained numerically for a given slip and γ as described in Section 2 6 of Chapter 2 The final values of the solution obtained for a period of $2\pi/3$ are substituted in equation (3 3) to obtain the initial vector This initial vector will directly lead to the steady state solution

The value of ϕ is obtained by linear interpolation technique The back-emf in each step of integration during the period of γ is computed as described in Section 2 6 of Chapter 2

3 2 6 Solution of Phase Variables Over One Cycle

From the computed results of the state variables V_{s1}, V_{s2}, V_{r1}, V_{r2}, the phase currents i_{1a}, i_{1b} and i_{1c} can be calculated using equations (2 10) and (2 4 - 2 6) Because of the 3-phase symmetry of the phase variables, the following relationships can be easily derived (see Appendix B)

$$i_{1a}(\omega t + 2\pi/3) = i_{1c}(\omega t) \qquad (3.12)$$

$$i_{1a}(\omega t + 4\pi/3) = i_{1b}(\omega t) \qquad (3\ 13)$$

Similar relationships exist for the stator voltage waveforms The electromagnetic torque gets repeated three times over one cycle

3 2 7 Example

Steady state waveforms of stator current i_{1a}, stator voltage v_{as} and electromagnetic torque T_e are computed with

the forcing voltages defined in Section 3 2.4 The algorithm given in Section 2 6 of Chapter 2 is used for the simulation Fig 3 5 shows the computed steady state waveforms of current, voltage and torque for a hold off angle (γ) of 50° and slip of 0 15 The computed results for γ = 100° and slip = 0 2 are shown in Fig 3 6 The dissimilar pattern of voltage and current waveforms during negative and positive half-cycle is evident from these results The torque waveform has a constant term with a predominant third harmonic The magnitude of the harmonic component changes with γ and this is evident from the torque waveforms given in Figs 3.5 and 3 6 It can be seen from Fig 3 5 that the peak value of current reaches about 4 p u at a slip of 0 15 This can cause excessive heating and damage the windings if the motor is run for longer duration at this value of slip The average value of the developed torque for constant values of γ is shown in Fig 3 7 The parameters of the motor are given in Table 2 1 of Chapter 2

3 3 SYMMETRICALLY TRIGGERED THYRODE CONTROLLER

Schematic diagram of a voltage controlled 3-phase induction motor with back-to-back connected thyristor-diode combination in each phase is shown in Fig 3 1 The three thyristors T_1, T_2 and T_3 are triggered symmetrically at intervals of $2\pi/3$ so as to obtain a balanced 3-phase voltage across the machine terminals The input voltage to the machine terminals

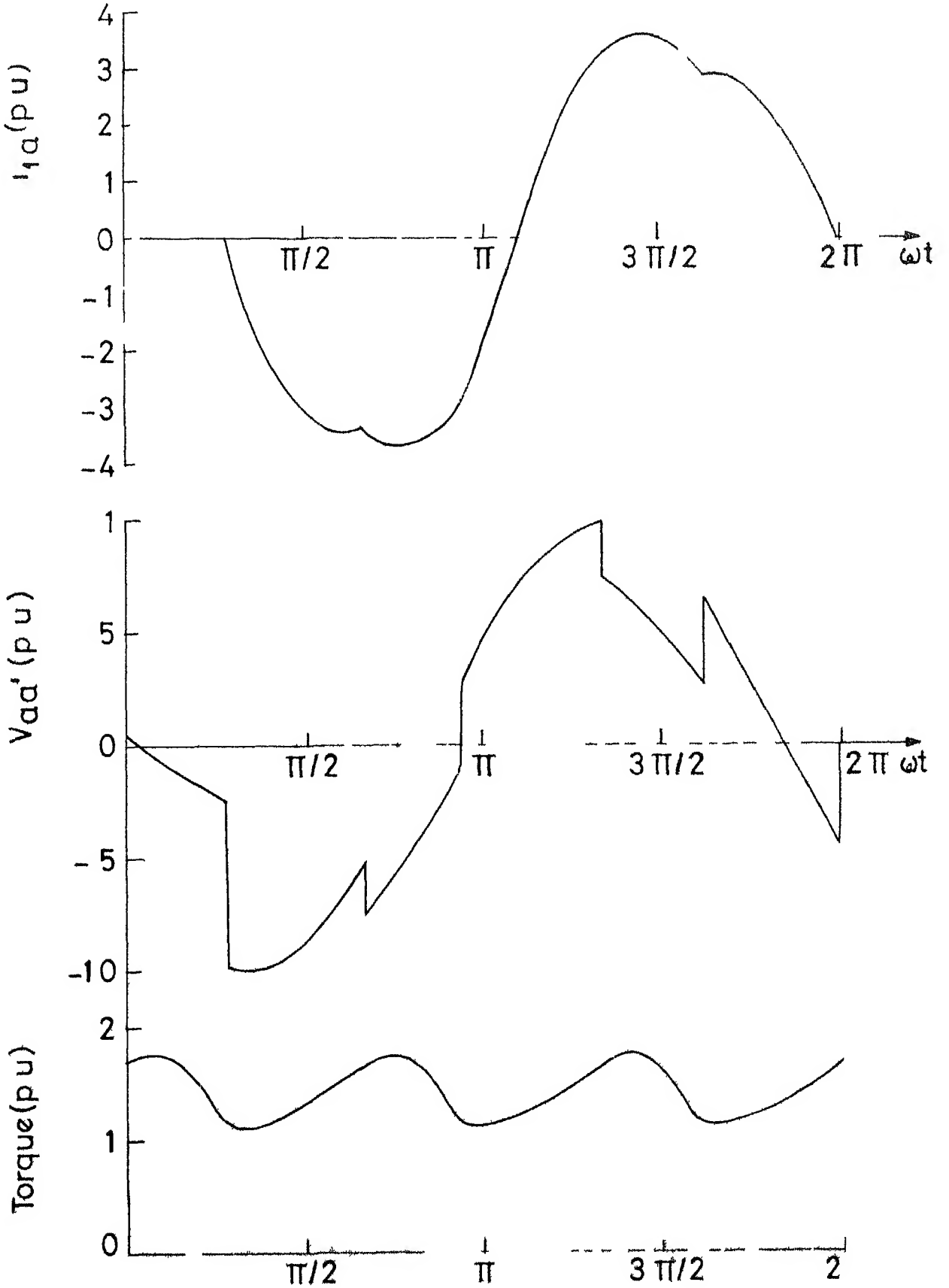

mputed results of a delta controlled
uction motor at $\gamma = 50^{c}$ and slip = 0 15

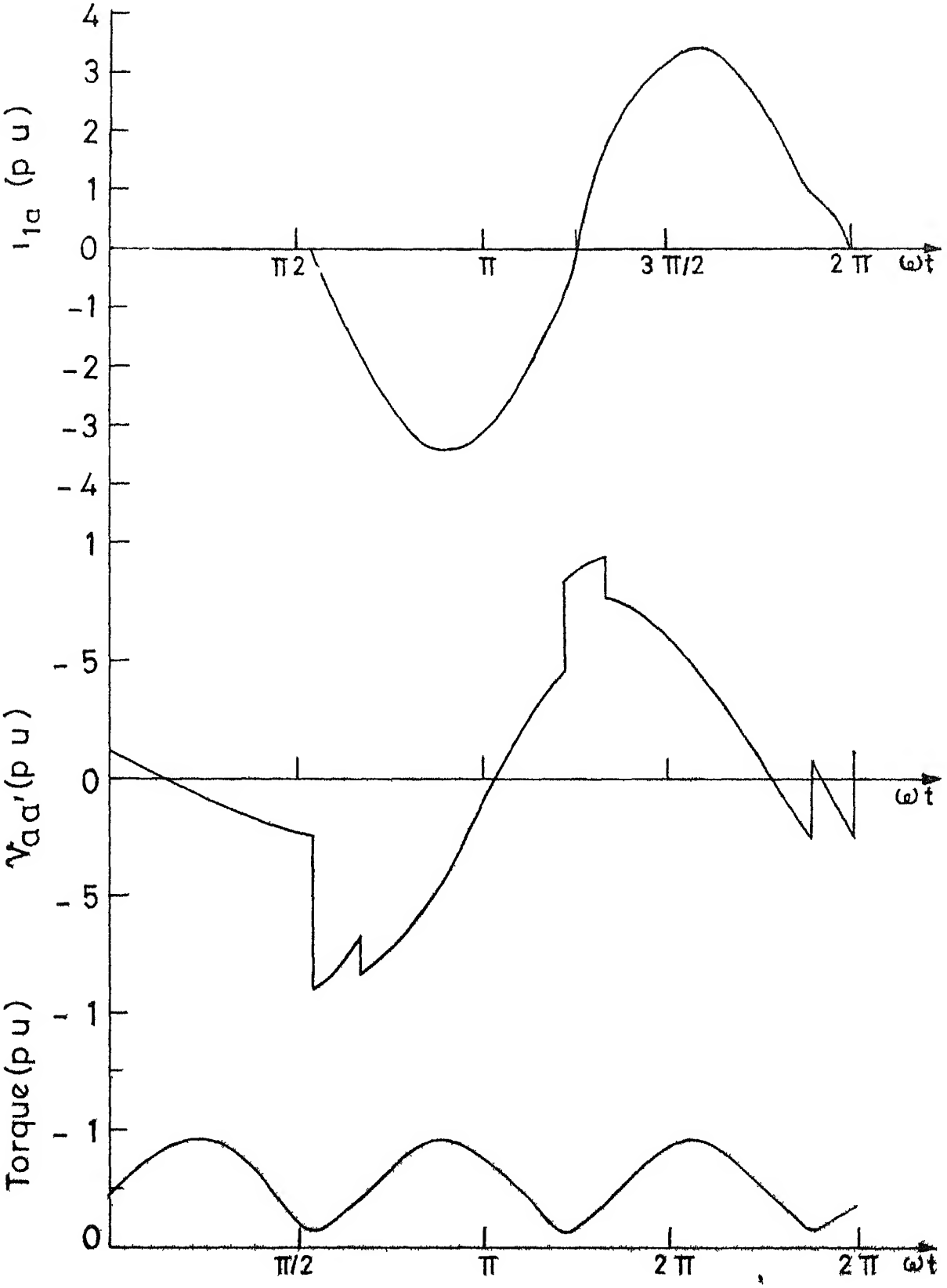

Fig 3 6 Computed results at ϑ=100° slips=0 2

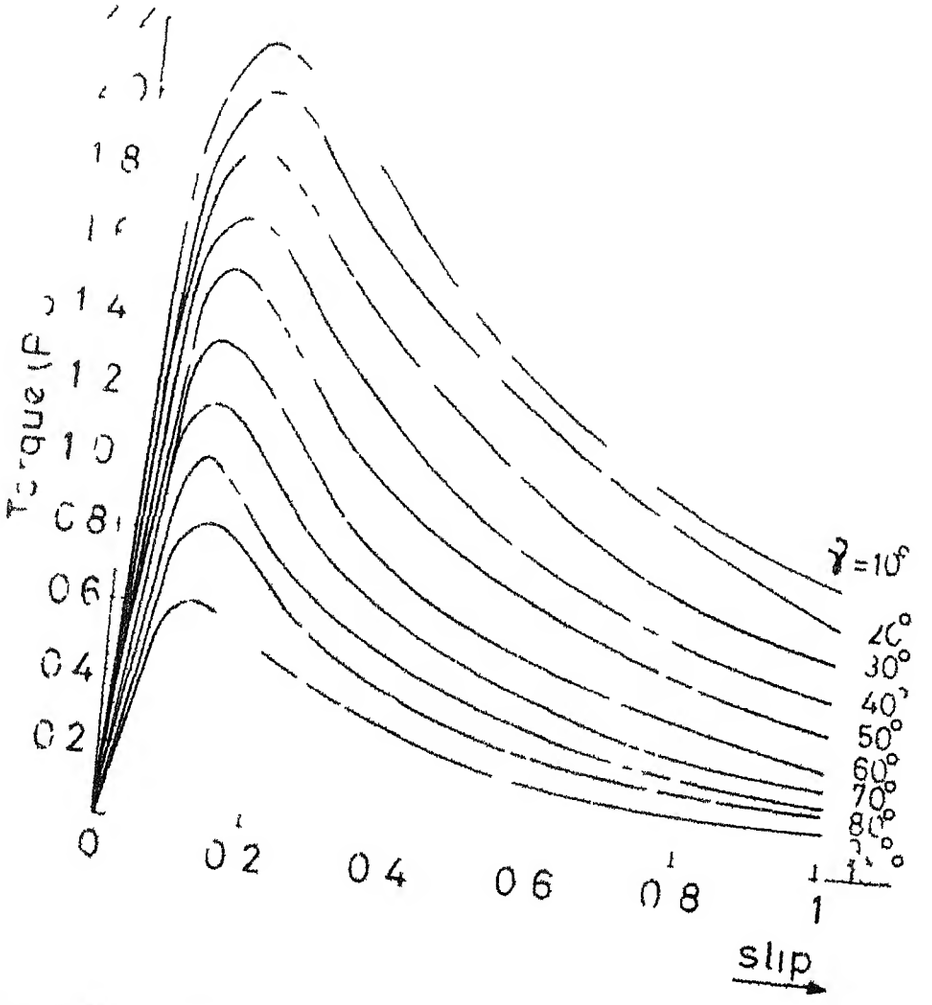

Fig 3 7 Computed Torque-speed characteristics of an induction motor with delta controller

can be controlled by varying the triggering angle α Because of the symmetrical triggering of the thyristors, the machine voltages and currents have 3-phase symmetry but there will not be any half wave symmetry due to the presence of diodes in each branch Depending upon the hold off angle γ of phase current, the motor operation is classified into two distinct modes If γ is less than $2\pi/3$, the machine is subjected to three phase and single phase operation alternately Three devices - either two thyristors and one diode or two diodes and one thyristor - will be conducting when 3-phase operation takes place During single phasing only two devices - a thyristor and diode - conduct Accordingly this mode of operation is identified as 3/2 mode When the value of γ is greater than $2\pi/3$, the machine is subjected to single phasing and open circuiting alternately This mode of operation is denoted as 2/0 mode The method of steady state solution of motor variables for both modes of operation are exactly identical to that of the delta controller described in Section 3 1 Equations (3 1 - 3 3) are also applicable to the present case

3 3 1 Definition of Forcing Voltages

For the purpose of defining the forcing voltages, the current zero instant of a-phase is chosen as reference point The d-q voltages for both modes of operation are to be defined over a period of $2\pi/3$ to obtain the solution of system differetial equation (2 15a)

Mode 2/3 $0 < \gamma < 2\pi/3$

Referring to Fig 3 8, the d-q voltages can be readily defined as

a) Time period I, $0 < \omega t < \gamma$

$$v_{ds} = \text{back-emf} \tag{3 14}$$

$$v_{qs} = \sqrt{3/2}\, V_m \cos(\omega t + \phi) \tag{3 15}$$

b) Time period II, $\gamma < \omega t < 2\pi/3$

$$v_{ds} = \sqrt{3/2}\, V_m \sin(\omega t + \phi) \tag{3.16}$$

$$v_{qs} = \sqrt{3/2}\, V_m \cos(\omega t + \phi) \tag{3 17}$$

Mode 2/0 $\gamma > 2\pi/3$

The d-q voltages as given in Fig 3 9 are

a) Time period I, $0 < \omega t < (\gamma - 2\pi/3)$

$$v_{ds} = \sqrt{3/2}\, (\text{back-emf}_1) \tag{3 18}$$

$$v_{qs} = \sqrt{3/2}\, (\text{back-emf}_2) \tag{3,19}$$

b) Time period II, $(\gamma - 2\pi/3) < \omega t < 2\pi/3$

$$v_{ds} = \sqrt{3/2}\, (\text{back-emf}) \tag{3 20}$$

$$v_{qs} = \sqrt{3/2}\, V_m \cos(\omega t + \phi) \tag{3.21}$$

3 3 2 Steady State Simulation

The procedure to obtain the steady state waveforms of current, voltage and torque are exactly similar to that of a

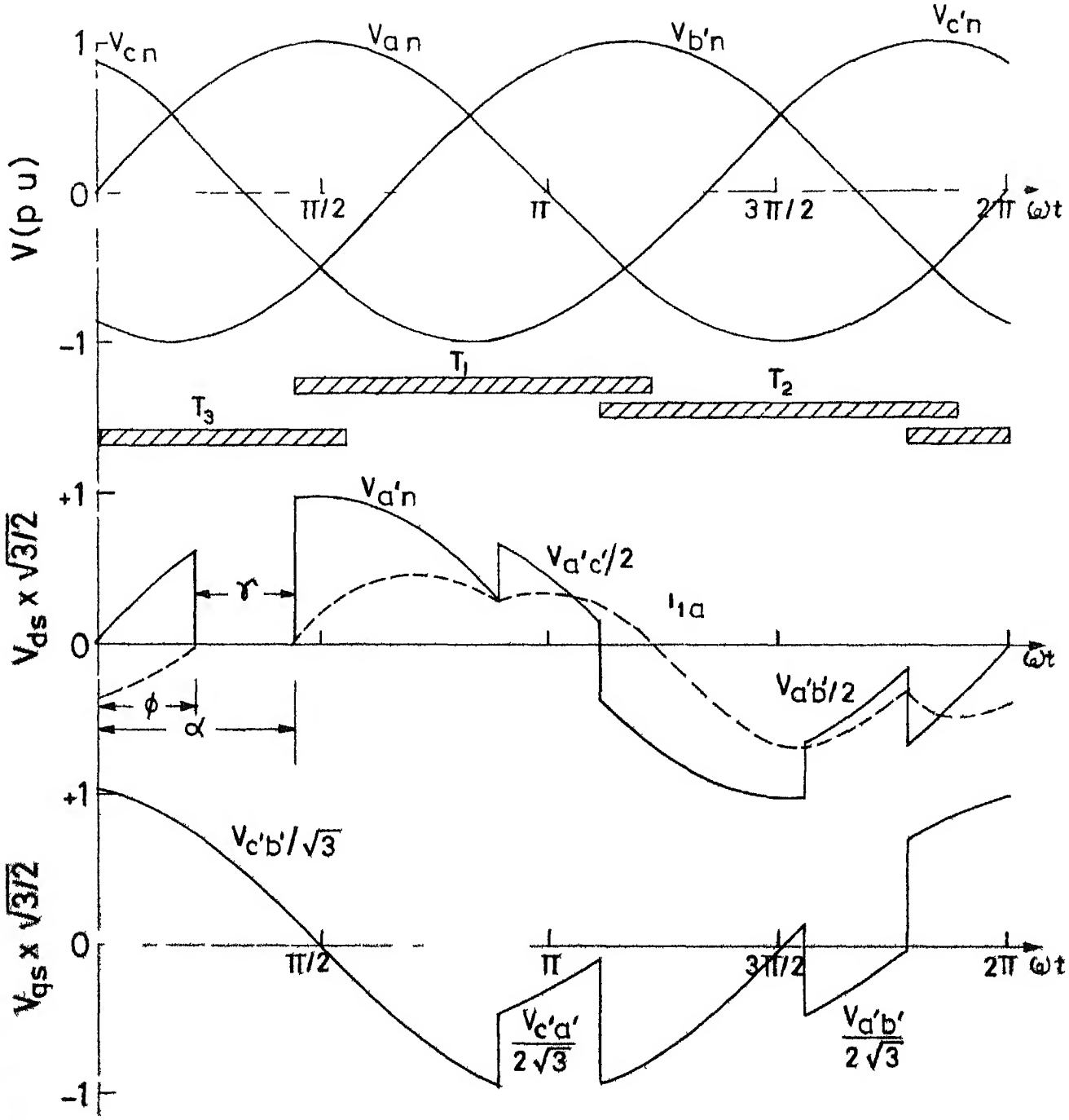

3 8 d-q voltages of a thyrode controlled induction motor during mode 2/3 (slip =1)

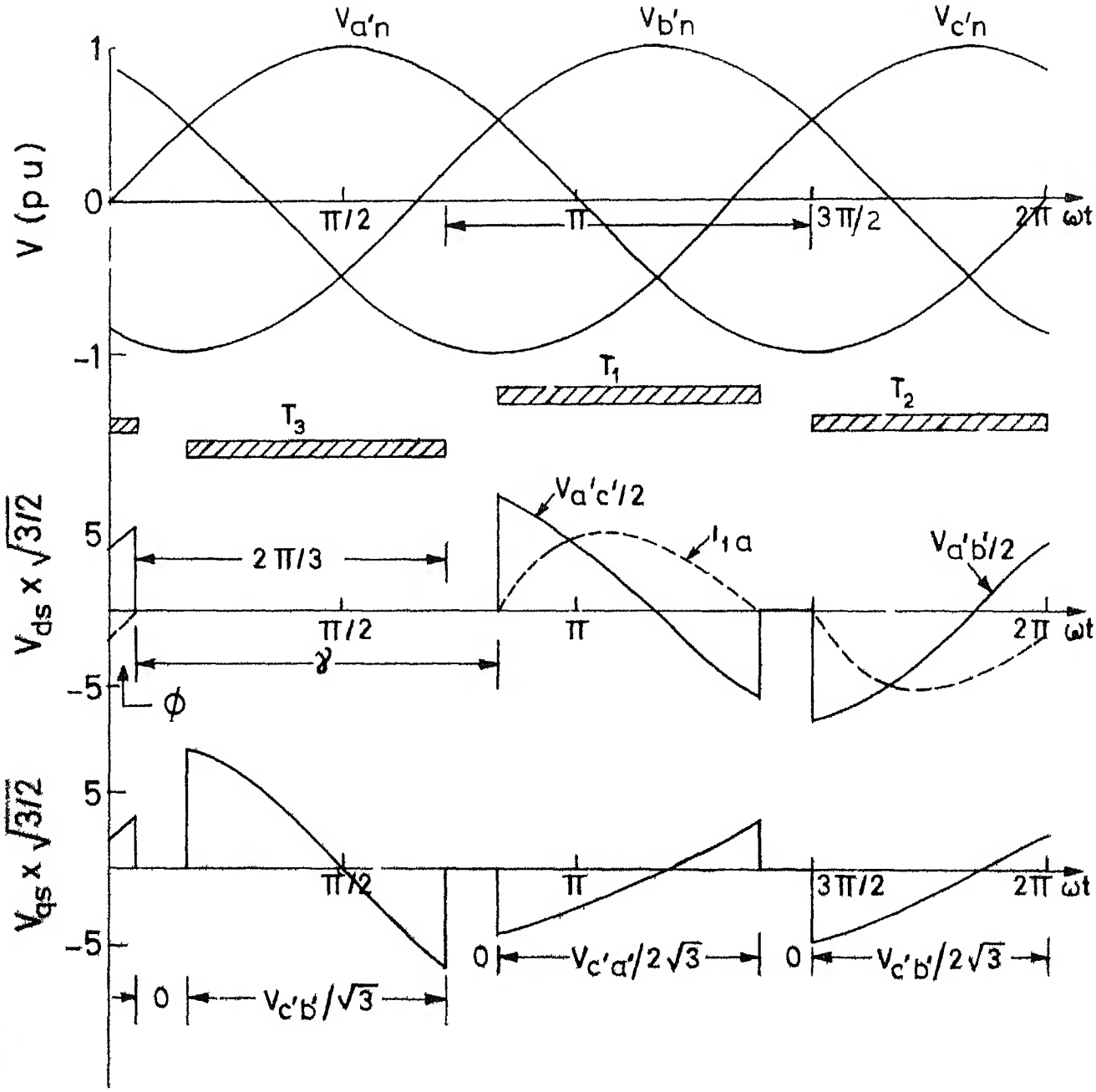

Fig 3 9 d-q voltages of thyrode controlled induction motor during 2/0 mode (slip=1)

delta controller described in Section 3 1 The forcing voltages needed for the solution of the system differential equation (2 15a) are given in equations (3 14 - 3 21)

3 3 3 Example

Steady state waveforms of phase current i_{1a} phase voltage v_{as} and electromagnetic torque obtained from the computer simulation are shown in Fig 3 10, for 2/3 mode of operation (γ = 40°, slip = 0 1) It can be observed from Fig 3 10 that there is no half-wave symmetry for the current and voltage waveforms The torque waveform has a predominant third harmonic component as in the case of the delta controller. Fig 3 11 shows the computed torque slip characteristics for constant values of γ

3 4 DISCUSSION

From the computed results, it can be seen that the torque in a delta and thyrode controlled machines has a predominant third harmonic component The third harmonic torque is produced by the second and fourth harmonic components of the stator current Although the shape of the current and the voltage waveforms (Figs 3 5 and 3 10) of the delta and thyrode controllers appears to be different, the r.m.s. current and average torque for a given slip and γ are exactly same for both cases This fact can be observed from Table 3 1

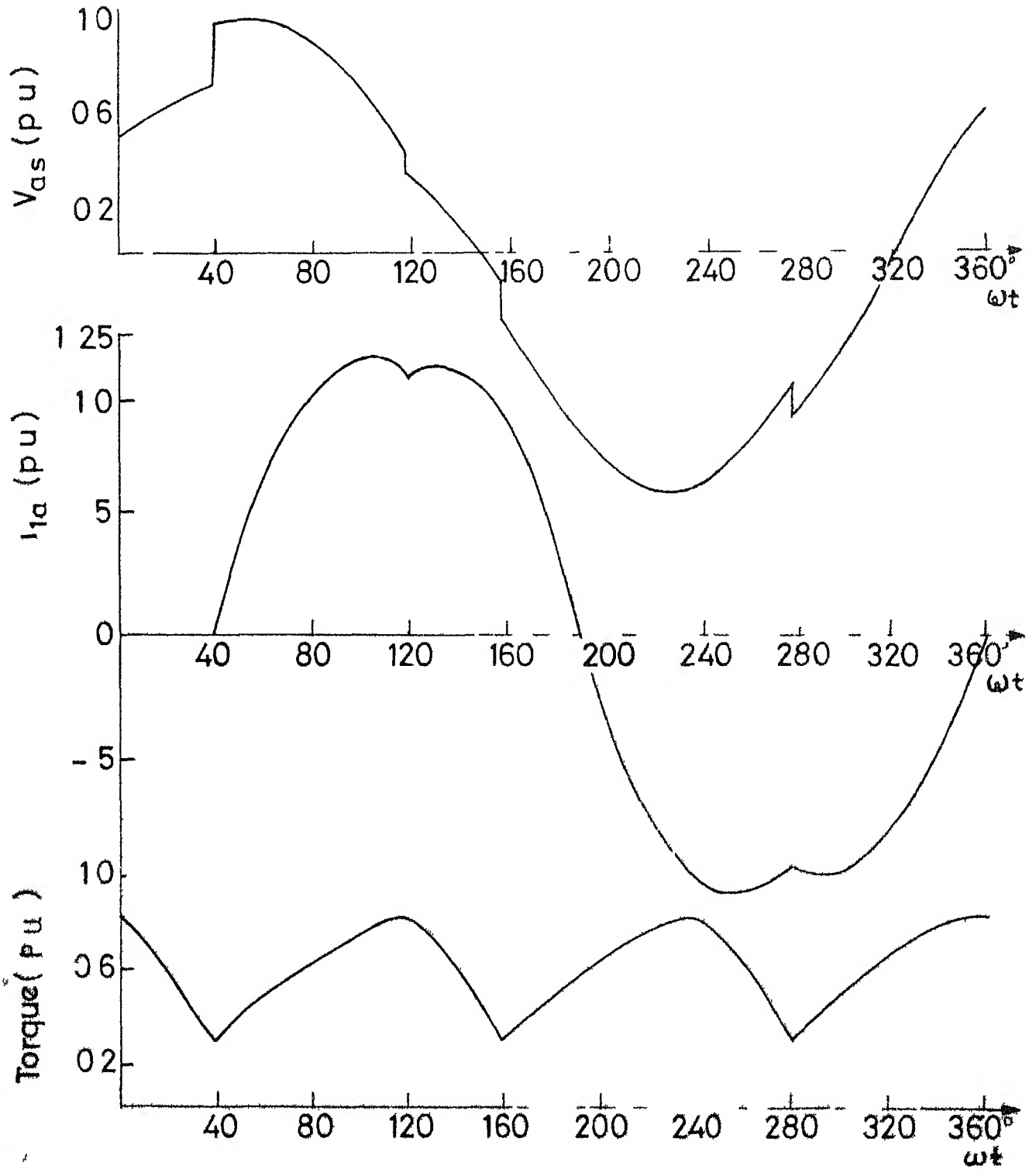

Fig 3 10 Computed results of a thyrode controlled motor (slip= 1, $\gamma = 40^{\circ}$)

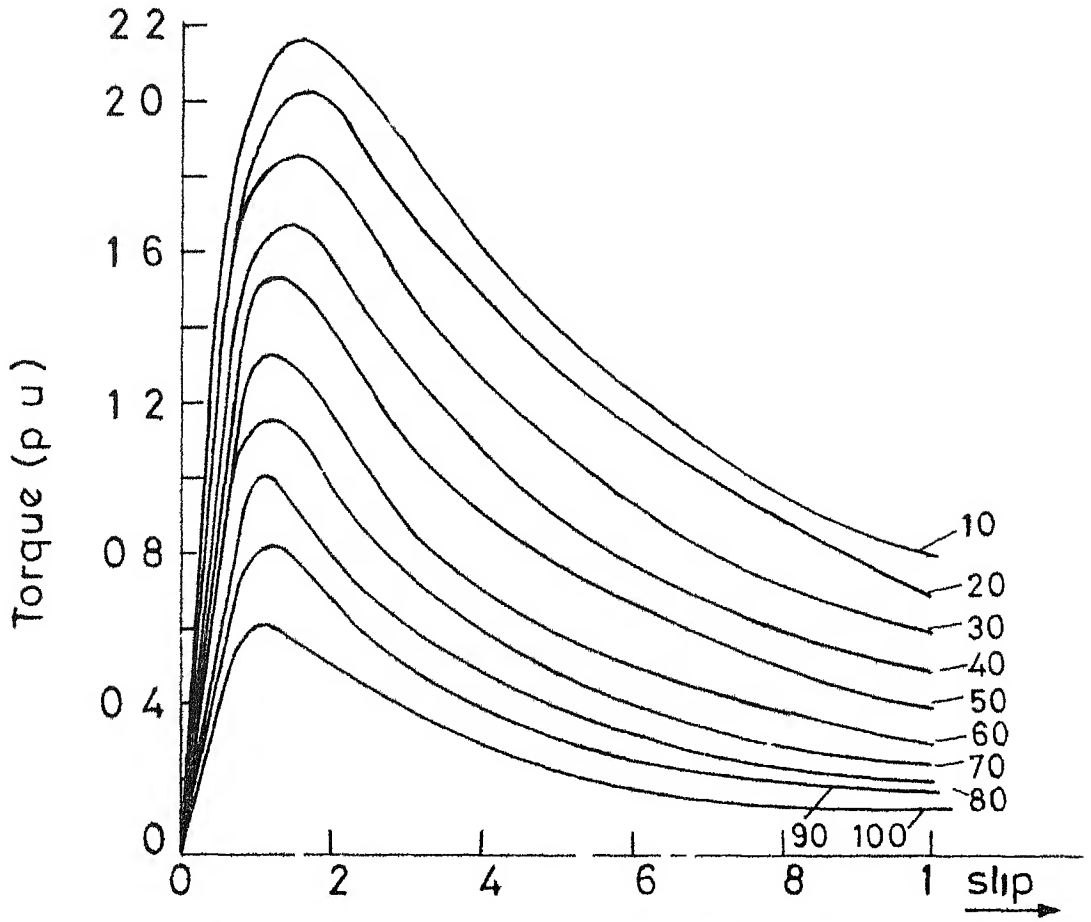

Fig 3 11 Torque-slip characteristics (thyrode controller)

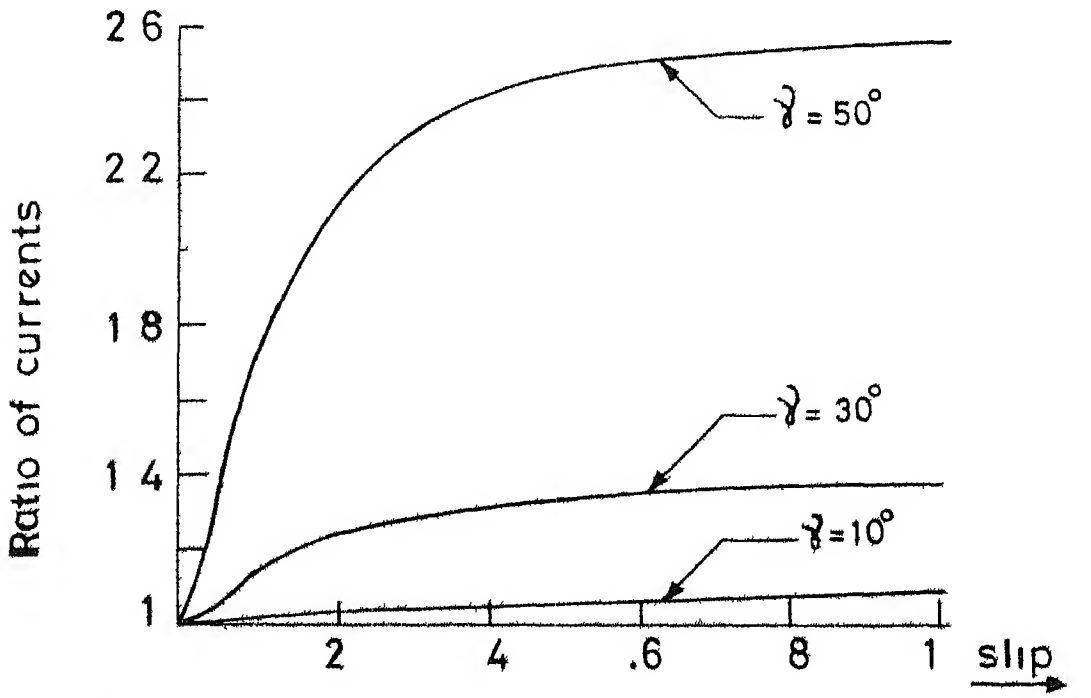

Fig 3 12 Ratio of motor currents for a delta (or tl rod·) and six-thyristor controller

TABLE 3 1

STEADY STATE SIMULATION RESULTS OF THYRODE AND DELTA CONTROLLERS

Sl No	γ	slip	Thyrode		Delta	
			$I_{r\,m\,s}$	T_{ave}	$I_{r\,m\,s}$	T_{ave}
1	10	0 05	1 587	1 483	1 587	1 483
2	10	0 10	2 387	2 032	2 387	2 032
3	10	0 20	3 371	2 140	3 371	2 140
4	10	0 30	3 858	1 900	3 858	1 900
5	10	0 40	4 140	1 640	4 140	1 640
6	30	0 05	1 550	1 310	1 550	1 310
7	30	0 10	2 250	1 780	2 250	1 780
8	30	0 20	3 090	1 760	3 090	1 760
9	30	0 30	3 490	1 490	3.490	1 490
10	30	0 40	3 715	1 260	3 715	1 260
11	50	0 05	1 467	1 100	1 467	1 10
12	50	0 10	2 110	1 449	2 110	1 449
13	50	0 20	2 838	1 338	2.838	1 338
14	50	0 30	3 091	1 086	3.091	1.086
15	50	0 40	3 227	0 893	3 227	0 893
16	70	0 05	1 376	0 917	1.376	0 917
17	70	0.10	1 997	1 087	1 997	1.087
18	70	0 20	2 510	0 937	2 510	0 937
19	70	0 30	2 694	0 743	2.694	0 743
20	70	0 40	2 790	0 600	2 790	0 600

(contd)

Sl No	γ	slip	Thyrode		Delta	
			I_{rms}	T_{ave}	I_{rms}	T_{ave}
21	90	0 05	1 379	0 724	1 379	0 724
22	90	0 10	1 817	0 790	1 817	0 790
23	90	0 20	2 280	0 680	2 280	0 680
24	90	0 30	2 359	0 507	2 359	0 507
25	90	0.40	2.386	0.392	2 386	0.392
26	110	0 05	1 354	0 550	1 354	0.550
27	110	0 10	1 696	0 649	1 696	0 649
28	110	0 20	1 978	0 508	1 978	0 508
29	110	0 30	2 060	0 351	2 060	1 351
30	110	0 40	2 130	0 284	2 130	0 284

The current and torque are in per unit

where the computed results are given for both controllers The torque-speed characteristics (Figs 3 7 and 3 11) for both controllers are also identical The forcing voltages defined in Sections 3 2 4 and 3 3 1 also indicate that the forcing voltages in both cases are the same except for a phase shift of 180° The motor is subjected to same duration of single-phase and three-phase operations for a given γ and slip and hence, both controllers should result in the same motor performance

Although there is some saving in terms of the thyristor cost, the current rating of the thyristors is higher than that of six thyristor scheme In addition, the motor is also subjected to higher heating in delta and thyrode controllers The ratio of the motor current (r m s) of the delta (or thyrode) controller to that of a six thyristor controller shown in Fig 3 12 clearly indicates that the current ratio increases with hold off angle γ The reason for the larger values of current in delta and thyrode controller is the presence of even harmonics in the motor current

3 5 CONCLUSION

BVA is extended to the analysis of two more cases of voltage controlled 3-phase induction motors in which different thyristor combinations are used In the first case, symmetrically triggered delta connected thyristors are used for the voltage control In the second case

thyristor-diode combination is used for the control In both cases the effective value of the motor voltage can be controlled over full range by varying the triggering angle Because of the symmetry of the system, a solution for the time period of a third of a cycle completely defines the motor operation It is observed from the computed results that performances of 3-phase induction motor controlled by symmetrically triggered delta connected thyristors and thyristor-diode combination are identical.

CHAPTER 4

DIGITAL SIMULATION OF THREE PHASE INDUCTION MOTORS USING HYBRID MODELS

4 1 INTRODUCTION

In this chapter two models of an induction motor, that are well suited for the transient and steady state analysis of three phase induction motors, under a wide range of terminal constraints, are given The major feature, of the models presented, is the development of an equivalent circuit for the stator or rotor windings, in which a dependent current source represents the coupling between the stator and the rotor This facilitates the formulation of the state equations for the motor with stator or rotor connected to any arbitrary network

One of the models presented is particularly suitable for stator controlled motors while the other is well suited for rotor controlled ones In the first model, the 3-phase rotor variables are transformed into equivalent 2-phase variables while the 3-phase stator variables are undisturbed This model gives the best approach [52] to the class of problems in which mixed terminal conditions exist In the second model, the stator variables are transformed into equivalent 2-phase variables and rotor variables are undisturbed so that any rotor terminal constraints can be directly

incorporated in the model Two examples are provided to illustrate the applicability of one of the models for wide range of terminal constraints.

4 2 DERIVATION OF THE MODELS

The following assumptions are made in setting up the machine equations

a) no magnetic saturation

b) uniform air-gap

c) negligible hysteresis and eddy current losses

d) sinusoidal distribution of air-gap flux

4 2 1 First Model With Equivalent Circuit for the Stator

The rotor is assumed to have two short circuited windings on $\alpha - \beta$ axes rotating at a speed of ω_r Referring to Fig 4 1 the stator and rotor voltages can be written as

$$\underline{v}_s = R_s \underline{i}_s + p \underline{\psi}_s \qquad (4\ 1)$$

$$\underline{v}_r = R_r \underline{i}_r + p \underline{\psi}_r \qquad (4.2)$$

where

$$R_s = \begin{bmatrix} R_1 & 0 & 0 \\ 0 & R_1 & 0 \\ 0 & 0 & R_1 \end{bmatrix}, \quad R_r = \begin{bmatrix} R_2 & 0 \\ 0 & R_2 \end{bmatrix}, \quad \underline{v}_s^T = [v_{as}\ v_{bs}\ v_{cs}],$$

$$\underline{v}_r^T = [0\ \ 0], \quad \underline{i}_s^T = [i_{1a}\ i_{1b}\ i_{1c}], \quad \underline{i}_r^T = [i_{2\alpha}\ i_{2\beta}],$$

$$\underline{\psi}_s^T = [\psi_{1a}\ \ \psi_{1b}\ \ \psi_{1c}] \text{ and } \quad \underline{\psi}_r^T = [\psi_{2\alpha}\ \psi_{2\beta}]$$

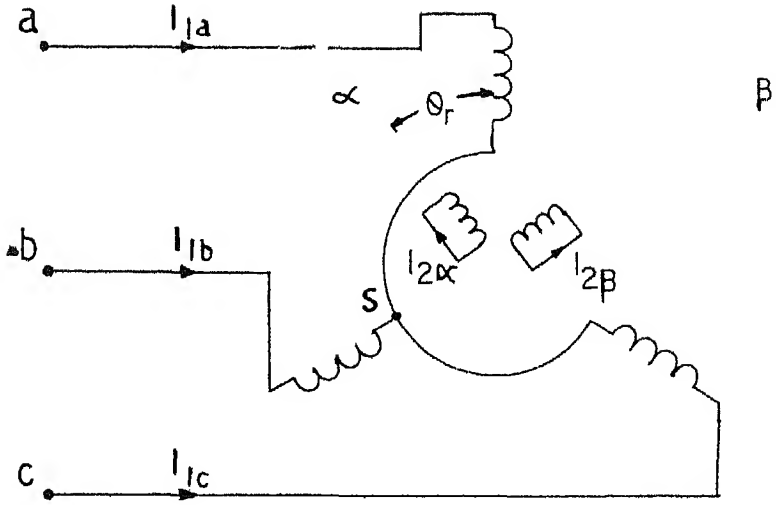

Fig 41 Schematic diagram of an induction motor with 3 phase stator and 2 phase rotor

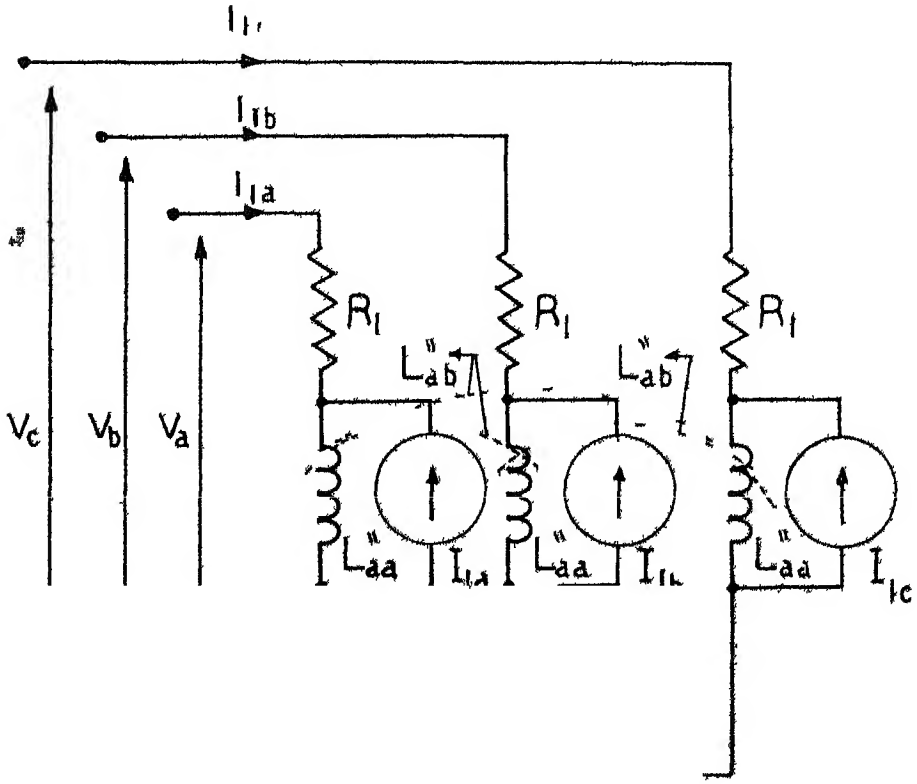

tator

The stator and rotor flux linkages are given by

$$\underline{\psi}_s = L_s \underline{i}_s + M \underline{i}_r \tag{4 3}$$

$$\underline{\psi}_r = L_r \underline{i}_r + M^T \underline{i}_s \tag{4 4}$$

where

$$L_s = \begin{bmatrix} L_1 & L_{11} & L_{11} \\ L_{11} & L_1 & L_{11} \\ L_{11} & L_{11} & L_1 \end{bmatrix}, \quad L_r = \begin{bmatrix} L_2 & 0 \\ 0 & L_2 \end{bmatrix},$$

and

$$M = L_{12} \begin{bmatrix} \cos\theta_r & \sin\theta_r \\ \cos(\theta_r - 2\pi/3) & \sin(\theta_r - 2\pi/3) \\ \cos(\theta_r + 2\pi/3) & \sin(\theta_r + 2\pi/3) \end{bmatrix}$$

From equation (4 4), $\underline{i}_r$ can be expressed as

$$\underline{i}_r = \{L_r^{-1} \underline{\psi}_r - L_r^{-1} M^T \underline{i}_s\} \tag{4 5}$$

Substituting equation (4,5) in (4 3), we get

$$\underline{\psi}_s = (L_s - M L_r^{-1} M^T) \underline{i}_s + M L_r^{-1} \underline{\psi}_r \tag{4.6}$$

Let

$$L_s'' = (L_s - M L_r^{-1} M^T) \tag{4 7}$$

$$\underline{I}_s = L_s''^{-1} M L_r^{-1} \psi_r \tag{4 8}$$

Then eqn (4 6) can be written as

$$\underline{\psi}_s = L''_s \, (\underline{\imath}_s + \underline{I}_s) \tag{4 9}$$

Equation (4 7) can be expanded as

$$L''_s = \begin{bmatrix} L''_{aa} & L''_{ab} & L''_{ab} \\ L''_{ab} & L''_{aa} & L''_{ab} \\ L''_{ab} & L''_{ab} & L''_{aa} \end{bmatrix} \tag{4 10}$$

where

$$L''_{aa} = L_1 - L_{12}^2/L_2, \quad L''_{ab} = L_{11} + L_{12}^2/(2L_2)$$

On expanding (4 8),

$$\underline{I}_s = I_\alpha \begin{bmatrix} \cos \theta_r \\ \cos(\theta_r - 2\pi/3) \\ \cos(\theta_r + 2\pi/3) \end{bmatrix} + I_\beta \begin{bmatrix} \sin \theta_r \\ \sin(\theta_r - 2\pi/3) \\ \sin(\theta_r + 2\pi/3) \end{bmatrix} \tag{4 11}$$

where

$$I_\alpha = \frac{L_{12}}{L_2 \, L''_1} \, \psi_{2\alpha}, \quad I_\beta = \frac{L_{12}}{L_2 \, L''_1} \, \psi_{2\beta}, \quad L''_1 = L''_{aa} - L''_{ab}$$

The stator voltage equation (4 1) can be rewritten as

$$\underline{v}_s = R_s \, \underline{\imath}_s + L''_s \, p(\underline{\imath}_s + \underline{I}_s) \tag{4.12}$$

Equation (4 12) can be represented by means of an equivalent circuit (Fig 4 2), which will be useful for the formulation of the state equations for any stator terminal constraints

Combining eqns (4 2) and (4 5), we get

$$p\,\underline{\psi}_r = -R_r(L_r^{-1}\,\underline{\psi}_r - L_r^{-1}\,M^T\,\underline{i}_s) \qquad (4\ 13)$$

On expanding,

$$p\begin{bmatrix}\psi_{2\alpha}\\ \psi_{2\beta}\end{bmatrix} = -\frac{R_2}{L_2}\begin{bmatrix}\psi_{2\alpha}\\ \psi_{2\beta}\end{bmatrix} + \frac{R_2L_{12}}{L_2}\begin{bmatrix}\cos\theta_r & \cos(\theta_r-2\pi/3) & \cos(\theta_r+2\pi/3)\\ \sin\theta_r & \sin(\theta_r-2\pi/3) & \sin(\theta_r+2\pi/3)\end{bmatrix}\begin{bmatrix}i_{1a}\\ i_{1b}\\ i_{1c}\end{bmatrix} \qquad (4\ 14)$$

While equation (4 14) can be directly used for digital simulation, it will be advantageous if the rotor flux linkages in eqns (4 11) and (4 14) are transformed into d-q variables (referred to a synchronously rotating reference frame) so that the transformed variables become constants during steady state operation with sinusoidal excitation Even for non-sinusoidal excitation such as due to the operation with periodic switching of supply, it can be shown that the rotor flux linkages ψ_{2d} and ψ_{2q} (in the synchronously revolving frame) are practically constants in steady state (at constant speed) operation

The transformation to d-q axis is defined by

$$\begin{bmatrix}\psi_{2\alpha}\\ \psi_{2\beta}\end{bmatrix} = \begin{bmatrix}\cos(\theta_o-\theta_r) & \sin(\theta_o-\theta_r)\\ -\sin(\theta_o-\theta_r) & \cos(\theta_o-\theta_r)\end{bmatrix}\begin{bmatrix}\psi_{2d}\\ \psi_{2q}\end{bmatrix} \qquad (4\ 15)$$

In terms of the d-q variables, equation (4 11) becomes

$$\underline{I}_s = I_1 \begin{bmatrix} \cos\theta_o \\ \cos(\theta_o - 2\pi/3) \\ \cos(\theta_o + 2\pi/3) \end{bmatrix} + I_2 \begin{bmatrix} \sin\theta_o \\ \sin(\theta_o - 2\pi/3) \\ \sin(\theta_o + 2\pi/3) \end{bmatrix} \qquad (4\ 16)$$

where

$$I_1 = \frac{L_{12}}{L_2 L_1''} \psi_{2d}\ , \qquad I_2 = \frac{L_{12}}{L_2 L_1''} \psi_{2q}$$

Using (4 15), eqn (4 14) can be transformed as

$$p \begin{bmatrix} \psi_{2d} \\ \psi_{2q} \end{bmatrix} = \begin{bmatrix} -R_2/L_2 & -S\omega \\ S\omega & -R_2/L_2 \end{bmatrix} \begin{bmatrix} \psi_{2d} \\ \psi_{2q} \end{bmatrix} + \sqrt{\frac{3}{2}} \frac{R_2 L_{12}}{L_2} \begin{bmatrix} i_{1d} \\ i_{1q} \end{bmatrix} \qquad (4.17)$$

where

$$\begin{bmatrix} i_{1d} \\ i_{1q} \end{bmatrix} = \sqrt{2/3} \begin{bmatrix} \cos\theta_o & \cos(\theta_o - 2\pi/3) & \cos(\theta_o + 2\pi/3) \\ \sin\theta_o & \sin(\theta_o - 2\pi/3) & \sin(\theta_o + 2\pi/3) \end{bmatrix} \begin{bmatrix} i_{1a} \\ i_{1b} \\ i_{1c} \end{bmatrix} \qquad (4.18)$$

Equation (4 17) represents the rotor flux linkage equation for any type of stator terminal conditions The instantaneous torque (as derived in Appendix C) and speed equations are given by

$$T_e = \sqrt{3/2}\ \frac{L_{12}}{L_2} (i_{1d}\ \psi_{2q} - i_{1q}\ \psi_{2d}) \qquad (4\ 19)$$

and

$$pS = -\frac{(T_e - T_m)}{\omega J} + \frac{(1-S)\ D}{J} \qquad (4\ 20)$$

Equations(4 12), (4 17), (4 19) and (4 20) completely describe the induction machine under dynamic conditions

The equivalent circuit (Fig 4.2) representing a general induction machine can be further simplified if the stator windings of the motor are wye connected with isolated neutral Since the sum of the stator currents and their derivatives are zero at any instant of time and by virtue of eqn (4 16), the stator voltage eqn (4 12) can be rewritten as

$$\begin{bmatrix} v_{as} \\ v_{bs} \\ v_{cs} \end{bmatrix} = R_1 \begin{bmatrix} i_{1a} \\ i_{1b} \\ i_{1c} \end{bmatrix} + L_1'' \, p \begin{bmatrix} i_{1a} + I_{1a} \\ i_{1b} + I_{1b} \\ i_{1c} + I_{1c} \end{bmatrix} \qquad (4\ 21)$$

The equation (4 21) is represented by means of an equivalent circuit (Fig 4 3) in which there is no mutual coupling between the stator windings In Appendix D, the relationship between the parameters of conventional passive equivalent circuit and those of the active equivalent circuits (Figs 4 2 and 4 3) are given

4 2 2 Second Model with Equivalent Circuit for the Rotor

In this model, the rotor variables are undisturbed while the stator variables, are first transformed into α- β variables Referring to Fig 4.4, the machine equations are

$$\underline{v}'_s = R'_s \, \underline{i}'_s + p \, \underline{\psi}'_s \qquad (4\ 22)$$

$$\underline{v}'_r = R'_r \, \underline{i}'_r + p \, \underline{\psi}'_r \qquad (4\ 23)$$

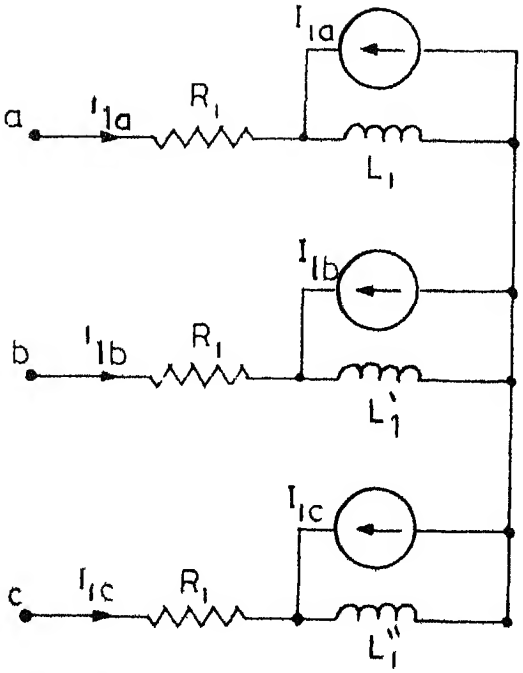

Fig 4 3 Circuit model of a wye-connected stator

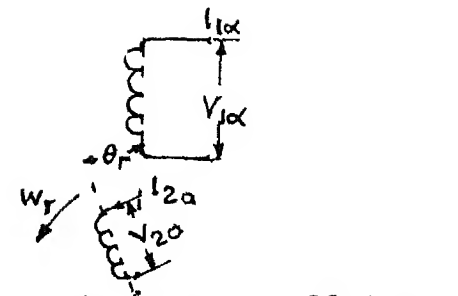

Fig 4 4 Schematic diagram of an induction motor with 2 phase stator and 3 phase rotor

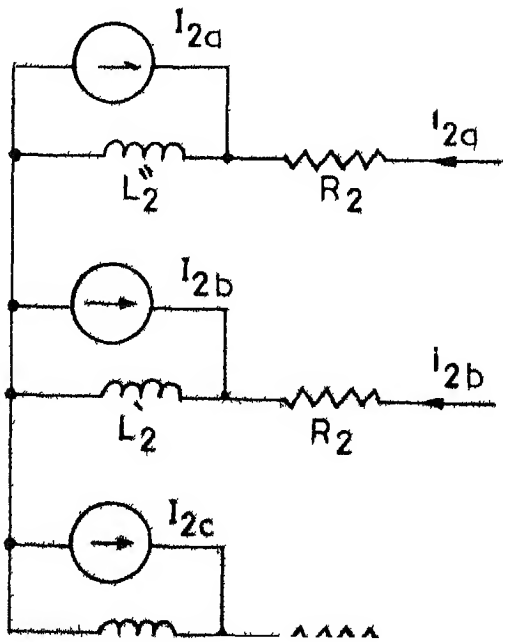

where

$$\underline{v}_s'^T = [v_{1\alpha} \quad v_{1\beta}], \quad \underline{v}_r'^T = [v_{2a} \quad v_{2b} \quad v_{2c}], \quad \underline{i}_s'^T = [i_{1\alpha} \; i_{1\beta}]$$

$$\underline{i}_r'^T = [i_{2a} \quad i_{2b} \quad i_{2c}], \quad \underline{\psi}_s'^T = [\psi_{1\alpha} \; \psi_{1\beta}], \quad \underline{\psi}_r'^T = [\psi_{2a} \; \psi_{2b} \; \psi_{2c}]$$

$$R_r' = \begin{bmatrix} R_2' & 0 & 0 \\ 0 & R_2' & 0 \\ 0 & 0 & R_2' \end{bmatrix}, \quad R_s' = \begin{bmatrix} R_1' & 0 \\ 0 & R_1' \end{bmatrix}$$

The relationship between 3-phase voltages and $\alpha - \beta$ voltages is given by

$$\begin{bmatrix} v_{as} \\ v_{bs} \\ v_{os} \end{bmatrix} = \begin{bmatrix} \sqrt{2/3} & 0 & 1/\sqrt{3} \\ -1/\sqrt{6} & -1/\sqrt{2} & 1/\sqrt{3} \\ -1/\sqrt{6} & 1/\sqrt{2} & 1/\sqrt{3} \end{bmatrix} \begin{bmatrix} v_{1\alpha} \\ v_{1\beta} \\ v_{1o} \end{bmatrix} \qquad (4\ 24)$$

$\underline{\psi}_s'$ and $\underline{\psi}_r'$ are defined by

$$\underline{\psi}_s' = L_s' \underline{i}_s' + M'^T \underline{i}_r' \qquad (4.25)$$

$$\underline{\psi}_r' = L_r' \underline{i}_r' + M' \underline{i}_s' \qquad (4\ 26)$$

where

$$L_s' = \begin{bmatrix} L_1' & 0 \\ 0 & L_1' \end{bmatrix}, \quad L_r' = \begin{bmatrix} L_2' & L_{22}' & L_{22}' \\ L_{22}' & L_2' & L_{22}' \\ L_{22}' & L_{22}' & L_2' \end{bmatrix}$$

$$M'^T = L_{12}' \begin{bmatrix} \cos\theta_r & \cos(\theta_r+2\pi/3) & \cos(\theta_r-2\pi/3) \\ -\sin\theta_r & -\sin(\theta_r+2\pi/3) & -\sin(\theta_r-2\pi/3) \end{bmatrix}$$

From equation (4 25), the stator current $\underline{\imath}'_s$ can be expressed as

$$\underline{\imath}'_s = \{ L'^{*1}_s \, \underline{\psi}'_s - L'^{-1}_s \, M'^{T} \, \underline{\imath}'_r \} \qquad (4\ 27)$$

Eliminating $\underline{\imath}'_s$ from equation (4 26) using (4 27)

$$\underline{\psi}'_r = (L'_r - M' \, L'^{-1}_s \, M'^{T}) \, \underline{\imath}'_r + M' \, L'^{-1}_s \, \underline{\psi}'_s \qquad (4\ 28)$$

$$= L''_r(\underline{\imath}'_r + \underline{I}'_r) \qquad (4\ 28)$$

where

$$L''_r = L'_r - M' \, L'^{-1}_s \, M'^{T} \qquad (4\ 29)$$

$$\underline{I}'_r = L''^{-1}_r \, M' \, L'^{-1}_s \, \underline{\psi}'_s \qquad (4\ 30)$$

The rotor voltage equation (4 23) can be rewritten as

$$\underline{v}'_r = P_r \, \underline{\imath}'_r + L''_r \, p \, (\underline{\imath}'_r + \underline{I}'_r) \qquad (4\ 31)$$

L''_r is a constant matrix given by

$$L''_r = \begin{bmatrix} L'_2 & L'_{22} & L'_{22} \\ L'_{22} & L'_2 & L'_{22} \\ L'_{22} & L'_{22} & L'_2 \end{bmatrix} - \frac{L'^2_{12}}{L'_1} \begin{bmatrix} 1 & -5 & -5 \\ -5 & 1 & -5 \\ -5 & -5 & 1 \end{bmatrix}$$

The stator flux linkage equation in terms of the rotor currents $\underline{\imath}'_r$ can be obtained from equations (4 22) and (4 27) as

$$p \, \underline{\psi}'_s = \underline{v}'_s - R'_s \, L'^{-1}_s \, \underline{\psi}'_s + R'_s \, L'^{-1}_s \, M'^{T} \, \underline{\imath}'_r \qquad (4\ 32)$$

After transforming the α - β components to d-q components using the relationship

$$\begin{bmatrix} \psi_{1\alpha} \\ \psi_{1\beta} \end{bmatrix} = \begin{bmatrix} \cos\theta_o & \sin\theta_o \\ -\sin\theta_o & \cos\theta_o \end{bmatrix} \begin{bmatrix} \psi_{1d} \\ \psi_{1q} \end{bmatrix} \tag{4.33}$$

We obtain

$$\underline{I}'_r = I'_1 \begin{bmatrix} \cos(\theta_o-\theta_r) \\ \cos(\theta_o-\theta_r-2\pi/3) \\ \cos(\theta_o-\theta_r+2\pi/3) \end{bmatrix} + I'_2 \begin{bmatrix} \sin(\theta_o-\theta_r) \\ \sin(\theta_o-\theta_r-2\pi/3) \\ \sin(\theta_o-\theta_r+2\pi/3) \end{bmatrix} \tag{4 34}$$

and

$$p \begin{bmatrix} \psi_{1d} \\ \psi_{1q} \end{bmatrix} = \begin{bmatrix} v_{1d} \\ v_{1q} \end{bmatrix} - \begin{bmatrix} R'_1/L'_1 & \omega \\ -\omega & R'_1/L'_1 \end{bmatrix} \begin{bmatrix} \psi_{1d} \\ \psi_{1q} \end{bmatrix} + \sqrt{\frac{3}{2}} \frac{R'_1 L'_{12}}{L'_1} \begin{bmatrix} i_{2d} \\ i_{2q} \end{bmatrix} \tag{4 35}$$

where

$$I'_1 = \frac{L'_{12}}{L'_1 L''_2} \psi_{1d} \quad , \quad I'_2 = \frac{L'_{12}}{L'_1 L''_2} \psi_{1q} \quad ,$$

$$L''_2 = L'_2 - L'_{22} - 3/2 \frac{L'^2_{12}}{L'_1} \quad ,$$

$$\begin{bmatrix} i_{2d} \\ i_{2q} \end{bmatrix} = \sqrt{2/3} \begin{bmatrix} \cos(\theta_o-\theta_r) & \cos(\theta_o-\theta_r-2\pi/3) & \cos(\theta_o-\theta_r+2\pi/3) \\ \sin(\theta_o-\theta_r) & \sin(\theta_o-\theta_r-2\pi/3) & \sin(\theta_o-\theta_r+2\pi/3) \end{bmatrix} \begin{bmatrix} i_{2a} \\ i_{2b} \\ i_{2c} \end{bmatrix}$$

and

$$\begin{bmatrix} v_{1d} \\ v_{1q} \end{bmatrix} = \sqrt{2/3} \begin{bmatrix} \cos\theta_o & \cos(\theta_o-2\pi/3) & \cos(\theta_o+2\pi/3) \\ \sin\theta_o & \sin(\theta_o-2\pi/3) & \sin(\theta_o+2\pi/3) \end{bmatrix} \begin{bmatrix} v_{as} \\ v_{bs} \\ v_{cs} \end{bmatrix}$$

For a wye-connected rotor winding with isolated neutral, the rotor voltage equation (4 31) becomes

$$\begin{bmatrix} v_{2a} \\ v_{2b} \\ v_{2c} \end{bmatrix} = R'_2 \begin{bmatrix} i_{2a} \\ i_{2b} \\ i_{2c} \end{bmatrix} + L''_2 \, p \begin{bmatrix} i_{2a} + I_{2a} \\ i_{2b} + I_{2b} \\ i_{2c} + I_{2c} \end{bmatrix} \qquad (4\ 36)$$

Equation (4 36) is represented by an equivalent circuit (Fig 4 5) where I_{2a}, I_{2b} and I_{2c} are dependent current sources which are functions of stator flux linkages ψ_{1d} and ψ_{1q} The instantaneous torque (as derived in Appendix E) and the speed equations are

$$T_e = \sqrt{3/2} \, \frac{L'_{12}}{L'_1} \, (i_{2q} \, \psi_{1d} - i_{2d} \, \psi_{1q}) \qquad (4\ 37)$$

$$pS = - \frac{(T_e - T_m)}{\omega J} + \frac{(1-S)\ D}{J} \qquad (4\ 38)$$

4 3 EXAMPLES OF STATOR CONTROLLED MOTORS

4 3 1 Example 1 Digital Simulation of a Wye-Connected Induction Motor

The schematic diagram shown in Fig 2 1 (Chapter 2) is considered for digital simulation The terminal voltage of the motor is varied by symmetrically triggered, back-to-back connected thyristor pairs in each line For dynamic and steady state analysis of such a system, the different possible modes of operation are

1) the 3-phase source is directly connected to the motor terminals allowing currents in all the three lines
2) line a'a is open while other two lines carry currents
3) line b'b is open while lines a'a and c'c carry currents
4) line c'c is open while lines a'a and b'b carry currents
5) currents in all the three lines are zero

This mode of operation will occur only when not more than one thyristor is in conducting mode

4 3 1 1 Formulation

The objective is to obtain a set of equations corresponding to each mode of operation from network analysis For a particular case when the supply is assumed to be a voltage source in series with an inductance, the network on the stator side is shown in Fig 4 6(a) Here it is assumed that the thyristors in all phases are conducting

There are three possible meshes for the network shown in Fig 4 6(a) although for a given mode, not more than two mesh currents are independent The equations for each mode would be given in terms of mesh currents For each of the five modes of operation, the state equation can be formulated as follows

Mode-1

Let i_1 and i_2 be the independent mesh currents The mesh equations in matrix form are given by

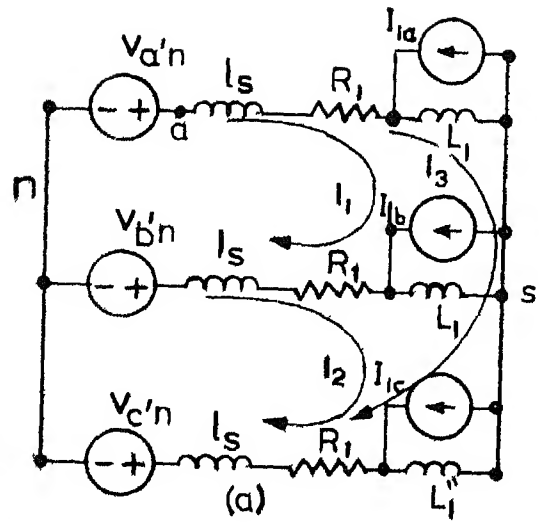

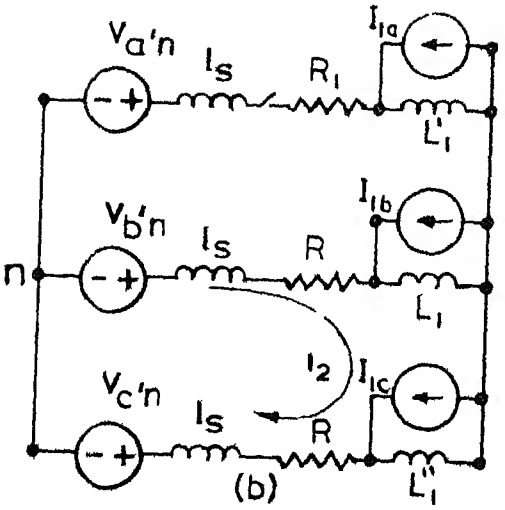

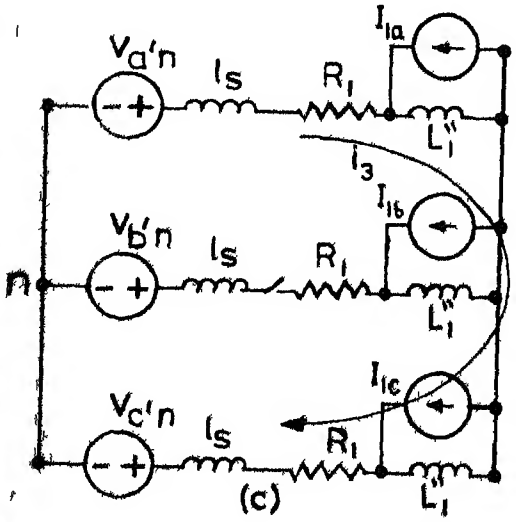

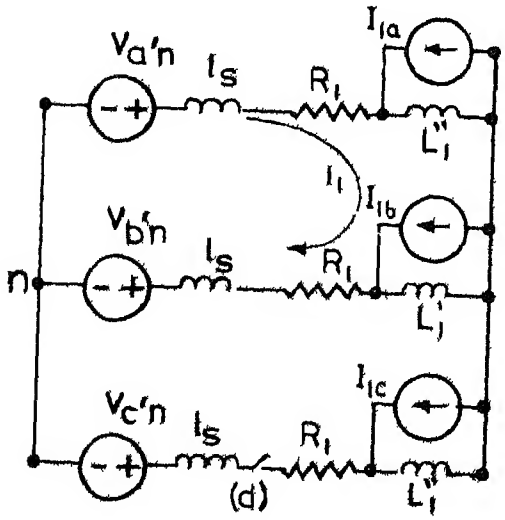

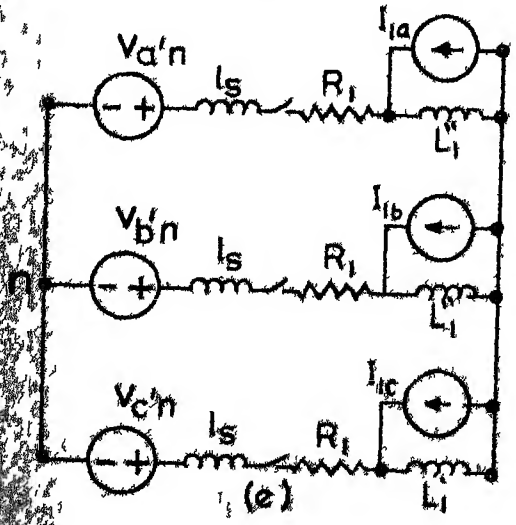

Fig 4 6 Various modes of operation

(a) mode 1 All the phases conducting
(b) " 2 Phase a non-conducting
(c) " 3 Phase b non-conducting
(d) " 4 Phase c non-conducting
(e) " 5 None of the phases conducting

$$\begin{bmatrix} v_{a'n} - v_{b'n} \\ v_{b'n} - v_{c'n} \end{bmatrix} = \begin{bmatrix} 2(l_s+L_1'') & -(l_s+L_1'') \\ -(l_s+L_1'') & 2(l_s+L_1'') \end{bmatrix} p \begin{bmatrix} i_1 \\ i_2 \end{bmatrix} + \begin{bmatrix} 2R_1 & -R_1 \\ -R_1 & 2R_1 \end{bmatrix} \begin{bmatrix} i_1 \\ i_2 \end{bmatrix} + \begin{bmatrix} L_1'' & -L_1'' \\ L_1'' & 2L_1'' \end{bmatrix} p \begin{bmatrix} I_{1a} \\ I_{1b} \end{bmatrix} \quad (4\ 39)$$

Equation (4 39) can be simplified to

$$(l_s+L_1'')\ p \begin{bmatrix} i_1 \\ i_2 \end{bmatrix} = -R_1 \begin{bmatrix} i_1 \\ i_2 \end{bmatrix} - L_1'' \begin{bmatrix} 1 & 0 \\ 1 & 1 \end{bmatrix} p \begin{bmatrix} I_{1a} \\ I_{1b} \end{bmatrix} + \begin{bmatrix} v_{a'n} \\ -v_{c'n} \end{bmatrix} \quad (4\ 40)$$

Equations (4.39) and (4 40) are obtained using the relations $v_{a'n} + v_{b'n} + v_{c'n} = 0$ and $I_{1a} + I_{1b} + I_{1c} = 0$ The relationship between the phase currents and mesh currents are

$$\begin{bmatrix} i_{1a} \\ i_{1b} \\ i_{1c} \end{bmatrix} = \begin{bmatrix} 1 & 0 & 0 \\ -1 & 1 & 0 \\ 0 & -1 & 0 \end{bmatrix} \begin{bmatrix} i_1 \\ i_2 \\ i_3 \end{bmatrix} \quad (4\ 41)$$

where i_3 is the third mesh current which is not considered in this mode of operation

Mode-2

When the stator current i_{1a} becomes zero, the thyristor in a-phase enters the blocking state During this mode, back-emf will appear across the a-phase winding due to induced rotor currents From the equivalent circuit (Fig 4.6(b)),

the expression for the back-emf is

$$v_{a(\text{back-emf})} = L_1' \, p \, I_{1a} \qquad (4\ 42)$$

and the state equation is

$$pi_2 = \frac{1}{2(l_s+L_1'')} \left(-2R_1 i_2 - L_1'' p(I_{1b}-I_{1c}) + v_{b'n} - v_{c'n}\right) \qquad (4\ 43)$$

The phase currents are

$$\begin{bmatrix} i_{1a} \\ i_{1b} \\ i_{1c} \end{bmatrix} = \begin{bmatrix} 0 & 0 & 0 \\ 0 & 1 & 0 \\ 0 & -1 & 0 \end{bmatrix} \begin{bmatrix} i_1 \\ i_2 \\ i_3 \end{bmatrix} \qquad (4\ 44)$$

Mode-3

From the equivalent circuit (Fig 4 6(c)), the state equation for this mode of operation is

$$pi_3 = \frac{1}{2(l_s+L_1'')} \left(-2R_1 i_3 - L_1'' p(I_{1a}-I_{1c}) + v_{a'n} - v_{c'n}\right) \qquad (4\ 45)$$

The stator phase currents are

$$\begin{bmatrix} i_{1a} \\ i_{1b} \\ i_{1c} \end{bmatrix} = \begin{bmatrix} 0 & 0 & 1 \\ 0 & 0 & 0 \\ 0 & 0 & -1 \end{bmatrix} \begin{bmatrix} i_1 \\ i_2 \\ i_3 \end{bmatrix} \qquad (4\ 46)$$

Mode-4

This mode of operation is identical to those of 2 and 3 except that the phase c is open-circuited. The state equation

and the stator currents are (ref Fig 4 6d)

$$pi_1 = \frac{1}{2(l_s+L_1'')} (-2R_1 i_1 - L_1'' p(I_{1a}-I_{1b}) + v_{a'n} - v_{b'n} \qquad (4\ 48)$$

$$\begin{bmatrix} i_{1a} \\ i_{1b} \\ i_{1c} \end{bmatrix} = \begin{bmatrix} 1 & 0 & 0 \\ -1 & 0 & 0 \\ 0 & 0 & 0 \end{bmatrix} \begin{bmatrix} i_1 \\ i_2 \\ i_3 \end{bmatrix} \qquad (4\ 49)$$

Mode-5

None of the stator windings carry current during this mode of operation but back-emf may appear across the stator windings due to the presence of rotor currents Referring to Fig 4 6e

$$i_{1a} = i_{1b} = i_{1c} = 0 \qquad (4\ 50)$$

$$\begin{aligned} v_{a(\text{back-emf})} &= L_1'' \ p \ I_{1a} \\ v_{b(\text{back-emf})} &= L_1'' \ p \ I_{1b} \\ v_{c(\text{back-emf})} &= L_1'' \ p \ I_{1c} \end{aligned} \qquad (4\ 51)$$

4 3 1 2 Simulation and results

The rotor flux linkages ψ_{2d} and ψ_{2q}, slip S and the mesh currents i_1, i_2 and i_3 are chosen as state variables The state equation defining ψ_{2d}, ψ_{2q} and S are derived in equations(4 17) and (4 20) The state equations of mesh currents consist of terms with derivatives of dependent current sources which can be obtained from equation (4 16) as

$$pI_{1a} = \frac{L_{12}}{L_2 L_1''} \{\cos\theta_o \; p\,\psi_{2d} + \sin\theta_o \; p\,\psi_{2q} + \omega(\cos\theta_o\,\psi_{2q} - \sin\theta_o\,\psi_{2d})\} \tag{4.52}$$

$$pI_{1b} = \frac{L_{12}}{L_2 L_1''} \{\cos(\theta_o - 2\pi/3) \; p\,\psi_{2d} + \sin(\theta_o - 2\pi/3) \; p\,\psi_{2q} + \omega(\cos(\theta_o - 2\pi/3)\,\psi_{2q} - \sin(\theta_o - 2\pi/3)\,\psi_{2d})\} \tag{4 53}$$

and

$$pI_{1c} = \frac{L_{12}}{L_2 L_1''} \{\cos(\theta_o + 2\pi/3) \; p\,\psi_{2d} + \sin(\theta_o + 2\pi/3) \; p\,\psi_{2q} + \omega(\cos(\theta_o + 2\pi/3)\,\psi_{2q} - \sin(\theta_o + 2\pi/3)\,\psi_{2q})\} \tag{4 54}$$

The state equations for the stator which depend upon the particular mode of operation, are solved simultaneously along with the rotor flux linkage equations (4 17) and speed equation (4 20) on a digital computer using fourth order Runge-Kutta method for a chosen triggering angle α and load torque T_m A step size of 0 00025 sec is chosen for computation Linear interpolation is used to obtain instants for the current zero and its detection of change of mode initiated by the blocking of a thyristor Results of the simulation are shown in Figs 4 7 to 4 11 Transient starting torque for $\alpha = 80°$ with zero load torque is shown in Fig 4 7 Figure 4 8 shows the starting characteristics (speed versus time) for different triggering angles where the high frequency oscillations at the starting period are not shown It can be observed from Figs 4 7 and 4 8 that the motor speed exceeds the synchronous speed momentarily and settles down to the

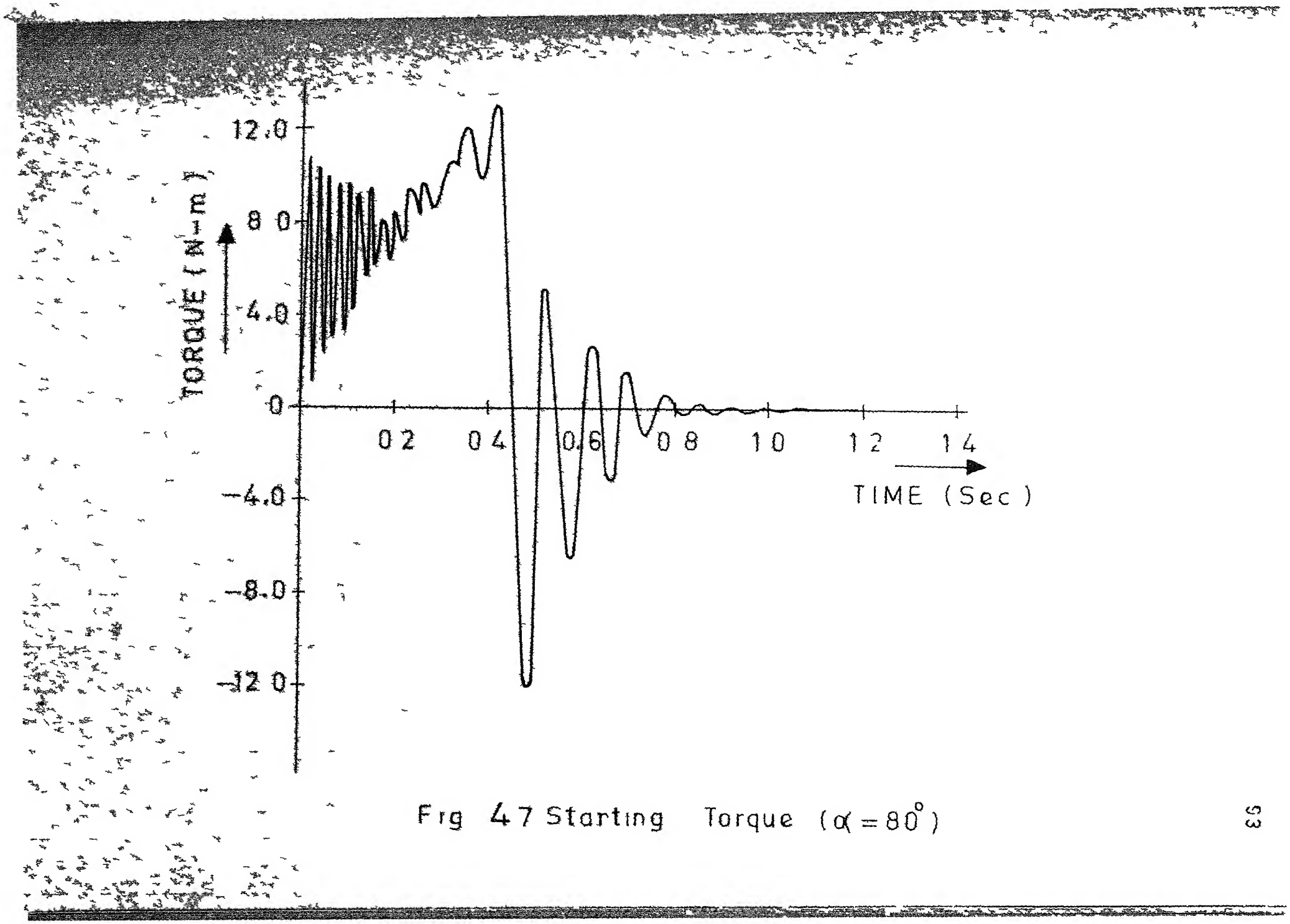

Frg 47 Starting Torque ($\alpha = 80^{\circ}$)

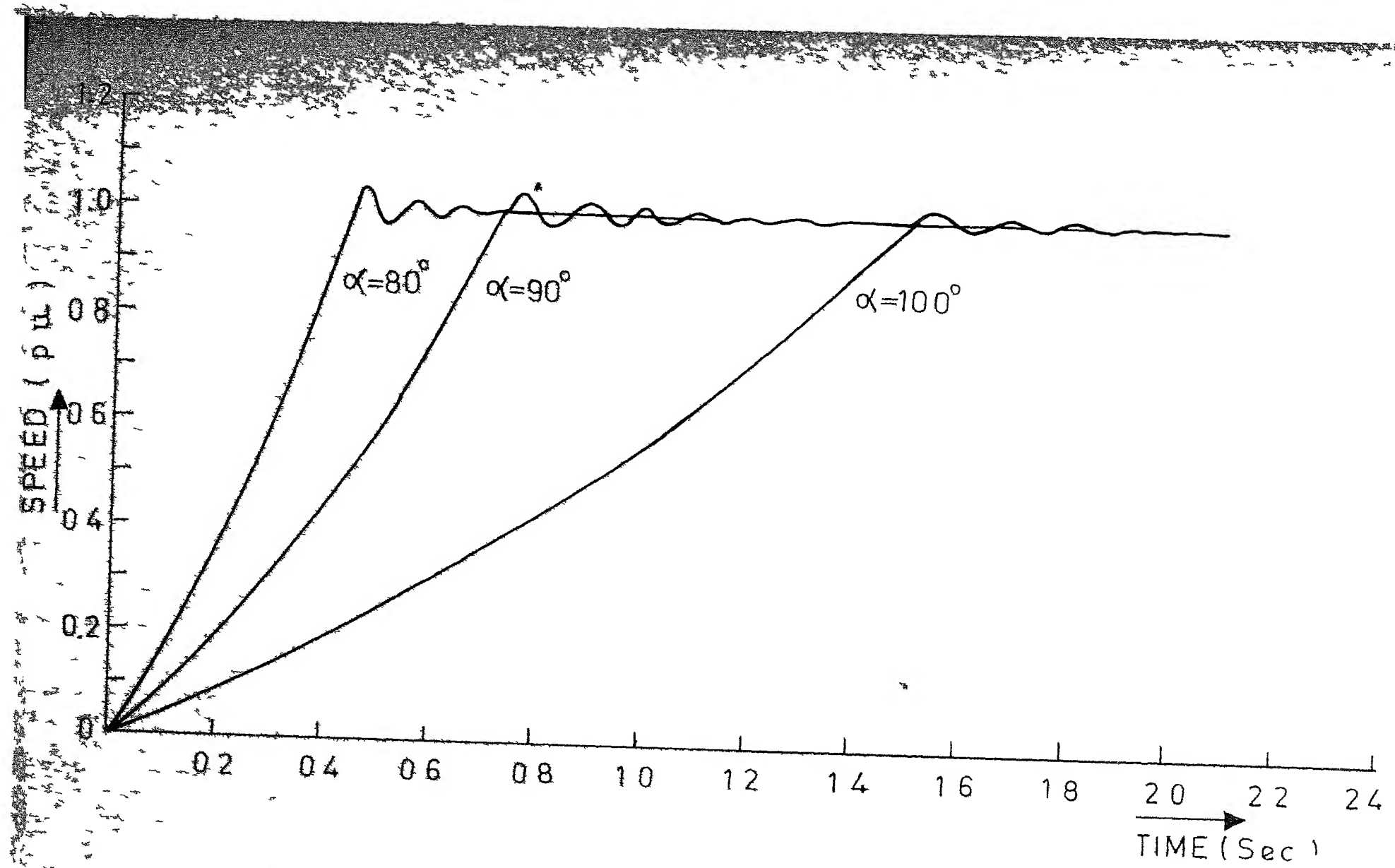

Fig 4.8 Starting Characteristics for different Triggering Angles

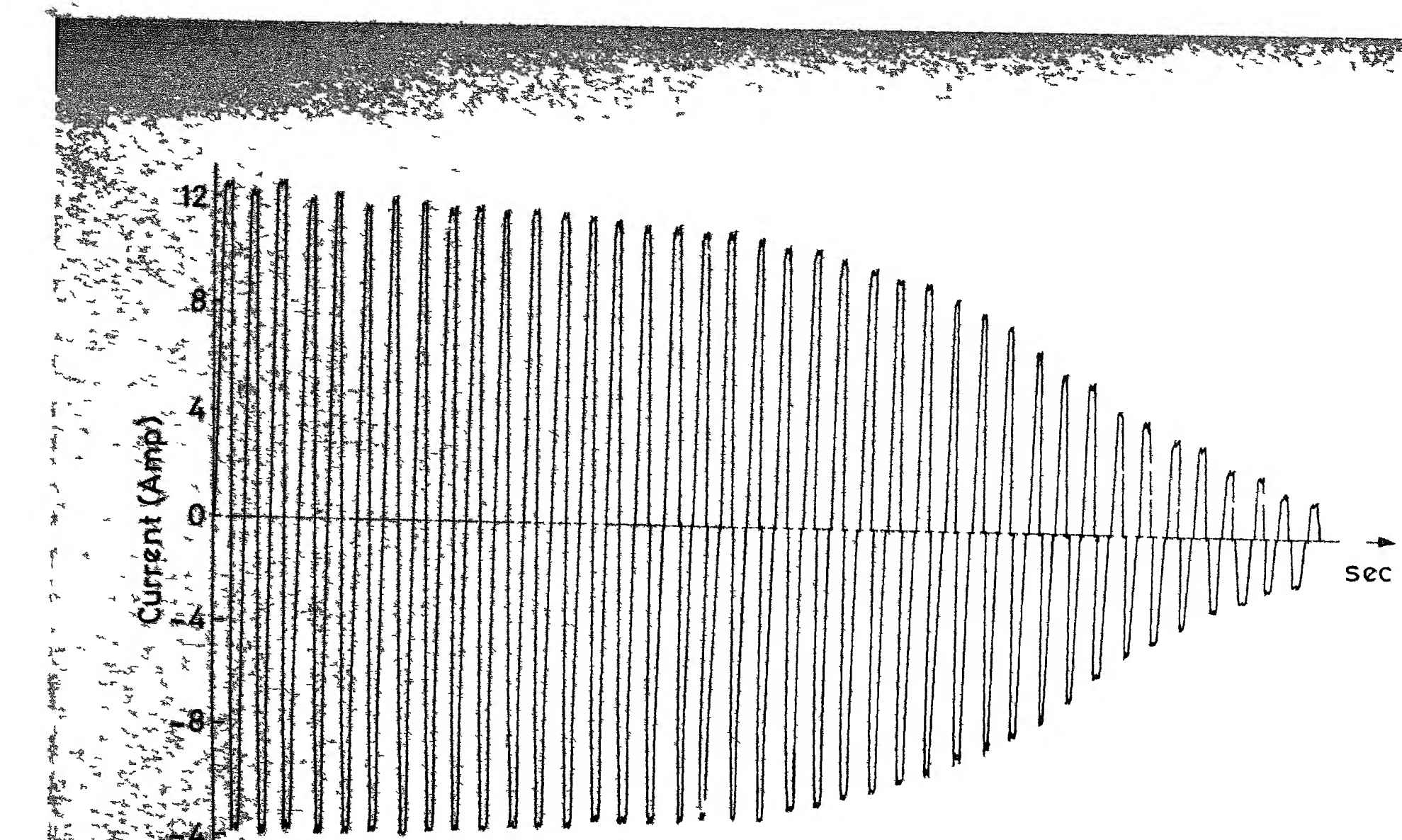

Fig 4.9 Starting current ($\alpha = 70^{\circ}$, $T_m = 3$ N-m)

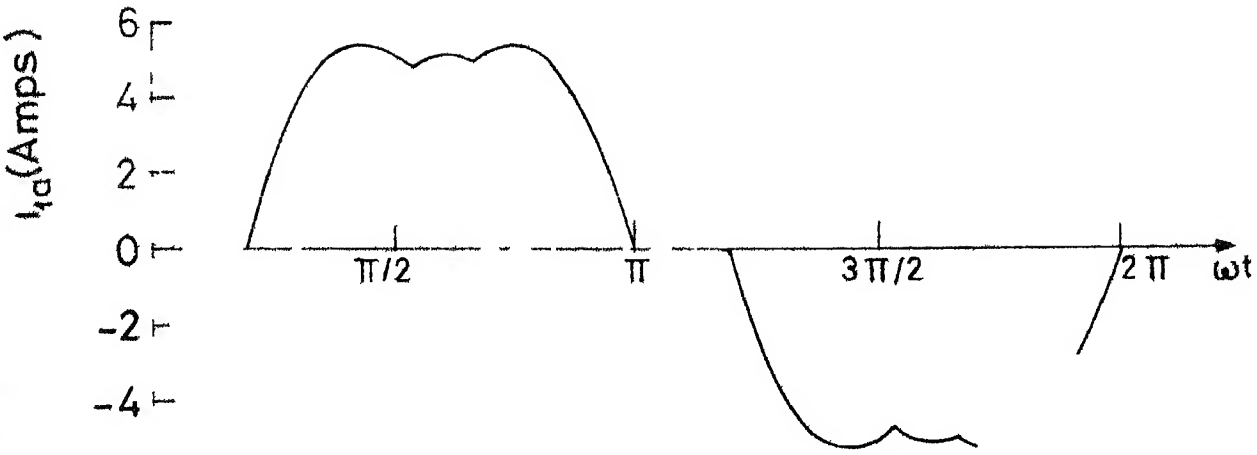
I_{1a}(Amps)
6
4
2
0
-2
-4
π/2
π
3π/2
2π
ωt

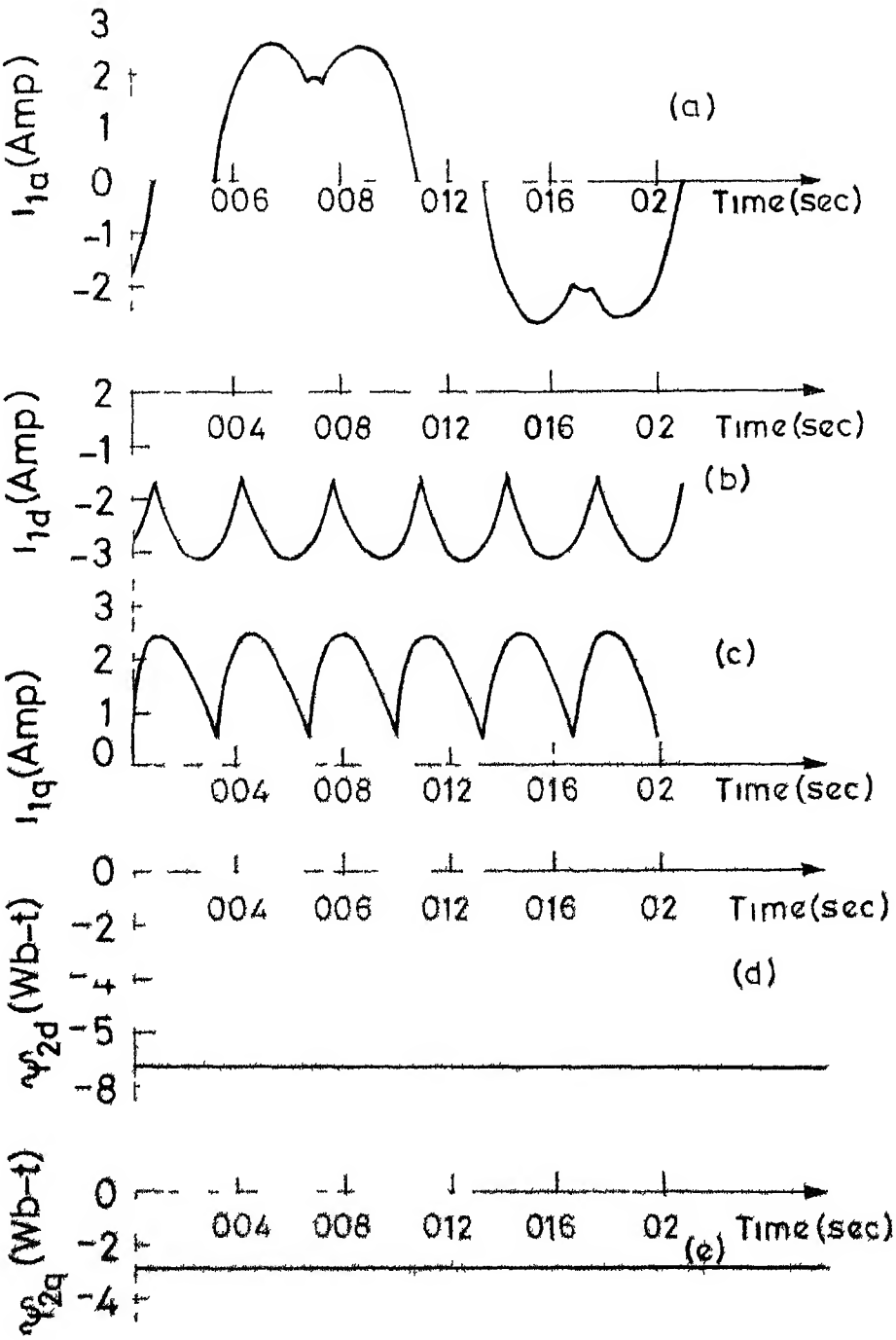

Fig 4.11 Steady-state characteristics of a voltage controlled 3 phase induction motor of slip = 0.0311 and alpha = 80°

(a) Stator current
(b) d-axis current
(c) q- " "
(d) d-axis rotor flux linkage
(e) q- " " "

steady state sub-synchronous speed after some oscillations The start-up transient current with a load torque of 3 N-m is shown in Fig 4 9 for a triggering angle of 70° Computed results of phase current i_{1a}, phase voltage v_{as} and electromagnetic torque T_e during steady state for a chosen triggering angle and load torque are shown in Fig 4 10 These waveforms have very close agreement with the results given in Fig 2 8 of Chapter 2 It will be interesting to observe from Fig 4 11 that the rotor flux linkages (ψ_{2d} and ψ_{2q}) are practically constant during steady state operation although the stator current contains large harmonic components The sixth harmonic components in the electromagnetic torque and the transformed stator currents (i_{1d} and i_{1q}) increases with increase in hold off angle γ. The details of the test machine are given in Table 2.1 of Chapter 2.

4 3 2 Example 2 Digital Simulation of a Delta Connected Induction Motor

The schematic diagram of a delta connected induction motor with voltage control is shown in Fig 4 12 The machine windings are permanently closed and a pair of back-to-back connected thyristors are included in each of the three lines The different possible modes of operation for such a scheme during transient and steady state are same as in the previous example and listed in Section 4 3 1 1

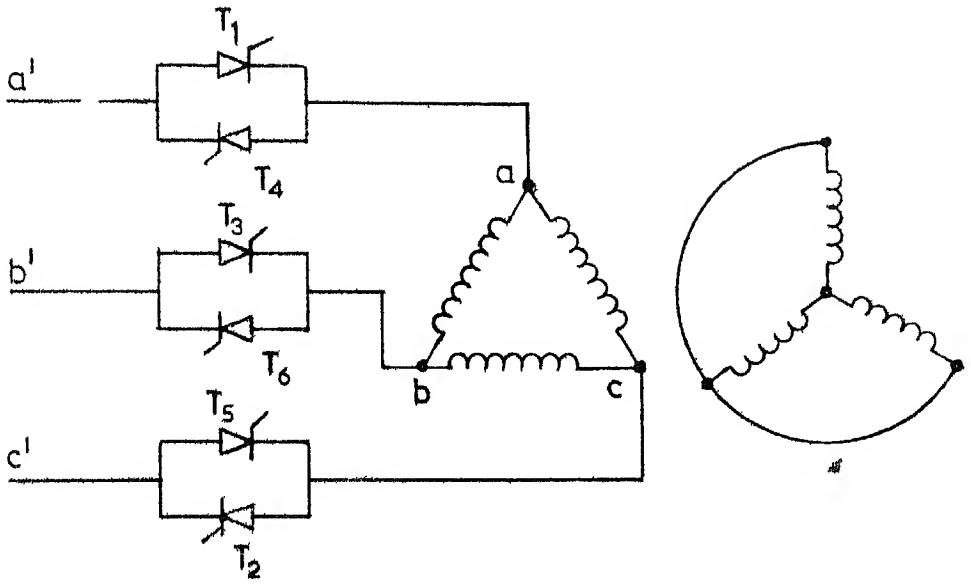

Fig 4 12 Schematic diagram - delta connected stator

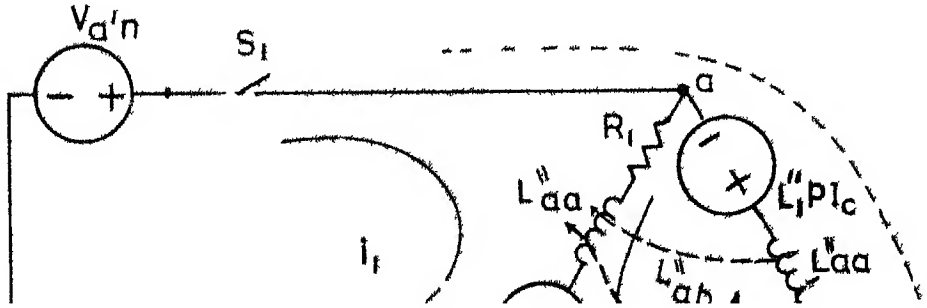

It may be observed that all the phase windings of the motor would be carrying currents irrespective of the mode of operation This is because of the delta connection of the motor winding. During mode-5 operation the current flow is due to the presence of possible third harmonic voltages Thus it is obvious that this example problem is different from the previous example in respect of analysis and performance

4 3 2 1 Formulation

The equivalent circuit of a delta connected induction motor as obtained from Fig. 4 2 is shown in Fig 4 13 in which the possible mesh currents are marked During mode-1 operation, there exist three independent mesh currents while during modes 2,3, and 4 operations only two independent mesh currents exist There is only one mesh current (i_o) during mode-5 operation The general expression relating the winding voltages and currents (refer equation (4.12)) is

$$L''_s \, p \, \underline{i}_s + R \, \underline{i}_s = \underline{v} - L'' \, p \, \underline{I} \qquad (4.54)$$

$$L'' = \begin{bmatrix} L''_1 & 0 & 0 \\ 0 & L''_1 & 0 \\ 0 & 0 & L''_1 \end{bmatrix}$$

$$\underline{i}_s^T = [i_{1a} \quad i_{1b} \quad i_{1c}], \quad \underline{I}^t = [I_{1a} \quad I_{1b} \quad I_{1c}]$$

The objective is to obtain state equations corresponding to each mode of operation in terms of the mesh currents and source

voltages This can be easily achieved utilising the mesh analysis given by Kron [53]

Mode-1

The mesh currents considered during this mode of operation are i_0, i_1 and i_2 The relationship between the phase currents and the mesh currents are

$$\underline{i}_{old} = C_1 \underline{i}_{new} \tag{4 55}$$

where

$$\underline{i}^T_{old} = [\, i_{1a} \quad i_{1b} \quad i_{1c} \,], \quad \underline{i}^T_{new} = [\, i_0 \quad i_1 \quad i_2 \,]$$

$$C_1 = \begin{bmatrix} 1 & 1 & 0 \\ 1 & 0 & 1 \\ 1 & 0 & 0 \end{bmatrix}$$

The matrix C_1 can be written by inspection from Fig 4 13 The state equations (in terms of the new currents) are

$$C_1^T L''_s C_1 \, p \, \underline{i}_{new} = -C_1^T R \, C_1 \underline{i}_{new} - C_1^T L'' \, p \, \underline{I} + C_1^T \underline{v} \tag{4.56}$$

where

$$C_1^T \underline{v} = \begin{bmatrix} 0 \\ v_{a'n} - v_{b'n} \\ v_{b'n} - v_{c'n} \end{bmatrix}$$

Mode-2

Line a'a is open and hence independent mesh currents during this mode of operation are i_0 and i_2

The connection matrix C_2 between old and new currents are

$$C_2 = \begin{bmatrix} 1 & 0 \\ 1 & 1 \\ 1 & 0 \end{bmatrix} \qquad (4\ 57)$$

The state equation is

$$C_2^T L_s'' C_2 p \underline{i}_{new} = -C_2^T R C_2 \underline{i}_{new} - C_2^T L'' p \underline{I} + C_2^T \underline{v} \qquad (4\ 58)$$

where

$$\underline{i}_{new}^T = [i_o \quad i_2], \qquad C_2^T \underline{v} = \begin{bmatrix} 0 \\ \\ v_{b'n} - v_{c'n} \end{bmatrix}$$

Mode-3

In this mode of operation, the line b'b is open circuited The mesh currents are i_o and i_1 where path of i_1 is indicated by dotted line (Fig 4 13) The connection matrix C_3 is

$$C_3 = \begin{bmatrix} 1 & 0 \\ 1 & 0 \\ 1 & -1 \end{bmatrix} \qquad (4\ 59)$$

The state equation is

$$C_3^T L_s'' C_3 p \underline{i}_{new} = -C_3^T R C_3 \underline{i}_{new} - C_3^T L'' p \underline{I} + C_3^T \underline{v} \qquad (4.60)$$

where

$$\underline{i}_{new}^T = [i_o \quad i_1], \qquad C_3^T \underline{v} = \begin{bmatrix} 0 \\ \\ v_{a'n} - v_{c'n} \end{bmatrix}$$

Mode-4

Line c'c is open circuited The independent mesh currents are i_o and i_1 The connection matrix between i_{1a}, i_{1b}, i_{1c} and the mesh currents are

$$C_4 = \begin{bmatrix} 1 & 1 \\ 1 & 0 \\ 1 & 0 \end{bmatrix} \qquad (4\ 61)$$

The state equation is

$$C_4^T L_s'' C_4 p \underline{i}_{new} = -C_4^T R C_4 \underline{i}_{new} - C_4^T L'' p \underline{I} + C_4^T \underline{v} \qquad (4\ 62)$$

where

$$\underline{i}_{new}^T = [i_o \quad i_1], \quad C_4^T \underline{v} = \begin{bmatrix} 0 \\ v_{a'n} - v_{b'n} \end{bmatrix}$$

Mode-5

Only one mesh current (i_o) exists during this mode of operation The connection vector $\underline{c}_5$ is

$$\underline{c}_5 = \begin{bmatrix} 1 \\ 1 \\ 1 \end{bmatrix} \qquad (4\ 63)$$

and the state equation is

$$\underline{c}_5^T L_s'' \underline{c}_5 p i_{new} = -\underline{c}_5^T R \underline{c}_5 i_{new} - \underline{c}_5^T L'' p \underline{I} \underline{c}_5^T \underline{v} \qquad (4.64)$$

where

$i_{new} = i_o$ and $\underline{c}_5^T \underline{v} = 0$

4 3 2 2 Digital simulation and results

The formulation described in Section 4 3 2 1 is used for the digital simulation. Transient and steady state characteristics are given in Fig 4 14 to 4 17 Starting torque as a function of time is shown in Fig 4 14 for $\alpha = 90°$ and load torque $T_m = 0\ 35$ N-m Figure 4 15 shows the speed versus time curve The motor settles down to normal speed after a few oscillations The steady state characteristics are shown in Fig 4 16 and 4 17 The stator phase current is continuous as expected The electromagnetic torque (Fig 4 16d) has a predominant sixth harmonic component The rotor flux linkages ψ_{2d} and ψ_{2q} are practically constant (Fig 4 17) although the stator currents i_{1d} and i_{1q} have high harmonic components

4 3 3 Discussion

For chosen values of α and T_m, digital simulation results of examples 1 and 2 are obtained for steady state operation The slip, ϕ and average values of ψ_{2d}, ψ_{2q}, i_{1d} and i_{1q} over one cycle are tabulated (Table 4 1) In order to facilitate a comparison between these results, same voltage per phase is taken for the wye and delta connected motors The results, given in Table 4 1, show that the characteristics of these drives are not identical especially at larger values of α The difference in characteristics in both cases is probably due to the presence of circulating current in the delta connected stator during single phasing For smaller

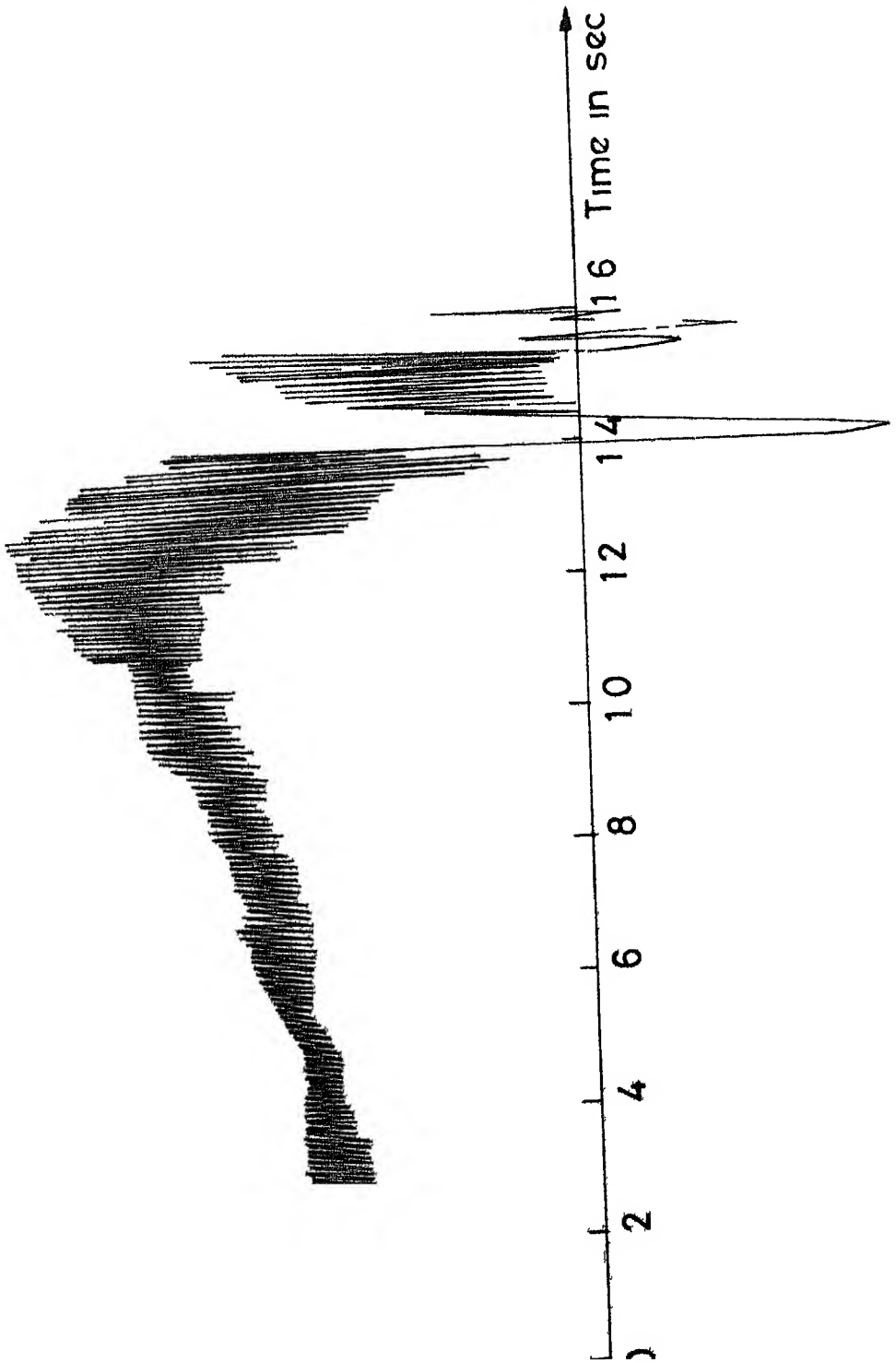

Fig 414 Starting Torque

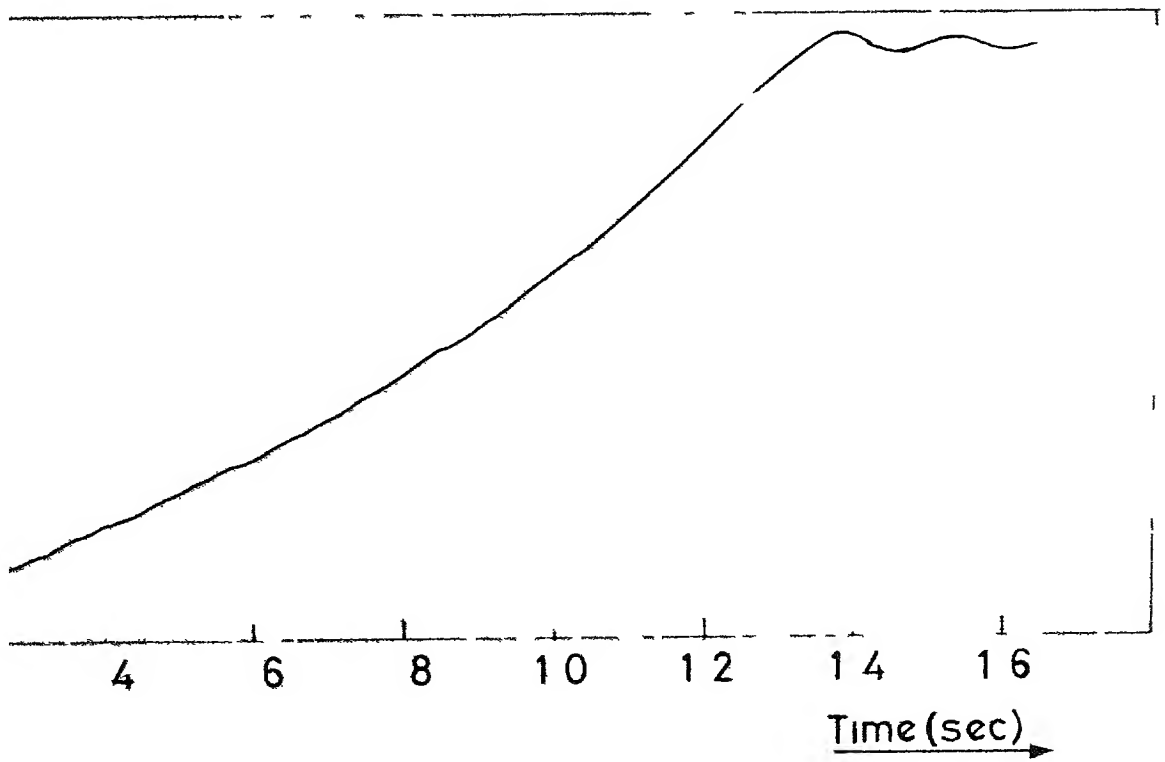

Fig 4 15 Starting characteristics

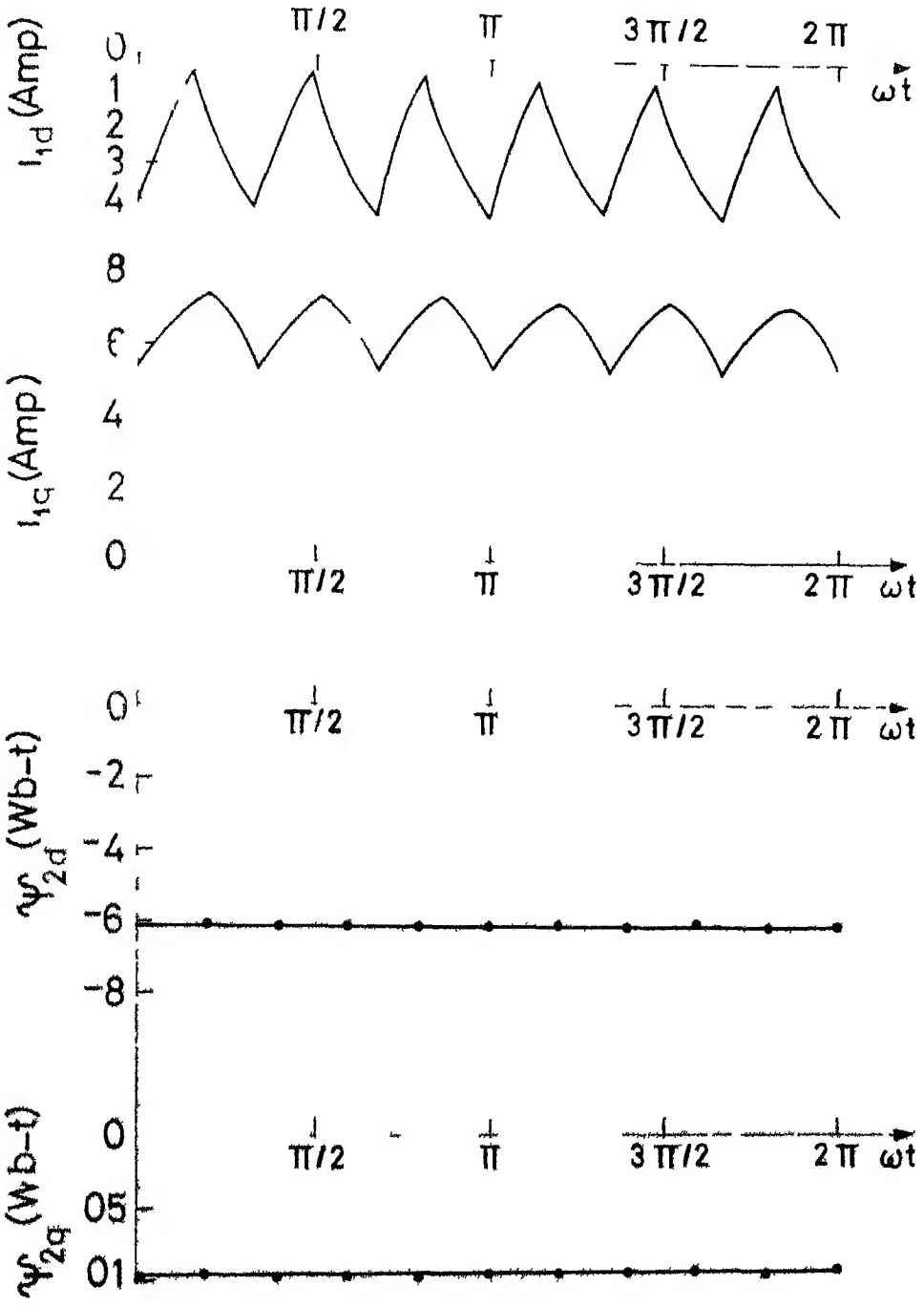

Fig.4.17 Steady state computed results for a Δ connected motor at $\alpha=70^{\circ}$ S=0.1057

(a) d-axis current
(b) q-axis current
(c) d-axis rotor
(d) q-axis rotor

TABLE 4 1

DIGITAL SIMULATION RESULTS DURING STEADY STATE

Sl No.	α	Load torque (N-m)	Star connected stator winding						
			slip	ψ_{2d}	ψ_{2q}	i_{1d}	i_{1q}	i_{rms}	ϕ
1	50	6 0	0 0260	-1 087	-0 077	-2.922	2 737	2 311	44 48
2	50	8 0	0.0414	-0 985	-0 185	-3 229	3 749	2 856	33 4
3	50	12 0	0 0969	-0 722	-0.349	-5 242	6 369	4 760	31 14
4	60	4 0	0 0164	-1 123	-0 020	-2 865	1 826	1 960	55 16
5	60	6 0	0 0320	-0 968	-0 185	-2 935	2 870	2 370	34 86
6	60	8 0	0 0550	-0 814	-0 303	-3 693	3 892	3 090	29 93
7	70	6.0	0 0471	-0 751	-0 313	-3 315	2 873	2 530	31 16
8	70	8 0	0 1065	-0 487	-0 391	-5 410	4 402	4 030	34 62
9	80	4 0	0 0358	-0 705	-0,290	-2 717	1 878	1 910	33 99
10	80	6 0	0 1740	-0 258	-0 334	-6 500	3 859	4 360	41 73
11	90	2 0	0 0153	-0 798	-0 163	-2 080	1 024	1.340	42 26
12	90	3 0	0 0534	-0 420	-0 335	-2 571	1 547	1 730	37.88
13	100	1 0	0 0068	-0 878	-0 327	-2 086	0 686	1 260	54 17
14	100	2 0	0 5897	-0 028	-0 099	-5 744	1 788	3 470	53 80

contd ..

TABLE 4 1 (continued)

Sl No	α	Load torque (N-m)	Delta connected stator winding						
			slip	ψ_{2d}	ψ_{2q}	i_{1d}	i_{1q}	i_{rms}	φ
1	50	6 0	0 0260	-0 981	0 478	-1 169	3 830	2 310	44 74
2	50	8 0	0 0413	-0 946	0 332	-0 912	4 870	2 851	33 46
3	50	12 0	0 0965	-0 802	0 059	-1 340	8 110	4 722	31 05
4	60	4.0	0 0163	-0 983	0 544	-1 570	3 020	1 962	55 30
5	60	6 0	0 0331	-0 936	0 314	-1 051	3 906	2 341	33 51
6	60	8 0	0 0550	-0 858	0 144	-1 257	5 197	3 082	29 82
7	70	6 0	0 0470	-0 808	0 103	-1 424	4 133	2 520	31 04
8	70	8 0	0 1060	-0 620	-0 096	-2 463	6 486	4.011	34 50
9	80	4 0	0 0359	-0 757	0 098	-1 400	2 969	1 889	33 80
10	80	6 0	0 1687	-0 399	-0 161	-3 633	6 490	4 290	41 40
11	90	2 0	0 0172	-0 776	0 236	-1 170	1 806	1 244	40 30
12	90	3 0	0 0544	-0 529	-0 088	-1 430	2 607	1 788	37 68
13	100	1 0	0 0067	-0 779	0 411	-1 463	1 598	1 253	54 10
14	100	2 0	0 5436	-0 080	-0 077	-3 926	4 357	3 383	53.48

values of γ the difference in characteristics is not appreciable The differences in the d and q axes current components between the two cases are due to the different references adopted in calculating these quantities Hence,only the r m s current magnitudes can be compared

Although the problem of the analysis of a voltage controlled delta connected induction motor has been mentioned in reference [22], a comprehensive analysis and simulation has not been attempted in the literature so far

4 4 CONCLUSION

Two models of an induction motor are described in which the first is particularly adapted for the simulation of motors where stator terminal switching is employed for speed control application The second model is well suited for rotor terminal switching conditions The major features of these models can be summarized as follows

1) The time dependence of the inductance matrix is eliminated
2) Identity of the motor terminals, where switching is employed, is retained
3) Simple but exact equivalent circuits are provided for either stator or rotor windings so that formulation of the problem with any arbitrary external network is easily obtained with well-known methods of network analysis

The major contribution in this chapter is the development of equivalent circuits for stator and rotor windings of the induction motor which are valid for both dynamic and steady state conditions

The transformation of variables into synchronously rotating reference frame has certain important significance, not only for sinusoidally excited machines, but also for thyristor controlled drives Simulation results indicate that the rotor flux linkages are essentially constant even when the stator current contains large harmonics due to thyristor switching The constant nature of flux linkages leads to two important features of the model presented in this chapter

1) The constant part of the developed torque (eqn 4 19) (the torque contains a constant term with harmonic components in all thyristor controlled machines) is produced by the fundamental component of stator current alone This property is applicable not only to voltage controlled machines but also to many other thyristor controlled drives such as voltage-fed inverters
2) The constancy of rotor flux linkages leads to certain simplified analysis which permits the development of transfer function between the torque and the control variable such as α This is particularly important in the design of speed controllers This aspect is considered in the next chapter

The formulation and simulation for two different configurations of voltage controlled induction motor are given to illustrate the applicability of the model Computed results of transient and steady state characteristics are furnished for each example In particular, the example of a voltage controlled delta connected induction motor has not been attempted in the past and the results of this example are compared with the results obtained for the wye-connected motor

CHAPTER 5

SIMPLIFIED ANALYSIS OF THE STEADY STATE PERFORMANCE OF A VOLTAGE CONTROLLED INDUCTION MOTOR DRIVE

5.1 INTRODUCTION

The previous chapters considered steady state performance of a voltage controlled induction motor using digital simulation. While this may be adequate for the analysis of a motor with open loop speed control, it is not sufficient for the analysis of a speed control system with feedback. What is essential is a method to directly relate the motor performance to the control variables, (such as firing angle, source voltage). This chapter present a simplified analysis based on the hybrid model given in Chapter 4, to calculate the steady state performance of a voltage controlled induction motor. While other configurations can also be considered, the analysis given here is applicable to a wye-connected motor with a pair of back-to-back thyristors connected in each line.

It was observed from the results of simulation given in Chapter 4 that the rotor flux linkages referred to a synchronously rotating reference frame are essentially constant even though the stator currents contain appreciable amount of harmonics. This observation can also be confirmed analytically and is done later in this chapter. This is an important

observation because it justifies the useful approximation of neglecting harmonics in the rotor flux linkages With this approximation and examination of the torque equation given in Chapter 4, it can be shown that only the fundamental components of the armature currents give rise to the constant component of the torque developed This fact is utilized in this chapter to derive three nonlinear algebraic equations from the solution of which, one can calculate the steady state performance of the motor for a given slip, firing angle and the source voltage.

The hybrid model given in Chapter 4 is used to first derive the expressions for the stator currents and terminal voltage of the motor The calculation of the current leads to a nonlinear algebraic equation in terms of the phase angle (ϕ) and the rotor flux linkages (ψ_{2d} and ψ_{2q}) The rotor flux linkages are solved in terms of the fundamental components of the stator currents which in turn are calculated from the fundamental components of the terminal voltage This leads to a set of two additional algebraic equations The combined set of nonlinear algebraic equations are solved using Newton-Raphson method to calculate the steady state performance of the motor The slip (S), the triggering angle (α), and source voltage magnitude (V_m) appear in the equations as parameters The fundamental current and voltage magnitudes, phase angle (ϕ) and the torque can be calculated in terms of α ,S and V_m

Two examples are presented to illustrate the analysis and its application

5 2 SIMPLIFIED STEADY STATE ANALYSIS

5 2 1 Assumptions

The major assumption used here is that the rotor flux linkages (ψ_{2d} and ψ_{2q}) referred to a synchronously revolving frame are constants during steady state operation From the simulation results given in Chapter 4 (Fig 4 11), it can be observed that these flux linkages are constants even if the armature currents are nonsinusoidal due to controlled switching The validity of this assumption is also proved analytically in a later section (5 4) Referring to the torque expression ($T_e = n (i_{1d} \psi_{2q} - i_{1q} \psi_{2d})/L_2$), it can be seen that the constant component of torque is produced by the d c components of i_{1d} and i_{1q} since ψ_{2d} and ψ_{2q} are constants The fundamental component of stator current contributes the d c components of i_{1d} and i_{1q}

The second assumption is that the analysis is restricted to mode-1 operation ($\gamma < 60°$) in which either three or two windings of the motor are connected to the power source The stator windings are assumed to be wye connected with isolated neutral

5 2 2 Analytical Expression for the Stator Current

Typical voltage and current waveforms during mode-1 operation are given in Fig 5 1 For convenience, the half

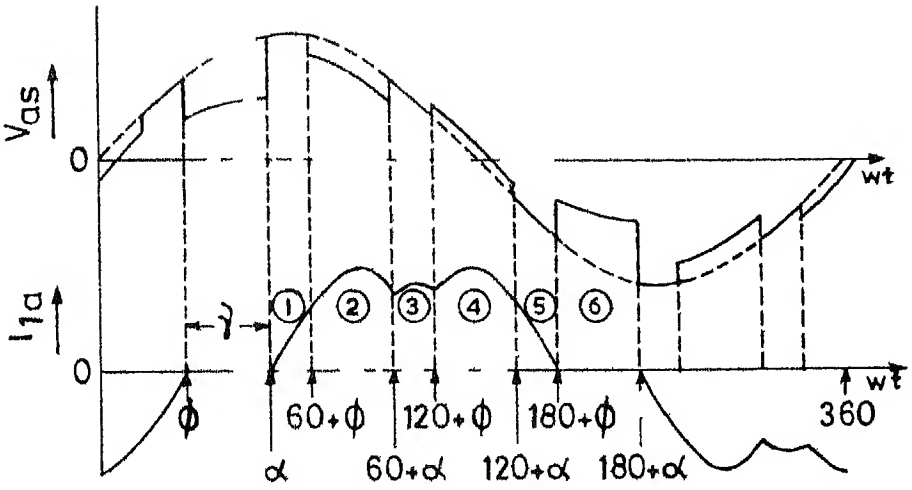

Fig 5 1 Typical voltage and current waveforms during mode-1

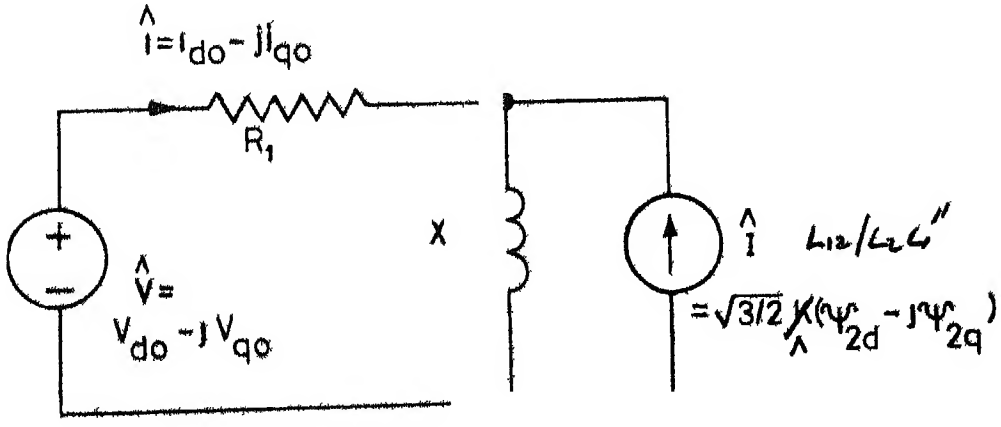

cycle period is divided into six sections starting from $\omega t = \alpha$ as shown in Fig 5.1. Referring to the circuit model (Fig 4.3) the differential equation defining the stator current i_{1a} can be written as

$$R_1 i_{1a} + L_1'' p(i_{1a} + I_{1a}) = v_{a'n} - v_s = v_{as} \qquad (5.1)$$

where v_s is the voltage at the star point of the motor with respect to the source neutral, $v_{a'n}$ is the source voltage and v_{as} is the voltage across the a-phase winding. From the circuit model (Fig 4.3) v_s can be calculated, using Millman's Theorem [54], for different modes of operation, as

$$v_s = 0 \quad \text{when all phases conducting} \qquad (5.2)$$

$$v_s = -(v_{b'n} - L_1'' p I_{1b})/2 \quad \text{when phase b non-conducting} \qquad (5.3)$$

$$v_s = -(v_{c'n} - L_1'' p I_{1c})/2 \quad \text{when phase c non-conducting} \qquad (5.4)$$

Since ψ_{2d} and ψ_{2q} are constants during steady state, the time derivatives of the dependent current sources are given by (see equation (4.16) of Chapter 4)

$$p I_{1a} = K(-\psi_{2d} \sin\theta_o + \psi_{2q} \cos\theta_o)/L_1'' \qquad (5.5)$$

$$p I_{1b} = K\{-\psi_{2d} \sin(\theta_o - 2\pi/3) + \psi_{2q} \cos(\theta_o - 2\pi/3)\}/L_1'' \qquad (5.6)$$

$$p I_{1c} = K\{-\psi_{2d} \sin(\theta_o + 2\pi/3) + \psi_{2q} \cos(\theta_o + 2\pi/3)\}/L_1'' \qquad (5.7)$$

where

$$K = \omega L_{12}/L_2$$

The solution of equation (5 1) for each section can be easily obtained as it is equivalent to a R-L circuit excited by a sinusoidal voltage with known initial condition The current expressions as derived in Appendix F are

section 1

$$i_{1a} = \frac{E}{|Z_1''|} \{ \sin(\theta_o + \delta) + C_1 \exp(-\beta(\theta_o - \alpha)) \} \qquad (5\ 8)$$

section 2

$$i_{1a} = \frac{E}{|Z_1''|} \{ \sqrt{3}/2 \sin(\theta_o + \pi/6 + \delta) + C_2 \exp(-\beta(\theta_o - \pi/3 - \phi)) \qquad (5\ 9)$$

section 3

$$i_{1a} = \frac{E}{|Z_1''|} \{ \sin(\theta_o + \delta) + C_3 \exp(-\beta(\theta_o - \pi/3 - \alpha)) \} \qquad (5\ 10)$$

section 4

$$i_{1a} = \frac{E}{|Z_1''|} \{ \sqrt{3}/2 \sin(\theta_o - \pi/6 + \delta) + C_4 \exp(-\beta(\theta_o - 2\pi/3 - \phi)) \} \qquad (5\ 11)$$

section 5

$$i_{1a} = \frac{E}{|Z_1''|} \{ \sin(\theta_o + \delta) + C_5 \exp(-\beta(\theta_o - 2\pi/3 - \alpha)) \} \qquad (5\ 12)$$

section 6

$$i_{1a} = 0 \qquad (5\ 13)$$

where

$$E = \{ E_d^2 + E_q^2 \}^{\frac{1}{2}}, \quad E_d = -K \psi_{2q}, \quad E_q = V_m + K \psi_{2d}, \quad Z_1'' = R_1 + J X_1'',$$

$$X_1'' = \omega L_1'', \quad \beta = R_1/X_1'', \quad \rho = \tan^{-1}(1/\beta), \quad \delta = \theta - \rho,$$

$$\theta = \tan^{-1}(E_d/E_q),$$

$$C_1 = -\sin(\alpha+\delta)$$

$$C_2 = C_1 \exp(-\beta(\pi/3+\phi-\alpha)+\sin(\pi/3+\phi+\delta)-\sqrt{3}/2\cos(\phi+\delta)$$

$$C_3 = C_2 \exp(-\beta(\alpha-\phi)) + \sqrt{3}/2\cos(\alpha+\delta) - \sin(\pi/3+\alpha+\delta)$$

$$C_4 = C_3 \exp(-\beta(\pi/3+\phi-\alpha))+\sin(2\pi/3+\phi+\delta)-\sqrt{3}/2\cos(\phi+\delta)$$

and

$$C_5 = C_4 \exp(-\beta(\alpha-\phi))+\sqrt{3}/2\cos(\alpha+\delta)-\sin(2\pi/3+\alpha+\delta)$$

At the end of section 5 ($\theta_o = \pi+\phi$), i_{1a} becomes zero Equating i_{1a} to zero at this instant, we get a nonlinear equation defining the phase angle ϕ as

$$C_{11}\exp(-\beta\alpha) + C_{12}\exp(-\beta\phi) = 0 \qquad (5\ 14)$$

where

$$C_{11} = -\sqrt{3}/2\cos(\phi+\delta)\{1+\exp(-\beta\pi/3)\} - \sin(\phi+\delta)\exp(\beta\pi/3) + \sin(2\pi/3+\phi+\delta) + \sin(\pi/3+\phi+\delta)\exp(-\beta\pi/3)$$

$$C_{12} = \sqrt{3}/2\cos(\alpha+\delta)\{1+\exp(-\beta\pi/3)\} - \sin(\alpha+\delta)\exp(-\beta 2\pi/3) - \sin(2\pi/3+\alpha+\delta) - \sin(\pi/3+\alpha+\delta)\exp(-\beta\pi/3)$$

The solution of equation (5 14) for an operating point (α, V_m, S) cannot be obtained as the term δ is a function of ψ_{2d} and ψ_{2q} A linear relationship between ψ_{2d}, ψ_{2q} and i_{1d}, i_{1q} during steady state is obtained from equation (4 17) by setting $p\ \psi_{2d}$ and $p\ \psi_{2q}$ to be equal to zero The relationship is given by

$$\begin{bmatrix} i_{1d} \\ i_{1q} \end{bmatrix} = \frac{1}{R_2 m} \begin{bmatrix} R_2 & S X_2 \\ -S X_2 & R_2 \end{bmatrix} \begin{bmatrix} \psi_{2d} \\ \psi_{2q} \end{bmatrix} \qquad (5\ 15)$$

where

$$m = \sqrt{3/2}\, L_{12}, \qquad X_2 = \omega L_2$$

5 2 3 Analytical Expressions for the Stator Voltage

In sections 1,3 and 5 (Fig 5 1) all the three phases conduct and hence, v_s in equation (5 1) is zero Therefore,

$$v_{as} = v_{a'n} = V_m \sin \theta_o \qquad (5\ 16)$$

During Section 2, c-phase is non-conducting while a and b phases carry current The a-phase voltage is given by

$$v_{as} = v_{a'n} - v_s$$

Replacing, v_s by equation (5 4) and eliminating the derivative of I_{1c} by equation (5 7), we get

$$v_{as} = \tfrac{1}{3}\{ \sqrt{3}\, V_m \sin(\theta_o + \pi/6) + E_1 \sin(\theta_o + 2\pi/3) \mp E_2 \cos(\theta_o + 2\pi/3)\} \qquad (5\ 17)$$

where

$$E_1 = K \psi_{2d}, \qquad E_2 = K \psi_{2q}$$

During section 4, only a and c phases conduct while b does not conduct The neutral voltage v_s is defined in equation (5 3) during this mode The stator voltage is given by

$$v_{as} = v_{a'n} - v_s$$

$$= \tfrac{1}{2} \{\sqrt{3}\, V_m \sin(\theta_o - \pi/6) + E_1 \sin(\theta_o - 2\pi/3) - E_2 \cos(\theta_o - 2\pi/3)\} \quad (5.18)$$

In section 6, a-phase is open-circuited A back-emf is induced in the a-phase winding due to presence of rotor currents and is given by

$$v_{as} = L_1'' \, p \, I_{1a}$$

$$= -E_1 \sin \theta_o + E_2 \cos \theta_o \quad (5\ 19)$$

5 2 4 Fourier Analysis of the Voltage Waveform

Since the voltage waveform is completely defined (5 16 - 5 19), it is possible to derive analytical expressions for the Fourier components The even harmonics and d c components are absent in the voltage waveform due to half wave symmetry The fundamental Fourier components of stator voltage as derived in Appendix G are

$$a_1 = \frac{3}{4\pi} \{ (V_m + E_1)(\cos 2\alpha - \cos 2\phi) + E_2 (\sin 2\alpha - \sin 2\phi + 2\alpha - 2\phi) \} = \sqrt{2/3}\, v_{do} \quad (5.20)$$

$$b_1 = \frac{3}{4\pi} \{ -E_2(\cos 2\alpha - \cos 2\phi) + \frac{4\pi}{3} V_m + (V_m + E_1)(\sin 2\alpha - \sin 2\phi - 2\alpha + 2\phi) = \sqrt{2/3}\, v_{qo} \} \quad (5\ 21)$$

Expression for a_n and b_n are given in Appendix G

In terms of the fundamental components of voltage and current, the stator side equivalent circuit can be represented on a per phase basis as given in Fig 5 2 Referring to Fig 5 2,

an expression relating the rotor flux linkages to the current and voltage can be derived as follows

Let,

$$\hat{i} = i_{do} - j\, i_{qo}\ , \quad \hat{v} = v_{do} - j\, v_{qo}, \quad \hat{I} = I_{do} - j\, I_{qo}$$

Referring to equation (4 16) of Chapter 4, the dependent current $\hat{I}$ can be related to the rotor flux linkages as

$$\hat{I} = \sqrt{3/2}\ \frac{L_{12}}{L_2 L_1''}\ (\psi_{2do} - j\, \psi_{2qo}) \qquad (5\ 22)$$

From the circuit model (Fig 5 2), the expression for $\hat{i}$ is given by

$$\hat{i} = \frac{\hat{v} - j\, \hat{I}\, X_1''}{Z_1''} \qquad (5\ 23)$$

where

$$X_1'' = \omega L_1'' , \qquad Z_1'' = R_1 + j\, X_1''$$

After simplification, we get

$$i_{do} - j\, i_{qo} = \frac{\{(v_{do} - \sqrt{3/2}\, K\, \psi_{2d}) - j(v_{qo} + \sqrt{3/2}\, K\, \psi_{2q})\}\ (R_1 - j\, X_1'')}{|Z_1''|^2} \qquad (5.24)$$

Equating real and imaginary parts of equation (5 24) and expressing in the matrix form, we get

$$\begin{bmatrix} i_{do} \\ i_{qo} \end{bmatrix} = \begin{bmatrix} a & -b \\ b & a \end{bmatrix} \begin{bmatrix} v_{do} \\ v_{qo} \end{bmatrix} + \sqrt{3/2}\, K \begin{bmatrix} -b & -a \\ a & -b \end{bmatrix} \begin{bmatrix} \psi_{2do} \\ \psi_{2qo} \end{bmatrix} \qquad (5\ 25)$$

where

$$a = R_1/|Z_1''|^2 , \qquad b = X_1''/|Z_1''|^2$$

It may be noted that the induction motor model shown in Fig 5 2 is equivalent to the conventional passive equivalent circuit for sinusoidal excitations in steady state This can be proved (see Appendix H) by showing that equation (5 23) is equivalent to the equation defining passive equivalent circuit

5 2 5 Prediction of Operating Vector

The operating vector of a voltage controlled induction motor consists of phase angle ϕ, fundamental components of current and voltage and constant component of torque The operating point is defined by triggering angle α, slip S and the source voltage magnitude V_m The problem is to predict the operating vector for a given operating point, An analytical expression for ϕ is given in equation (5 14) During steady state, ψ_{2d} and ψ_{2q} are linearly related to i_{1d} and i_{1q} by equation (5 15) Since the harmonic components i_{1d} and i_{1q} have very little effect on ψ_{2d} and ψ_{2q}, it is sufficient to know the fundamental components of stator current to determine ψ_{2d} and ψ_{2q} during steady state The fundamental component of current results from the fundamental component of applied voltage The current and voltage are related by the parameters of the passive equivalent circuit as

$$v_{do} - j\, v_{qo} = (i_{do} - j\, i_{qo})(R_{eq} + j\, X_{eq}) \qquad (5\ 26)$$

where R_{eq} and X_{eq} are the equivalent resistance and reactance of the passive equivalent circuit, given by

$$R_{eq} = R_1 + \frac{X_m^2}{(R_2/S)^2 + (X_m + X_{rl})^2} \frac{R_2}{S} \qquad (5\ 27)$$

and

$$X_{eq} = X_{sl} + \frac{(R_2/S)^2 + X_{rl}(X_{rl} + X_m)}{(R_2/S)^2 + (X_m + X_{rl})^2} X_m \qquad (5\ 28)$$

where R_1, R_2, X_{sl}, X_{rl} and X_m are the parameters of conventional passive equivalent circuit

On separating the real and imaginary parts of the equation (5 26), we get

$$v_{do} = i_{do} R_{eq} + i_{qo} X_{eq} \qquad (5\ 29)$$

$$v_{qo} = i_{qo} R_{eq} - i_{do} X_{eq} \qquad (5\ 30)$$

Combining equations (5.29) and (5 30) with (5 20) and (5 21), we get

$$\sqrt{\frac{2}{3}}\ \frac{4\pi}{3}(i_{do} R_{eq} + i_{qo} X_{eq}) - (V_m + K\psi_{2d})(\cos 2\alpha - \cos 2\phi) - K\psi_{2q}(\sin 2\alpha - \sin 2\phi + 2\alpha - 2\phi) = 0 \qquad (5\ 31)$$

$$\sqrt{\frac{2}{3}}\ \frac{4\pi}{3}(i_{qo} R_{eq} - i_{do} X_{eq}) + K\psi_{2q}(\cos 2\alpha - \cos 2\phi) - (V_m + K\psi_{2d})(\sin 2\alpha - \sin 2\phi - 2\alpha + 2\phi) - \frac{4\pi}{3} V_m = 0 \qquad (5\ 32)$$

Making use of (5 15), the nonlinear equations (5 14), (5 31) and (5 32) in ϕ, i_{do} and i_{qo} are solved simultaneously by

Newton-Raphson method [55] for a given operating point It may be remembered that the equations derived in Section 5 2 are applicable only for mode 1 operation ($\gamma < 60°$) Hence, the mode of operation is to be checked during the solution of the nonlinear equations A flow diagram giving the details of mode identification and the solution is shown in Fig 5 3 If the hold off angle γ is greater than 60°, the programme returns without computation Proper initial values (ϕ_i, i_{di} and i_{qi}) which are generated using passive equivalent circuit parameters, are provided for faster convergence The Jacobian which consists of the derivation of the three functions with respect to ϕ, i_{do} and i_{qo} are easily calculated because of the availability of analytical expressions for these functions Once the steady state solution is obtained the torque is calculated using equation (4 19) The expressions for the r m s values of current and voltage are given by

$$I_{rms} = \frac{1}{\sqrt{3}} \{ i_{do}^2 + i_{qo}^2 \}^{\frac{1}{2}} \qquad (5\ 33)$$

$$V_{rms} = \frac{1}{\sqrt{3}} \{ v_{do}^2 + v_{qo}^2 \}^{\frac{1}{2}} \qquad (5\ 34)$$

5 3 EXAMPLE

5 3 1 Computed Results

The steady state performance characteristics of the test machine (Table 2 1) were predicted using the simplified analysis discussed in the earlier Sections Predicted values of ϕ ,

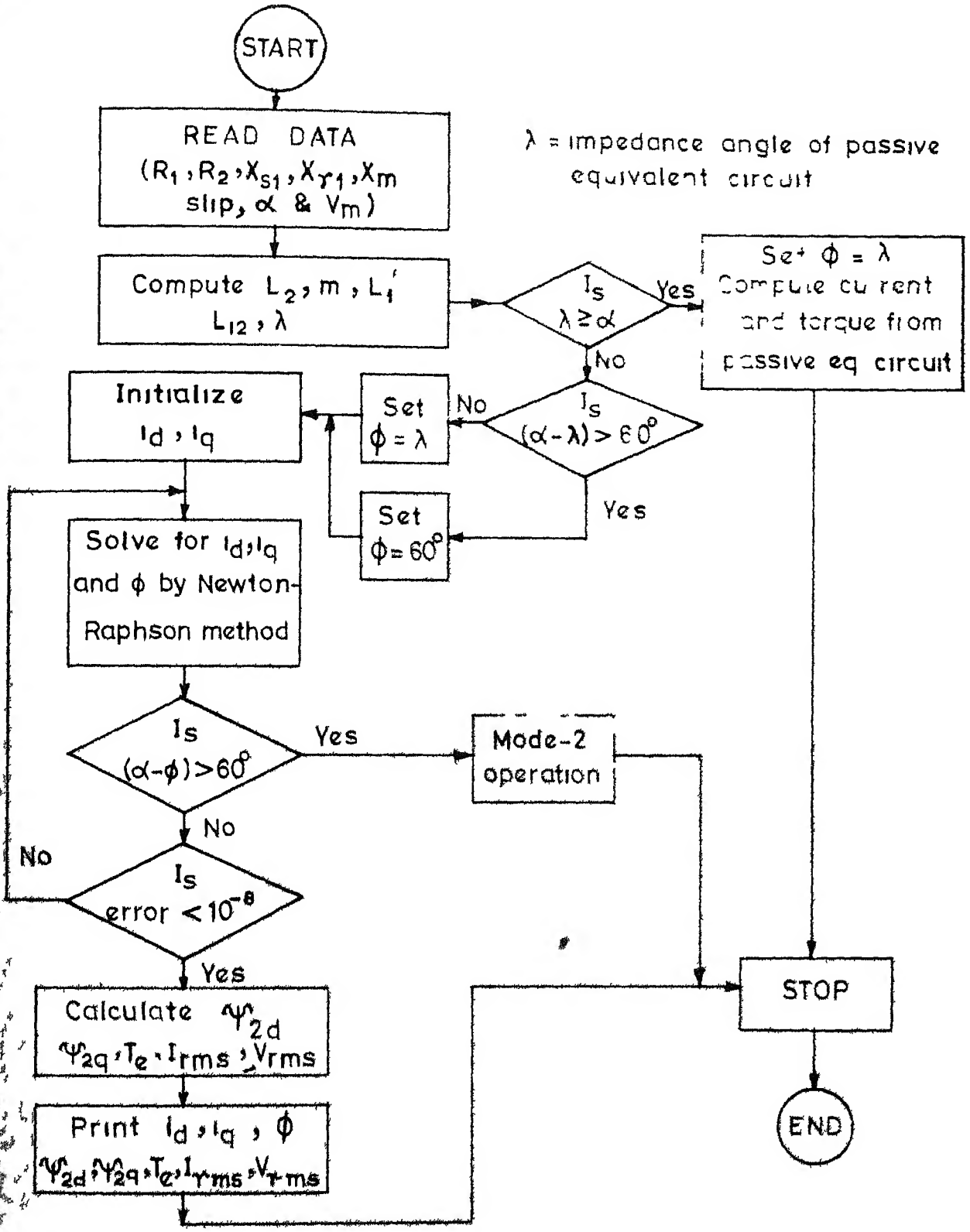

Fig 5 3 Flow diagram to predict operating vector

ψ_{2d}, ψ_{2q}, V_{rms}, I_{rms} and fundamental power factor (cosine of the angle between fundamental components of voltage and current) for mode-1 operation are plotted against slip S in Figs 5.4 to 5.7. It can be observed that all these variables change rapidly for small changes in slip when the motor is near maximum speed. This is because of the fact that the phase angle ϕ changes rapidly (Fig 5.4) near the maximum speed for small variations in slip resulting in large variations in the hold off angle γ. For larger values of slip ($S > 0.2$), the variations are not very significant. Variations of the rotor flux linkages for different values of α are plotted against slip S in Fig 5.5. The magnitude of the fundamental components of voltage and current are given in Figs 5.6 and 5.7. In Table 5.1, predicted and simulation results (ϕ, ψ_{2d} and ψ_{2q}) are furnished for comparison.

In order to check the accuracy of the predicted results, the steady state characteristics of a motor described in reference [14] are computed. The computed torque-speed characteristics of this motor is plotted in Fig 5.8 for constant values of α for comparing with the published results [14]. The parameters of the motor are given in Table 2.2.

5.3.2 Discussion

On comparing with the results published in [14], it can be seen that the predicted torque-slip characteristics

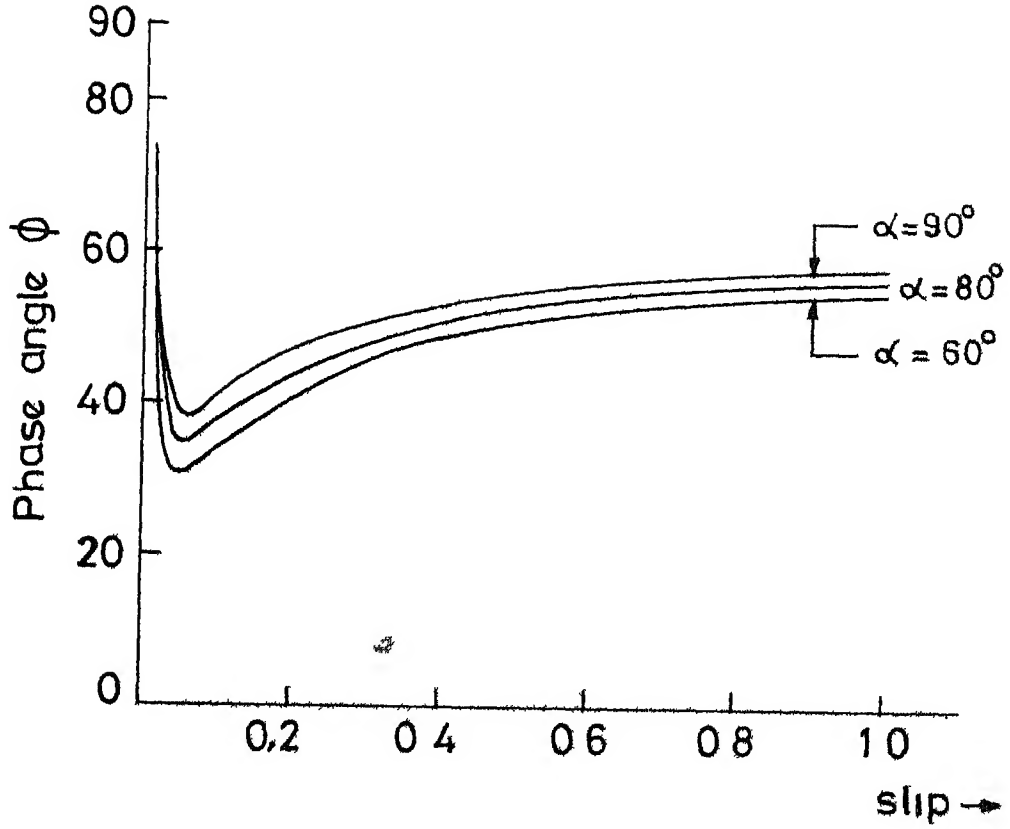

Fig 5 4 Variation of ϕ as a function of slip

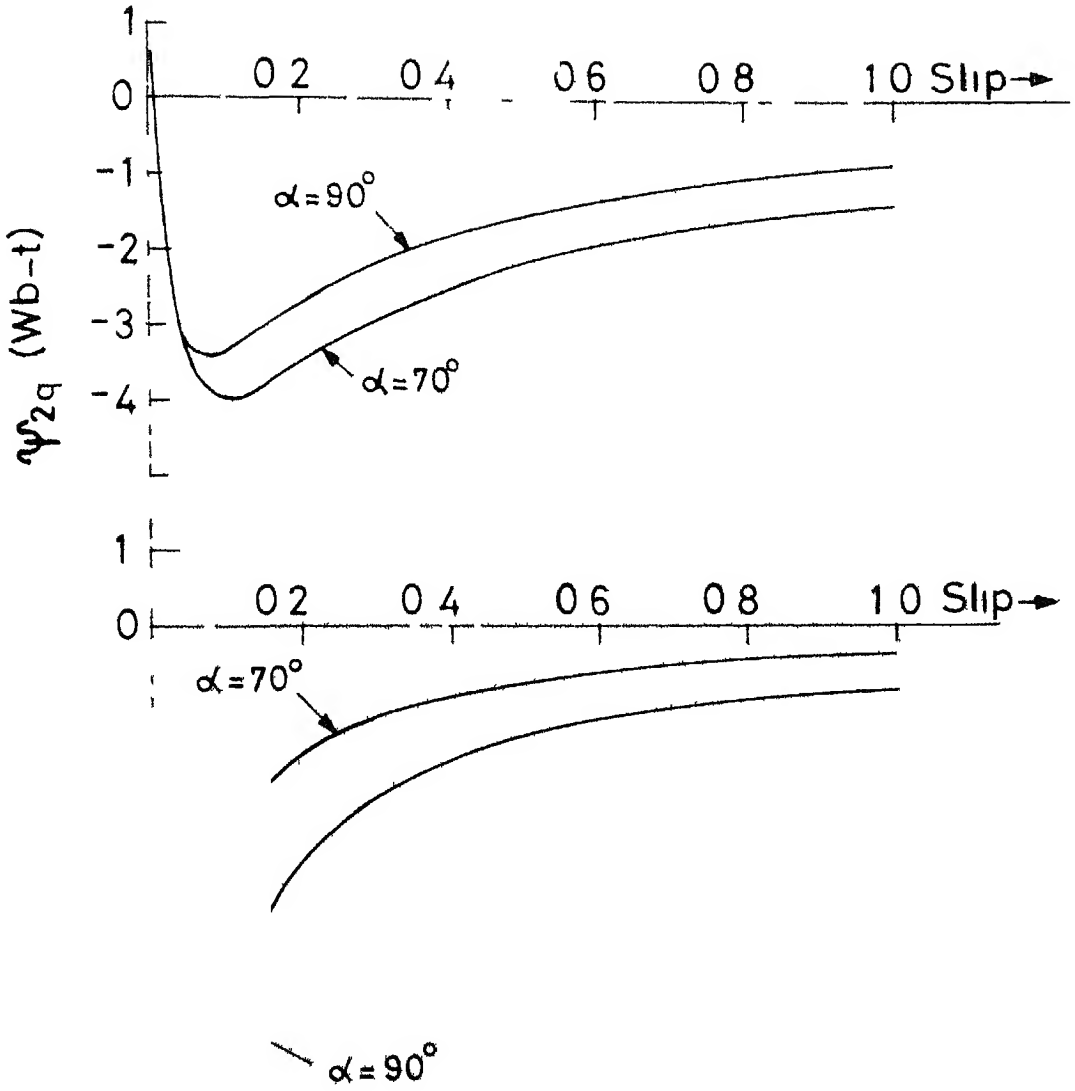
1
0
-1
-2
-3
-4
0 2
0 4
0 6
0 8
1 0 Slip
ψ_{2q} (Wb-t)
α=90°
α=70°
1
0
0 2
0 4
0 6
0 8
1 0 Slip
α=70°
α=90°

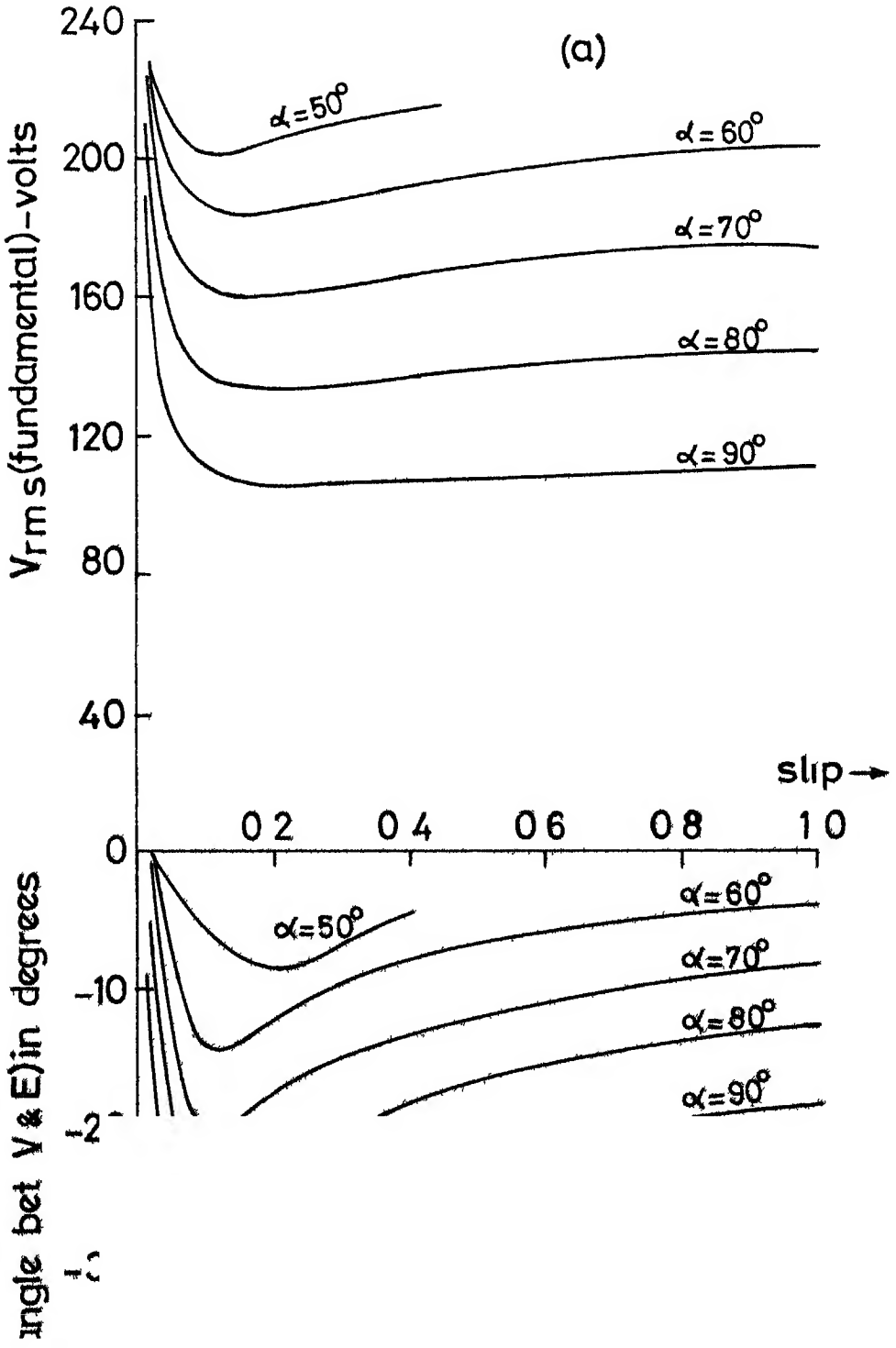
(a)
240
200
160
120
80
40
0
-10
-2
Vrms(fundamental)-volts
angle bet V & E)in degrees
slip →
0 2
0 4
0 6
0 8
1 0
α=50°
α=60°
α=70°
α=80°
α=90°

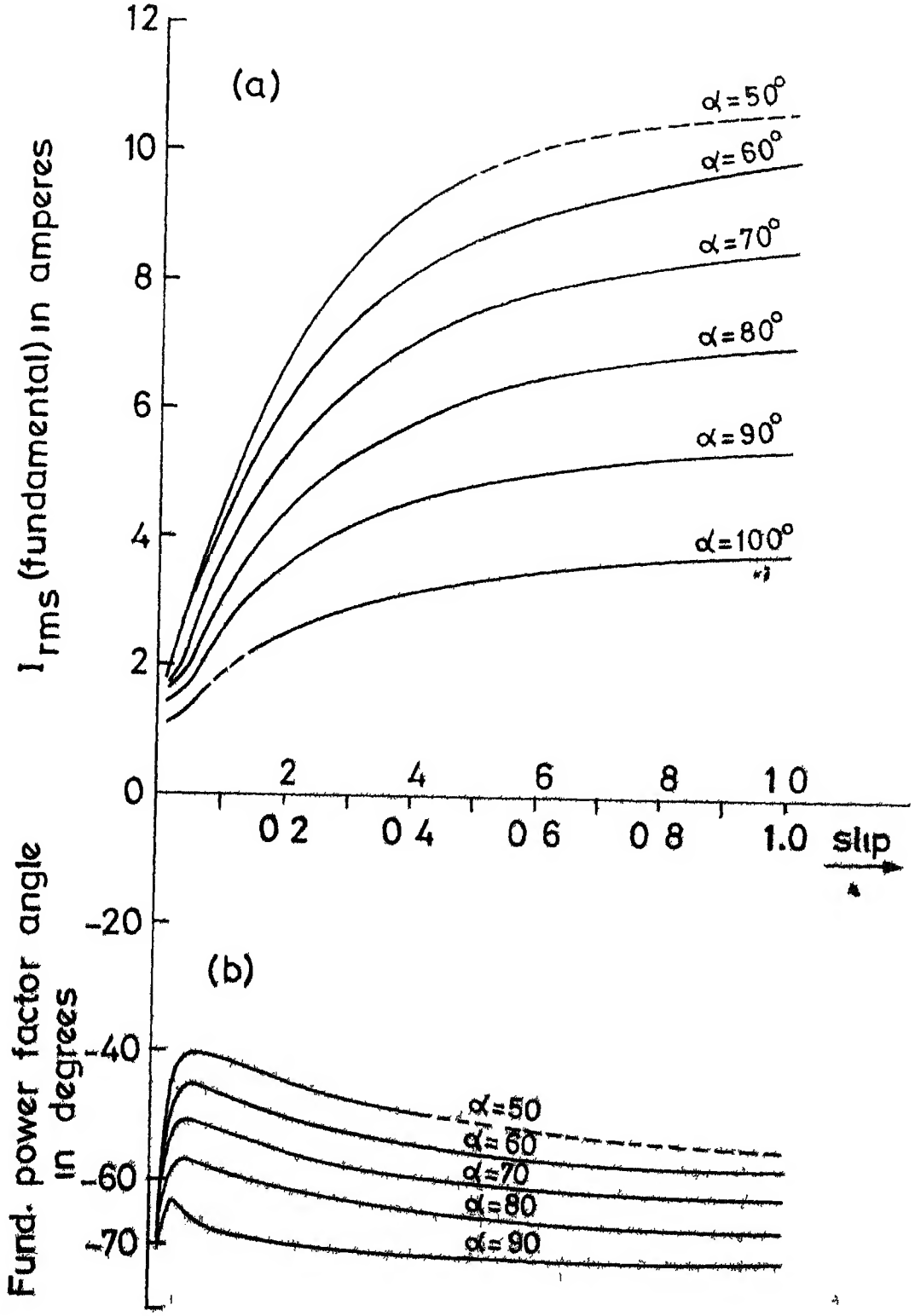

Fig. 5.7 (a) Variation of I_{rms} (fundamental)
(b) Phase angle between source voltage and fundamental component of current

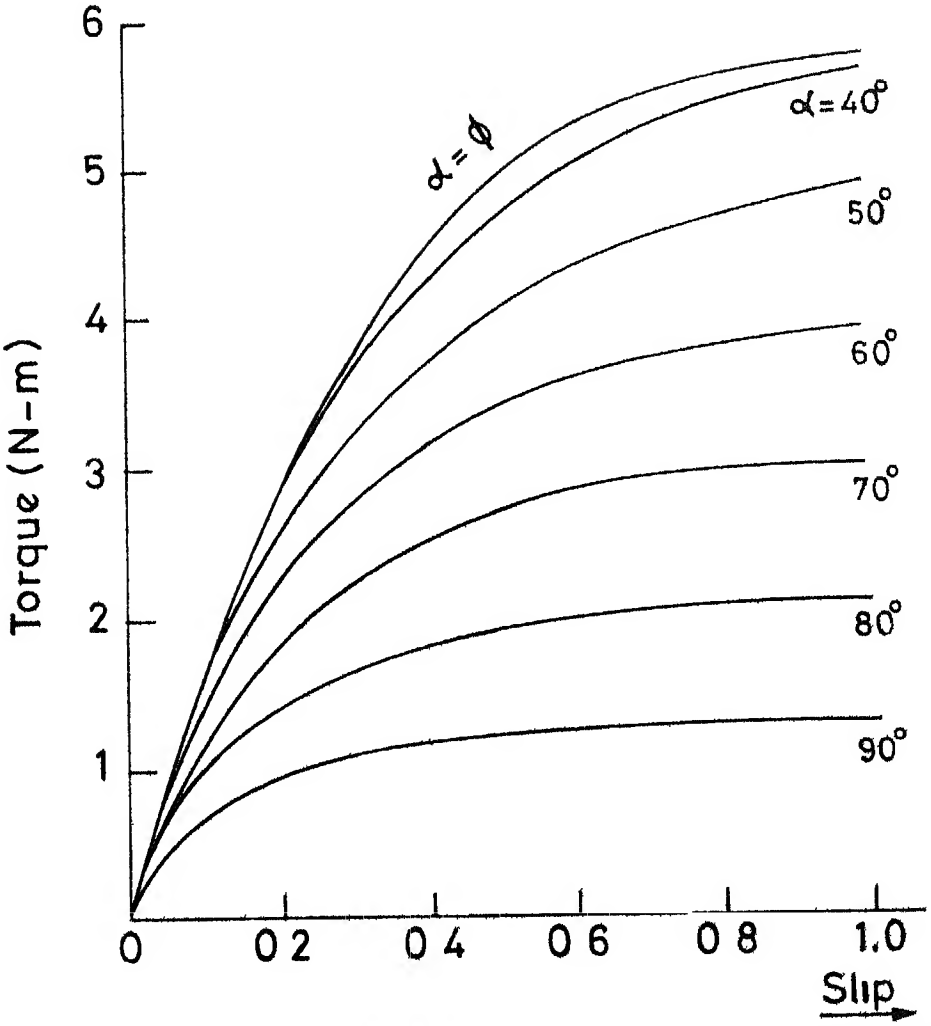

Fig 5 8 Predicted torque slip characteristics

TABLE 5.1

COMPARISON BETWEEN PREDICTED AND SIMULATION RESULTS

Sl No	α (degrees)	Slip (p u)	Predicted Results			Simulation Results		
			ϕ (degrees)	ψ_{2d} (Wb-t)	ψ_{2q} (Wb-t)	ϕ (degrees)	ψ_{2d} (Wb-t)	ψ_{2q} (Wb-t)
1	50	0 026	44 13	-1 086	-0 079	44 20	-1 086	-0 079
2	50	0 041	33 17	-0 983	-0 187	33 38	-0 983	-0 185
3	50	0 064	29 68	-0 857	-0 288	29 88	-0 857	-0 286
4	50	0 239	39 95	-0 423	-0 343	40 40	-0 422	-0 342
5	60	0 017	54 12	-1 119	-0 027	54 21	-1 119	-0 026
6	60	0 031	35 49	-0 985	-0 165	35 70	-0 985	-0 162
7	60	0 058	29 64	-0 798	-0 316	29 80	-0 797	-0 312
8	60	0 124	33 95	-0 544	-0 387	34 11	-0 544	-0 384
9	60	0 514	49.12	-0 186	-0 234	49 21	-0 185	-0 232
10	60	0 963	53 88	-0 104	0 149	53 90	-0 103	-0 149
11	70	0 026	43 01	-1 018	-0 099	43 21	-1 018	-0.097
12	70	0 056	30 95	-0 670	-0 348	31 14	-0 690	-0 344

Table 5 1(continued)

Sl No	α (degrees)	Slip (p u)	Predicted Results			Simulation Results		
			ϕ (degrees)	ψ_{2d} (Wb-t)	ψ_{2q} (Wb-t)	ϕ (degrees)	ψ_{2d} (Wb-t)	ψ_{2q} (Wb-t)
13	70	0 160	38 40	-0 371	-0 373	38 49	-0 372	-0 370
14	70	0 350	4€ 40	-0 200	-0 273	46 48	-0 200	-0 270
15	80	0 004	77 03	-1 165	0 055	77 11	-1 165	0 055
16	80	0 019	41 20	-0 924	-0 135	41 15	-0 922	-0 136
17	80	0 055	33 70	-0 559	-0 361	33 89	-0 562	-0 357
18	80	0 184	42 19	-0 247	-0 329	42 23	-0 248	-0 328
19	80	0 372	48 36	-0 135	-0 243	48 41	-0 137	-0 232
20	80	0 570	51 49	-0 094	-0 176	55 55	-0 090	-0 173
21	90	0 013	47 01	-0 901	-0 090	46 75	-0 888	-0 094
22	90	0 071	38 73	-0 345	-0 347	38 84	-0 348	-0 344
23	90	0 145	43 28	-0 199	-0 305	43 31	-0 201	-0 303
24	90	0 232	46 74	-0 133	-0 251	46 73	-0 135	-0 248
25	90	0 416	50 72	-0 079	-0 178	50 73	-0 079	-0 176
26	90	0 600	52.79	-0 054	-0 137	52 78	-0 054	-0 134

(Fig 5 8) have very good correlation with the exact values This validates the correctness of the assumptions made in the simplified analysis According to the induction motor model developed in Chapter 4 (equation 4 19), the constant component of the torque is produced by the fundamental component of stator current primarily because the rotor flux linkages referred to the synchronously involving axes are practically constant

The predicted values of ϕ , ψ_{2d}, ψ_{2q} for different values of α and S are shown in Table 5 1 for the test machine Results obtained from digital simulation (Chapter 4, example 1) are also given in the same table to enable a comparison between the two results Very good agreement between the two results is evident from Table 5 1

5 4 EFFECT OF STATOR CURRENT HARMONICS ON ROTOR FLUX LINKAGES ψ_{2d} AND ψ_{2q}

It is stated in Section 5 2 that ψ_{2d} and ψ_{2q} are essentially constant during steady state and harmonic components of stator current have very little effect on them The digital simulation results illustrate the validity of this assumption An analytical expression to justify this assumption is derived in this section

Consider the differential equations defining the rotor flux linkages derived in Section 4 2 1 of Chapter 4 given by

$$p\,\psi_{2d} = -R_2\,\psi_{2d}/L_2 - S\omega\,\psi_{2q} + R_2\,m\,i_{1d}/L_2 \qquad (5\ 35)$$

$$p\,\psi_{2q} = -R_2\,\psi_{2q}/L_2 + S\omega\,\psi_{2d} + R_2\,m\,i_{1q}/L_2 \qquad (5\ 36)$$

The harmonic components of ψ_{2d} and ψ_{2q} in steady state result from harmonic components of i_{1d} and i_{1q} These can be calculated as follows

Multiplying equation (5 36) by -j and adding to (5 35),

$$p(\psi_{2d}-j\,\psi_{2q}) = -R_2(\psi_{2d}-j\,\psi_{2q})/L_2 - j\,S\,\omega(\psi_{2d}-j\,\psi_{2q}) + R_2\,m(i_{1d}-j\,i_{1q})/L_2$$

In vector notation,

$$L_2\,p\,\hat{\psi}_2 = -(R_2 + j\,S\,X_2)\,\hat{\psi}_2 + R_2\,m\,\hat{i} \qquad (5\ 37)$$

where

$$\hat{\psi}_2 = \psi_{2d} - j\,\psi_{2q}, \qquad i = \hat{i}_{1d} - j\,i_{1q}$$

During steady state, operator 'p' can be replaced by $jn\omega$ where n represents the order of harmonics and we get

$$(R_2 + j(n+S)X_2)\,\hat{\psi}_{2n} = R_2\,m\,\hat{i}_n \qquad (5\ 38)$$

where

$$\hat{\psi}_{2n} = \psi_{2dn} - j\,\psi_{2qn}, \qquad \hat{i}_n = i_{dn} - j\,i_{qn}$$

The expressions for i_{dn} and i_{qn} in terms of the Fourier components of stator currents (see Appendix I) are

$$i_{dn} = \sqrt{3/2}\,\{(a_{n-1}+a_{n+1})^2 + (b_{n-1}+b_{n+1})^2\}^{\frac{1}{2}} \qquad (5\ 39)$$

$$i_{qn} = \sqrt{3/2}\,\{(a_{n-1}-a_{n+1})^2 + (b_{n-1}-b_{n+1})^2\}^{\frac{1}{2}} \qquad (5\ 40)$$

where a_n and b_n are the Fourier components of stator current

On rearranging the terms in (5 38), we get

$$\psi_{2dn} = \frac{R_2\, m(R_2\, i_{dn} - (n+S)\, X_2\, i_{qn})}{R_2^2 + (n+S)^2\, X_2^2} \qquad (5\ 41)$$

$$\psi_{2qn} = \frac{R_2\, m(R_2\, i_{qn} + (n+S)\, X_2\, i_{dn})}{R_2^2 + (n+S)^2\, X_2^2} \qquad (5\ 42)$$

Equations (5.41) and (5 42) indicate that ψ_{2dn} and ψ_{2qn} are reducing rapidly as the order of the harmonics increases since the reactance increases from S X_2 for d c component (of i_{1d} and i_{1q}) to (n+S) X_2 for the nth harmonic As an example, at a slip of 0 1, the reactance for the sixth harmonic, is about 61 times greater than that for the d c component

Using equations (5 41) and (5 42), ψ_{2dn} and ψ_{2qn} are calculated and the results are given in Table 5 2 along with the corresponding values of i_{dn} and i_{qn} It can be observed from Table 5 2 that ψ_{2dn} and ψ_{2qn} are approaching zero for higher values of n Even for the sixth harmonic (the lowest order harmonic in i_{dn} and i_{qn}) component of i_{1d} and i_{1q}, the magnitude of the flux linkages (harmonic) becomes quite small

Fourier components of a_n and b_n of the stator current can be obtained in three different ways The first method is to derive analytical expressions for a_n and b_n from the current

TABLE 5 2

HARMONIC COMPONENTS OF D-Q CURRENTS AND FLUX LINKAGES

$\alpha = 50°$, slip = 0 1

n	$i_d(n)$	$i_q(n)$	$\psi_{2d}(n)$	$\psi_{2q}(n)$
0	-5 390	6.410	-0 711	-0 350
6	0 845	0 761	-0 0012	0 0014
12	0 233	0 208	-0 0002	0 0002
18	0 025	0 032	-0 0000	0 0000

$\alpha = 60°$, slip = 0 1

n	$i_d(n)$	$i_q(n)$	$\psi_{2d}(n)$	$\psi_{2q}(n)$
0	-5 460	5 370	-0 6161	-0 3831
6	1 101	1 183	-0 0019	0 0018
12	0.090	0 113	-0 0001	0 0001
18	0 102	0 110	-0 0001	0 0001

Table 5 2 (continued)

α = 70°, slip = 0.1

n	$i_d(n)$	$i_q(n)$	$\psi_{2d}(n)$	$\psi_{2q}(n)$
0	-5 500	4 330	-0 4866	-0 3939
6	1.186	1 498	-0 0024	0 0019
12	0 119	0 173	-0 0001	0 0001
18	0 083	0 107	-0 0001	0 0000

α = 80°, slip = 0 1

n	$i_d(n)$	$i_q(n)$	$\psi_{2d}(n)$	$\psi_{2q}(n)$
0	-4.855	3 023	-0 3867	-0 3797
6	1 152	1 542	-0 0025	0 0019
12	0 205	0 357	-0 0003	0.0002
18	0 056	0 078	-0 0000	0 0000

α = 90°, slip = 0 1

n	$i_d(n)$	$i_q(n)$	$\psi_{2d}(n)$	$\psi_{2q}(n)$
0	-4.115	1 918	-0 2684	-0 3362
6	1 160	1 406	-0 0022	0 0019
12	0.216	0 399	-0 0003	0 0002
18	0.076	0 179	-0 0001	0 0000

expressions (equations (5 8 - 5 13)) Another method is to make use of the Fourier components of voltages and harmonic equivalent circuits [19] The third method is to obtain a_n and b_n numerically while doing digital simulation The calculations for the results given in Table 5 2 are performed using the first method and checked using the third method

5 5 CONCLUSION

The analysis presented in this chapter has two special features The first one is the faster computation of steady state characteristics for any given operating point Although the analysis is based on certain assumptions, the accuracy of the computed results is very good The computation time needed to predict the characteristics is approximately 1/50th of the time needed by state-variable method

The second and most important feature of the analysis is that it can be used to study the dynamic performance under perturbations in load torque and supply voltage From the analytical expressions developed in this chapter, linearized model and transfer functions of the voltage controlled induction motor can be developed which would help in the design and development of closed loop control schemes This aspect is considered in the next chapter

CHAPTER 6

DYNAMIC ANALYSIS AND DESIGN OF A CLOSED-LOOP SPEED CONTROLLER

6 1 INTRODUCTION

In Chapter 5, analytical expressions for the steady state currents and voltages are derived and expressions for the phase angle ϕ and fundamental Fourier components of stator voltage and current are obtained as function of triggering angle, supply voltage and rotor flux linkages This enables the development of a linearized model of the drive and its associated transfer functions for the study of dynamic response under perturbations in load torque, triggering angle or supply voltage This can be used for the design of closed-loop control systems to regulate speed.

This chapter presents the linearized state space model of the drive Stability of the drive, based on the eigenvalue analysis, is discussed Transfer functions of the drive are developed to predict dynamic response Using these transfer functions, a feedback control scheme is developed to regulate speed An example showing the design of the controller using classical control theory [56] is given The response of the closed-loop system is predicted analytically and checked by experimental investigations

6 2 LINEARIZED MODEL OF AN INDUCTION MOTOR WITH THYRISTOR VOLTAGE CONTROL

In developing this model the stator transients are ignored and the motor is represented by a third order model given by (see Section 4 2 1 of Chapter 4)

$$p\,\psi_{2d} = -R_2\,\psi_{2d}/L_2 - S\omega\,\psi_{2q} + R_2\,m\,i_{1d}/L_2 \qquad (6\ 1)$$

$$p\,\psi_{2q} = -R_2\,\psi_{2q}/L_2 + S\omega\,\psi_{2d} + R_2\,m\,i_{1q}/L_2 \qquad (6\ 2)$$

$$p\,S = -(T_e - T_m)/(\omega\,J) + (1-S)\,D/J \qquad (6\ 3)$$

and

$$T_e = m(i_{1d}\,\psi_{2q} - i_{1q}\,\psi_{2d})/L_2 \qquad (6\ 4)$$

On linearizing equations (6 1 - 6 4) and arranging in matrix form, we get

$$p\begin{bmatrix}\Delta\psi_{2d}\\ \Delta\psi_{2q}\\ \Delta S\end{bmatrix} = [A_1]\begin{bmatrix}\Delta\psi_{2d}\\ \Delta\psi_{2q}\\ \Delta S\end{bmatrix} + B_1\begin{bmatrix}i_{1d}\\ i_{1q}\end{bmatrix} + \underline{c}\,\Delta T_m \qquad (6\ 5)$$

where

$$A_1 = \begin{bmatrix} -R_2/L_2 & -S\omega & -\omega\,\psi_{2q} \\ S\omega & -R_2/L_2 & \omega\,\psi_{2d} \\ \dfrac{m\,i_{1q}}{\omega\,J\,L_2} & \dfrac{-m\,i_{1d}}{\omega\,J\,L_2} & -D/J \end{bmatrix},$$

$$B_1 = \begin{bmatrix} R_2 m/L_2 & 0 \\ 0 & R_2 m/L_2 \\ \dfrac{-m\,\psi_{2q}}{\omega\,J\,L_2} & \dfrac{m\,\psi_{2d}}{\omega J\,L_2} \end{bmatrix}, \qquad \underline{c} = \begin{bmatrix} 0 \\ 0 \\ \dfrac{1}{\omega J} \end{bmatrix}$$

The vector containing Δi_{1d} and Δi_{1q} in equation (6 5) is to be replaced in terms of the state variables $\Delta\psi_{2d}$, $\Delta\psi_{2q}$ and ΔS The relationship between the fundamental components of voltage, current and flux linkages (see equation (5 18) of Chapter 5) is given by

$$\begin{bmatrix} i_{1d} \\ i_{1q} \end{bmatrix} = [V_1] \begin{bmatrix} v_d \\ v_q \end{bmatrix} + [S_1] \begin{bmatrix} \psi_{2d} \\ \psi_{2q} \end{bmatrix} \qquad (6\ 6)$$

where

$$[V_1] = \frac{1}{|Z_1''|^2} \begin{bmatrix} R_1 & -X_1'' \\ X_1'' & R_1 \end{bmatrix}, \quad [S_1] = \frac{\omega_m}{L_2 |Z_1''|^2} \begin{bmatrix} -X_1'' & -R_1 \\ R_1 & -X_1'' \end{bmatrix}$$

On linearizing equation (6 6), we get

$$\begin{bmatrix} \Delta i_{1d} \\ \Delta i_{1q} \end{bmatrix} = [V_1] \begin{bmatrix} \Delta v_d \\ \Delta v_q \end{bmatrix} + [S_1] \begin{bmatrix} \Delta\psi_{2d} \\ \Delta\psi_{2q} \end{bmatrix} \qquad (6\ 7)$$

The fundamental components of the stator voltages (see Section 5 2 4 of Chapter 5) are defined by

$$v_d = \sqrt{\frac{3}{2}}\ \frac{3}{4\pi} \{ (V_m + K\psi_{2d})(\cos 2\alpha - \cos 2\phi) + K\psi_{2q}(\sin 2\alpha - \sin 2\phi + 2\alpha - 2\phi) \} \qquad (6\ 8)$$

$$v_q = \sqrt{\frac{3}{2}}\ \frac{3}{4\pi} \{ -K\psi_{2q}(\cos 2\alpha - \cos 2\phi) + \frac{4\pi}{3} v_m + (V_m + K\psi_{2d})(\sin 2\alpha - \sin 2\phi - 2\alpha + 2\phi) \} \qquad (6\ 9)$$

Linearizing (6 8) and (6.9) and arranging in matrix form, we get

$$\begin{bmatrix} \Delta v_d \\ \Delta v_q \end{bmatrix} = [\,Q\,] \begin{bmatrix} \Delta\psi_{2d} \\ \Delta\psi_{2q} \end{bmatrix} + \underline{q}_1 \Delta\alpha + \underline{q}_2 \Delta\phi + \underline{q}_3 \Delta V_m \qquad (6\ 10)$$

where

$$Q = \sqrt{\frac{3}{2}}\ \frac{3K}{4\pi} \begin{bmatrix} \cos 2\alpha - \cos 2\phi & \sin 2\alpha - \sin 2\phi + 2\alpha - 2\phi \\ \sin 2\alpha - \sin 2\phi - \alpha + 2\phi & -(\cos 2\alpha - \cos 2\phi) \end{bmatrix}$$

$$\underline{q}_1 = \sqrt{\frac{3}{2}}\ \frac{3}{2\pi} \begin{bmatrix} -(V_m + K\psi_{2d})\sin\alpha + K\psi_{2q}(\cos 2\alpha + 1) \\ K\psi_{2q}\sin 2\alpha + (V_m + K\psi_{2d})(\cos 2\alpha - 1) \end{bmatrix}$$

$$\underline{q}_2 = \sqrt{\frac{3}{2}}\ \frac{3}{2\pi} \begin{bmatrix} (V_m + K\psi_{2d})\sin 2\phi - K\psi_{2q}(\cos 2\phi + 1) \\ -K\psi_{2q}\sin 2\phi + (V_m + K\psi_{2d})(-\cos 2\phi + 1) \end{bmatrix}$$

and

$$\underline{q}_3 = \sqrt{\frac{3}{2}}\ \frac{3}{4\pi} \begin{bmatrix} \cos 2\alpha - \cos 2\phi \\ \sin 2\alpha - \sin 2\phi - 2\alpha + 2\phi + 4\pi/3 \end{bmatrix}$$

The term $\Delta\phi$ in equation (6 10) can be obtained from the nonlinear equation defining ϕ The expression for $\Delta\phi$ as derived in Appendix J is

$$\Delta\phi = g^T \begin{bmatrix} \Delta\psi_{2d} \\ \Delta\psi_{2q} \end{bmatrix} + g_3 \Delta\alpha + g_4 \Delta V_m \qquad (6\ 11)$$

g, g_3 and g_4 are defined in Appendix J

Eliminating $\Delta\phi$ from (6 10), we get

$$\begin{bmatrix} \Delta v_d \\ \Delta v_q \end{bmatrix} = [H] \begin{bmatrix} \Delta\psi_{2d} \\ \Delta\psi_{2q} \end{bmatrix} + \underline{h}_1 \Delta\alpha + \underline{h}_2 \Delta V_m \qquad (6\ 12)$$

where

$$[H] = [Q] + [\underline{g}_2 \underline{g}^T], \quad \underline{h}_1 = \underline{g}_1 + \underline{g}_2 g_3 , \quad \underline{h}_2 = \underline{g}_3 + \underline{g}_2 g_4$$

Substituting, equation (6 12) in (6 7),

$$\begin{bmatrix} \Delta i_{1d} \\ \Delta i_{1q} \end{bmatrix} = S_2 \begin{bmatrix} \Delta\psi_{2d} \\ \Delta\psi_{2q} \end{bmatrix} + \underline{j}_1 \Delta\alpha + \underline{j}_2 \Delta V_m \qquad (6\ 13)$$

where

$$[S_2] = [S_1] + [V_1 H] , \quad \underline{j}_1 = [V_1] \underline{h}_1 \text{ and } \underline{j}_2 = [V_1] \underline{h}_2$$

Finally, equation (6 5) becomes of the form

$$\underline{x} = A \underline{x} + \underline{b} u + \underline{c} v + \underline{d} w \qquad (6\ 14)$$

where

$$\underline{x}^T = [\Delta\psi_{2d} \quad \Delta\psi_{2q} \quad \Delta S] , \quad u = \Delta\alpha, \quad v = \Delta T_m , \quad w = \Delta V_m ,$$

$$A = [A_1] + [A_2], \quad [A_2] = [B_1 S_2 \mid C] , \quad \underline{b} = [B_1] \underline{j}_1 , \text{ and}$$

$$\underline{d} = [B_1] \underline{j}_2$$

Let the output vector be defined by

$$y = \Delta S = [0 \quad 0 \quad 1] \underline{x} \qquad (6\ 15)$$

During steady state, the solution of $\underline{x}$ is given by

$$X(s) = (sI-A)^{-1} (\underline{b}\, u(s) + \underline{c}\, v(s) + \underline{d}\, w(s)) \qquad (6\ 16)$$

and output Y(s) is given by

$$Y(s) = [0 \quad 0 \quad 1]\ X(s)$$

$$= G_1(s)\, u(s) + G_2(s)\, v(s) + G_3(s)\, w(s) \qquad (6\ 17)$$

6 3 AN EXAMPLE

The A matrix and its eigenvalues and vectors $\underline{b}$, $\underline{c}$ and $\underline{d}$ of the test machine are numerically computed for an operating point defined by $\alpha = 70°$, $S = 0.05$ and $V_m = 325$ V. Load torque is considered to be proportional to speed, in this example The effect of such a load is to increase the damping coefficient (D) from D to $(D + T_m/\omega_r)$ The computed results are

$$A = \begin{bmatrix} -40\ 868 & -46\ 200 & 103,025 \\ 37\ 206 & 5\ 845 & -229\ 317 \\ -\ 4\ 290 & -\ 2,222 & -\ 2\ 903 \end{bmatrix}, \quad \underline{b} = \begin{bmatrix} 20.92 \\ -26.11 \\ 6.30 \end{bmatrix}$$

$$\underline{c} = \begin{bmatrix} 0 \\ 0 \\ 0\ 796 \end{bmatrix}, \quad \underline{d} = \begin{bmatrix} -0\ 138 \\ 0\ 088 \\ -0\ 027 \end{bmatrix}$$

The eigenvalues are

$$\lambda_{1,2} = -4.889 \pm j\ 34\ 87, \qquad \lambda_3 = -28\ 149$$

The open-loop transfer functions G_1, G_2 and G_3 are

$$G_1(s) = \frac{6\ 315(s^2+30s+851)}{(s+28\ 15)(s^2+9\ 78s+1239\ 8)}$$

$$G_2(s) = \frac{0\ 796(s^2+35s+1480)}{(s+28\ 15)(s^2+9\ 785s+1239\ 8)}$$

$$G_3(s) = \frac{-0\ 027(s^2+20\ 48s+828\ 9)}{(s+28\ 15)(s^2+9\ 78s+1239\ 8)}$$

The block diagram of the motor is given in Fig 6 1

6 4 STABILITY ANALYSIS

The stability of the drive under dynamic operation is determined from the location of the roots of the characteristic equation or eigenvalues of the system The eigenvalues of A matrix defined in (6 14) are obtained numerically for different operating points The loci of complex eigenvalues of the test machine (Table 7 1) are given in Fig 6 2 for constant values of α It is interesting to observe from Fig 6 2 that there is a possibility of instability at speeds very near to rated synchronous speed This phenomena is rather unexpected and is not observed on machines supplied by constant voltage source at rated frequency [57] In order to study this phenomena in more detail and verify its existence nine more machines are studied whose parameters are taken from reference [40] These machines can be divided into two groups (1) with $(R_s/R_r) > 1$ and (2) with $(R_s/R_r) < 1$ where (R_s/R_r) is the ratio of stator to rotor resistance The parameters of these machines are given in Table 6 1. Fig 6 3 gives the loci of eigenvalues for the

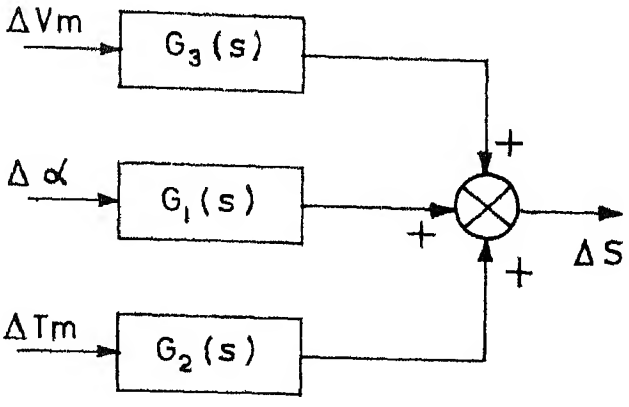

Fig 6 1 Block diagram representation of an induction motor with voltage control

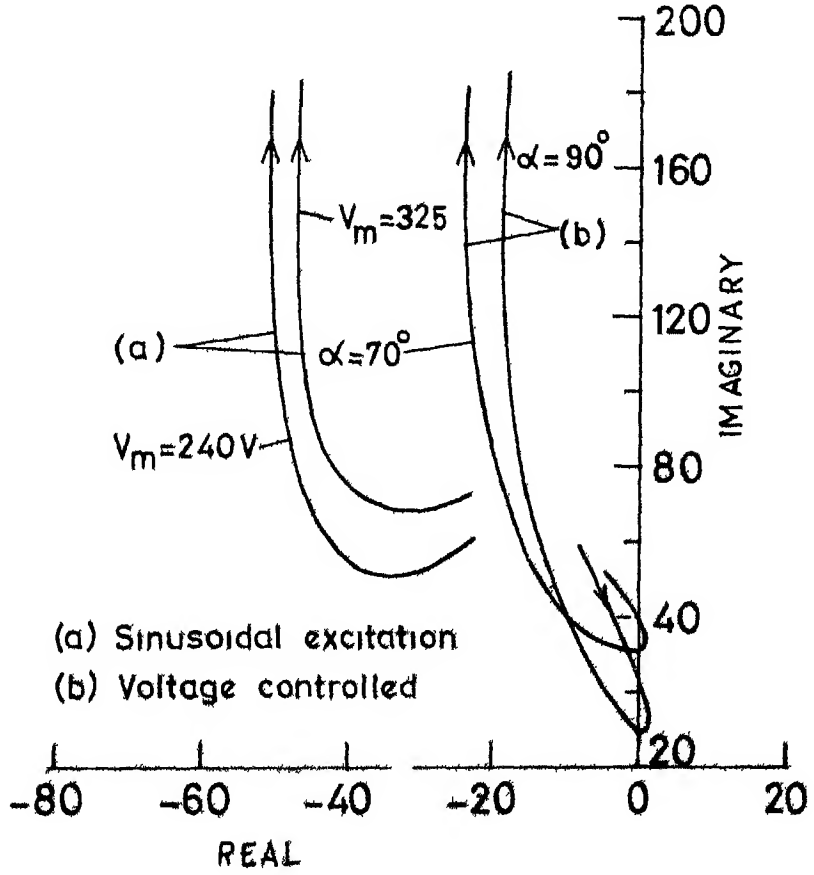

Fig.6.2 Locus of eigenvalues of the test machine

$\alpha' = R_s / R_r$

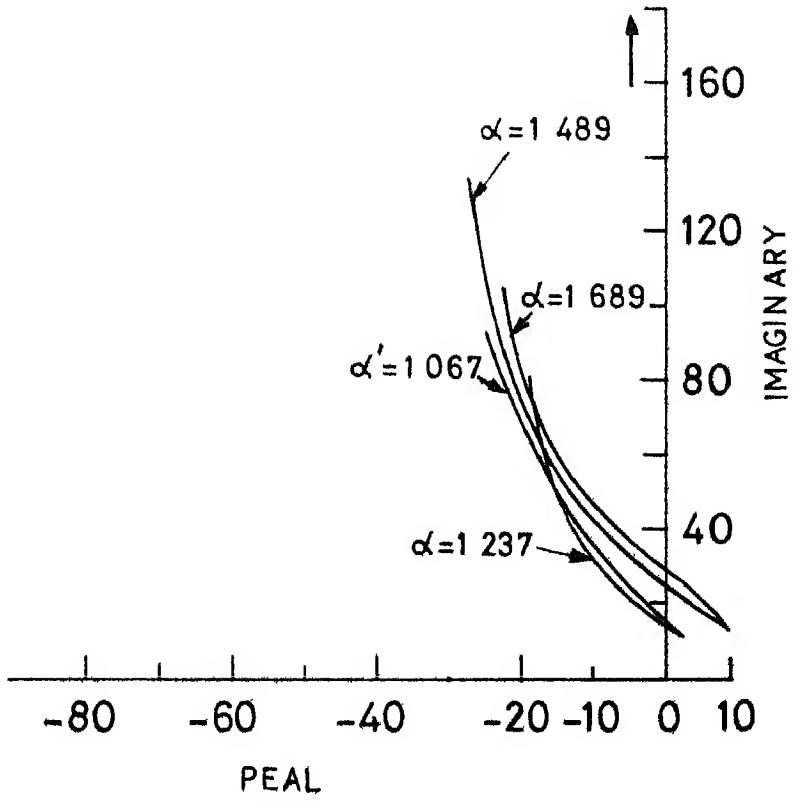

Fig 6 3 Locus of eigenvalues of machines with $\alpha' > 1$

TABLE 6 1

MOTOR PARAMETERS

Sl No	hp	V_{LL}	Poles	Freq	R_r (p u)	$X_1=X_2$ (p u)	X_m (p u)	J	α
1	15	230	4	60	0199	1270	2 073	0 150	1 489
2	30	325	6	50	0250	0873	3 877	2 736	1 067
3	110	364	4	50	0170	1215	4 140	5 000	1 237
4	250	2300	4	60	0141	0864	3 026	3 459	1 698
5	3	220	4	60	0377	0349	1 208	0 044	0 533
6	3	208	6	60	0324	0566	1 026	0 312	0 645
7	3.75	400	4	50	0799	0526	1 127	0 1023	0 415
8	25	460	4	60	0472	0498	1 951	0 277	0.465
9	50	460	4	60	0402	0532	2 306	0 831	0 382

Per unit quantities calculated from $Z_B = V_{LL}^2/(hp \times 746)$

All motors are assumed to be wye connected.

machine with $(R_s/R_r) > 1$ Instability is observed in all these cases It is to be observed that the test machine also has $(R_s/R_r) > 1$ The loci of complex eigenvalues for machines with $(R_s/R_r) < 1$ are plotted in Fig 6 4 It can be observed that the characteristics are quite different from that given in Fig 6 3 There is no instability for voltage controlled motors having (R_s/R_r) less than unity In both cases, real eigenvalue shifts to the right half plane of the s-plane when the operating point shifts to the negative slope region of torque-slip characteristics From these results, it may be conjunctured that voltage controlled induction motors with (R_s/R_r) greater than unity may experience instability very close to the synchronous speed However, this phenomena may not be observed in practice since it occurs for a small region near synchronous speed

Loci of the complex eigenvalues of the test machine with sinusoidal excitation obtained from a linearized third order model (Appendix K) are shown in Fig 6 2 for different input voltages. For a voltage controlled induction motor with sinusoidal excitation, there is no unstable region as can be seen from Fig 6 2, although the value (R_s/R_r) is greater than unity. The complex pair of eigenvalues always lie in the left half of s-plane The dissimilarity of characteristics between the sinusoidal excited operation and thyristor fed, voltage controlled operation

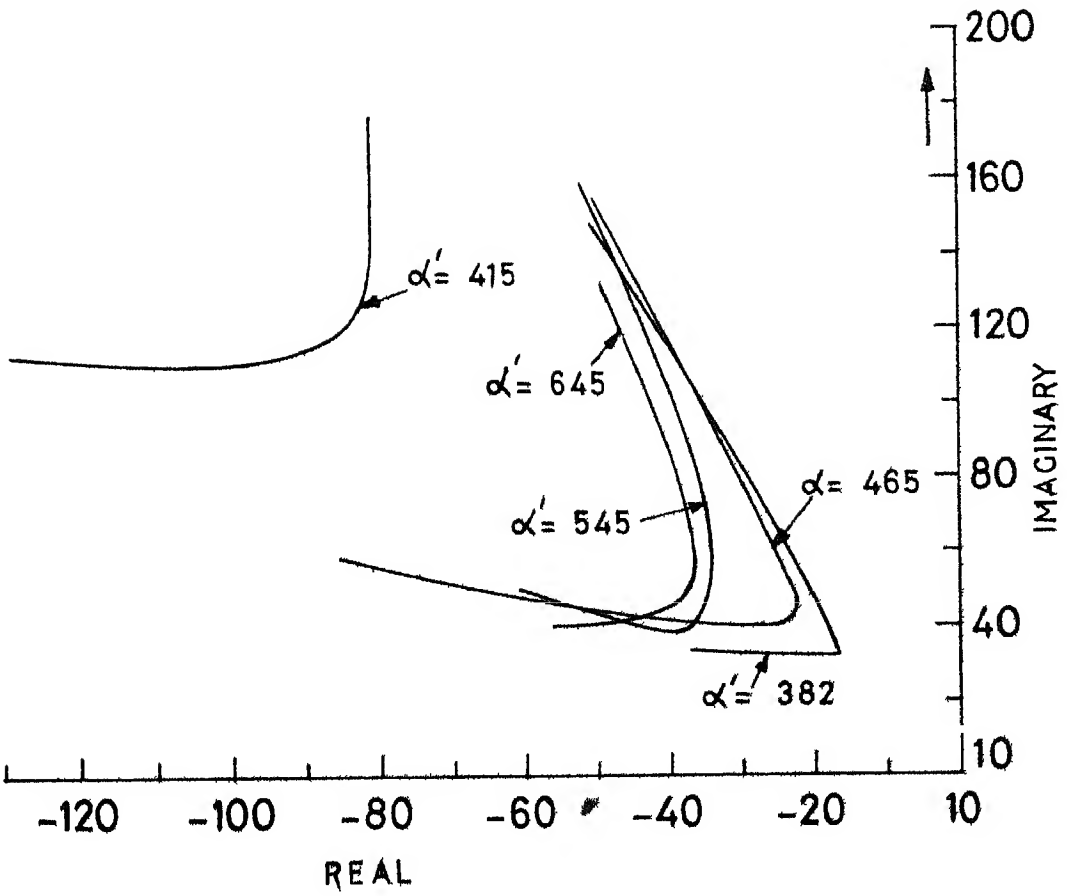

Fig 6 4 Locus of eigenvalues for machines

can be ascribed to the differences in the two cases given below

1) The effective terminal voltage in the case of voltage controlled induction motor is a function of the rotor flux linkages while for a sinusoidally excited motor it is independent of the rotor variables This is noticed from the fact that Δv_d and Δv_q are functions of $\Delta\psi_{2d}$ and $\Delta\psi_{2q}$ (see equation 6 10)

2) The variation of the rotor flux linkages with slip follows a different pattern in the case of thyristor fed motor (see Fig 5.5 of Chapter 5)

3) The effective terminal voltage of a voltage controlled motor changes rapidly with small changes in the slip when the motor is operating near synchronous speed (see Fig 5 6).

Since the region of instability is very small for the test machine, this phenomena could not be observed experimentally.

6.5 DESIGN OF THE CLOSED-LOOP SYSTEM FOR SPEED CONTROL

For precise speed control applications, a closed-loop system with speed feedback is essential In this section, a voltage controlled induction motor in a closed-loop configuration with speed feedback is discussed The transfer functions and block diagram of the open-loop system developed in Sections 6 2 and 6.3 are used for the design of the closed-loop system

6 5.1 Description of the System

A squirrel cage induction motor (test machine) is used as a drive with a mechanically coupled d.c generator for loading. A tacho-generator coupled to the induction motor is used for obtaining a voltage signal proportional to speed The output of the tacho-generator is stepped down by means of a potential divider arrangement The output of the tacho-generator has high ripple content due to the commutator action and it is filtered by means of a first order R-C filter This filtered output which is proportional to the shaft speed is compared with a reference voltage corresponding to the set speed of the drive The error signal is fed to a proportional plus integral (PI) controller to adjust the triggering angle α such that the error signal at the input of the PI controller tends to become zero A precision half wave limiter [51] is used at the output side of the PI controller so that α always lies in the normal working range (0 to 180°) The block diagram of the closed-loop system is given in Fig 6 5

PI Controller for the Speed-loop

The functional diagram of a PI controller is given in Fig 6.6 and the transfer function is given by

$$G_c(s) = \frac{k_c(1+sT_c)}{s} \qquad (6\ 18)$$

where

$$T_c = C_c R_{c2} \quad , \quad k_c = \frac{1}{C_c R_{c1}}$$

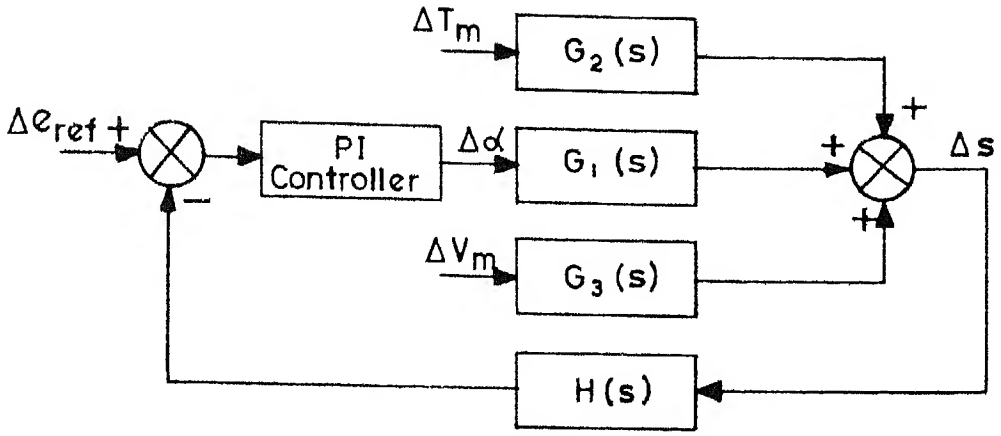

Fig 6 5 Block diagram-closed loop system

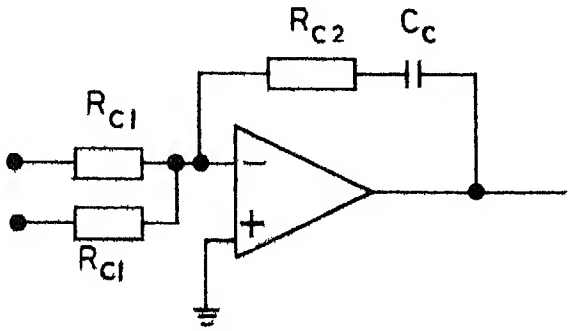

Fig 6 6 PI Controller

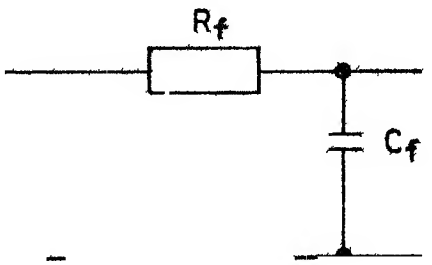

A half wave precision limiter with unity gain is used at the output side of the PI controller to limit the voltage within the allowable limits.

Tacho-generator

The tacho-generator output is stepped down to 3V using a potential divider arrangement corresponding to the maximum speed of the motor (S = 0) The output voltage is assumed to vary linearly and the transfer function is given by

$$H_c(s) = \frac{E(s)}{S(s)} = -3 \qquad (6\ 19)$$

Filter

A first order R-C filter (Fig 6 7) is used to reduce the ripple content of the tacho-generator voltage The transfer function is given by

$$G_f(s) = \frac{1}{1+s\ T_f} \qquad (6\ 20)$$

where

$$T_f = R_f\ C_f$$

Triggering Circuitry

The triggering angle α varies between π and 0 corresponding to an input voltage variation of 0 and 3V and hence the transfer function is given by

$$G_t(s) = \frac{\Delta\alpha(s)}{\Delta e_o(s)} = -\pi/3 = -1 \qquad (6\ 21)$$

6 5.2 Controller Design

Let the operating point be defined by $\alpha = 70°$ and slip $S = 0.05$. The numerical values of the motor transfer functions are given in Section 6.3 for the same α and S. The design of the closed-loop controller involves the determination of gain and time constant of the PI controller and filter used in the feedback path.

The filter time constant T_f is kept large enough to reduce the ripple amplitude and small enough to keep the cut-off frequency $1/T_f$ greater than the gain crossover frequency ω_c. Accordingly T_f is chosen as 8.33 msec.

From stability considerations, the PI-controller time constant T_c is chosen such that the gain crossover frequency occurs at -1 slope and $1/T_c < \omega_c < 1/T_f$ [58,59]. Accordingly T_c is chosen as 250 msec.

The open-loop transfer function of the complete system becomes

$$GH(s) = \frac{0.45\, k_c\, (1 + \frac{s}{4})(1 + \frac{s}{28.3} + \frac{s^2}{851})}{s(1 + \frac{s}{120})(1 + \frac{s}{26.2})(1 + \frac{s}{130} + \frac{s^2}{1185.6})} \qquad (6.22)$$

With the help of a Bode plot, the gain of the controller k_c in equation (6.22) can be determined.

Let

$$GH(s) = \frac{k' A(s) B(s)}{C(s)}$$

where

$$k' = 0.45 k_c$$

$$A(s) = \frac{(1+s/4)}{s(1+s/120)(1+s/26.2)}, \quad B(s) = (1 + s/28.3 + s^2/851)$$

$$C(s) = (1 + s/130 + s^2/1185.6)$$

Bode plots of A(s), B(s), C(s) and GH(s)/k' are shown in Fig 6.8. The gain crossover frequency for a phase margin of 50° is 60 rad/sec and the value of k' corresponding to this value is 15 dB. Therefore,

$$k_c = 12.5$$

6.6 DETERMINATION OF DYNAMIC RESPONSE OF THE CLOSED-LOOP SYSTEM

6.6.1 Experimental Results

On the basis of the design described in the previous section, an electronic circuitry was developed for the controller (see Fig 6.9) and experiments were conducted to determine the dynamic response under closed-loop operation. The PI-controller gain is chosen as 6 although the designed value is 12.5. Mal-operation of the triggering circuit is observed for gain greater than 6. The inability of the circuit to respond to fast input variations may be the cause of mal-operation. Photographs of the dynamic responses due to load perturbations and change in

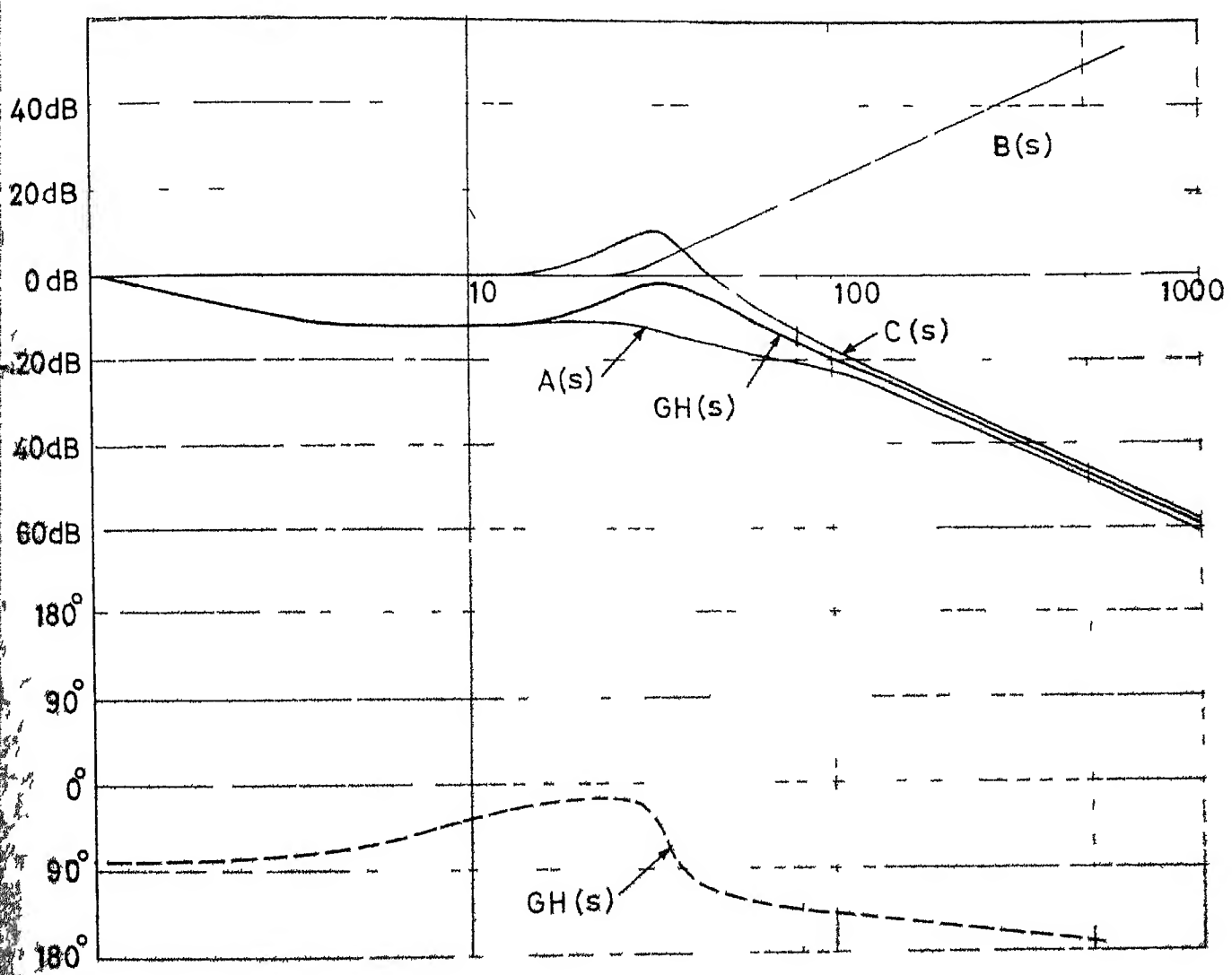

Fig 6 8 Frequency response of the closed loop system

C_{c_1} = 10 μF
R_{c_2} = 2.5 K
R_3 = 5.8 K
R_4 = 9.1 K
= 16.5 K

R_5 = 1.2 K
R_6 = 5.8 K
R_7 = 2.5 K
LI = LM 324
Z_1 = 1Z3 1A

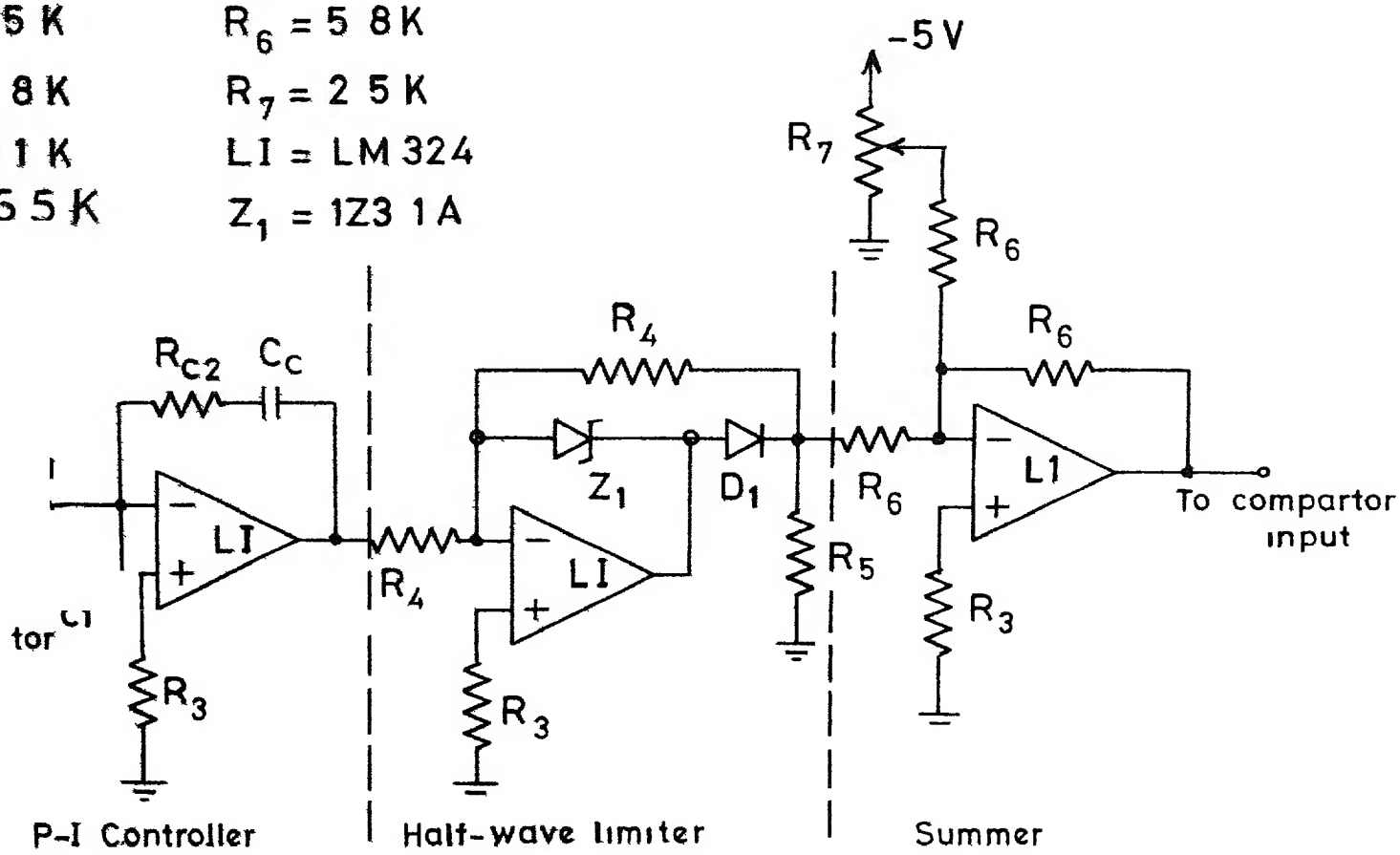

Fig 6.9 Closed loop speed controller

reference voltage are given in Figs. 6.10 to 6.12. Test results for both positive and negative step inputs in load torque shown in Figs.6.10 and 6.11 indicate that the controller is effective during both acceleration and retardation of the motor. It can also be observed that the steady state error in speed due to perturbations in load torque is practically nil. When triggering angle α becomes less than or equal to ϕ, the controller becomes ineffective because any further advancement of α does not have any effect on the motor voltages. In Fig. 6.12, the response due to changes in the reference voltage is given. The response is well damped and the speed settles down to a new value with little overshoot.

In Fig.6.13, the photograph of the experimental set up is shown.

6.6.2 Analytical Results

Transient response of the closed-loop system for perturbations in load torque and reference voltage is obtained by solving the system differential equations. The closed-loop transfer function is transformed into a set of first order differential equations. These equations are numerically solved using fourth order Runge-Kutta method for a unit step input of the disturbance.

The open-loop transfer functions given in Section 6.3 for an operating point of $S = 0.05$ and $\alpha = 70°$ are used for the analysis.

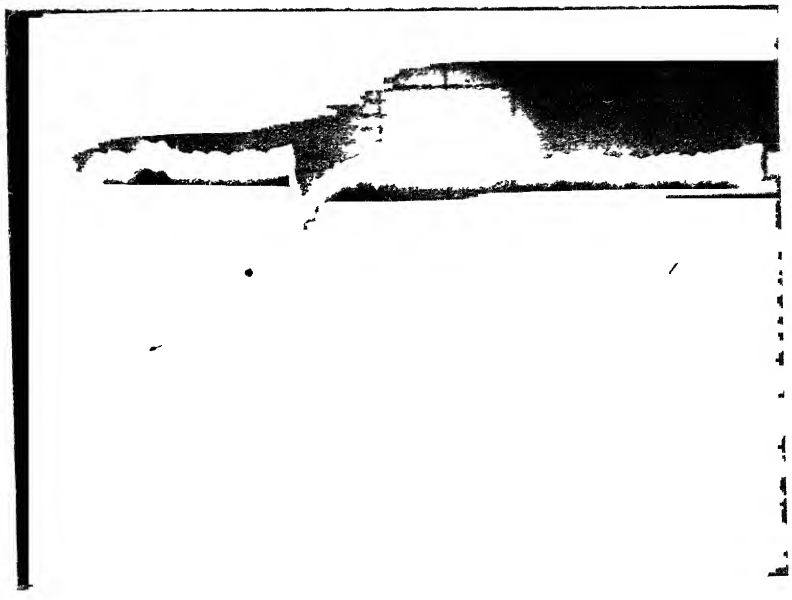

Fig. 6.10 Response due to load perturbation (positive step input) (25 rpm/division, 2 sec/div)

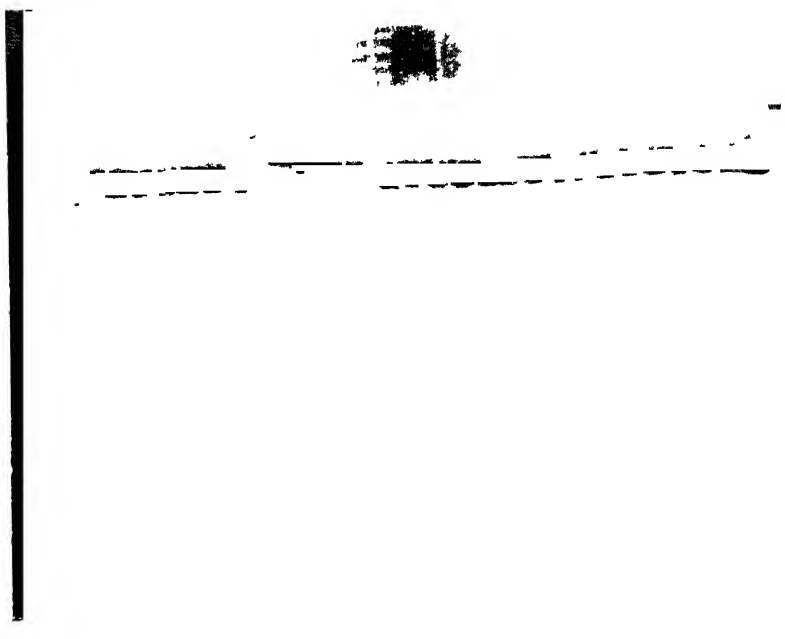

Fig. 6.11 Response due to load perturbation (negative step input)(25 rpm/division, 2 sec/div)

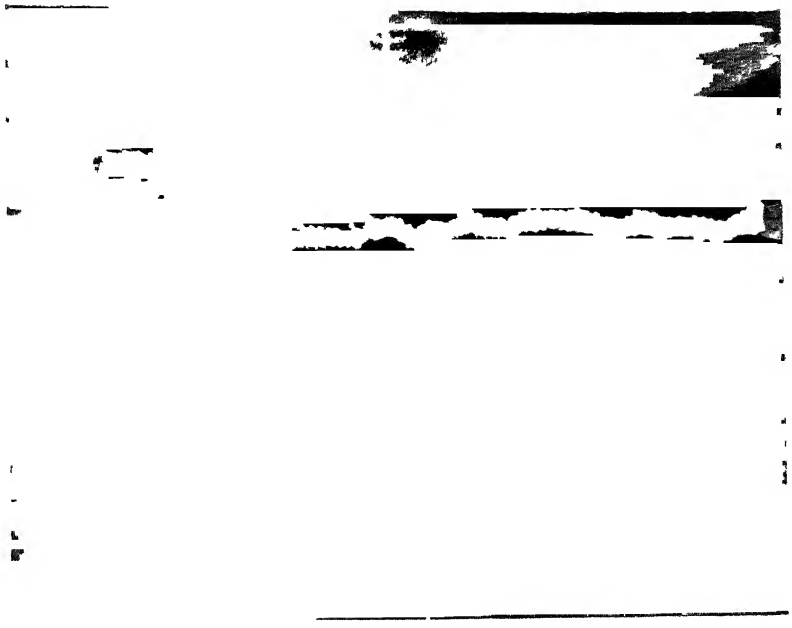

Fig. 6.12 Response due to reference speed perturbation (25 rpm/div, 2 sec/div)

Fig. 6.13 Experimental set-up

For the closed-loop system shown in Fig. 6.5, the closed-loop transfer function is given by

$$\frac{x}{u}(s) = \frac{b_o s^5 + b_1 s^4 + b_2 s^3 + b_3 s^2 + b_4 s + b_5}{s^5 + a_1 s^4 + a_2 s^3 + a_3 s^2 + a_4 s + a_5} \qquad (6.23)$$

The equation (6.23) can be transformed into state space form [60,61] and is given by

$$p \begin{bmatrix} x_1 \\ x_2 \\ x_3 \\ x_4 \\ x_5 \end{bmatrix} = \begin{bmatrix} 0 & 1 & 0 & 0 & 0 \\ 0 & 0 & 1 & 0 & 0 \\ 0 & 0 & 0 & 1 & 0 \\ 0 & 0 & 0 & 0 & 1 \\ -a_5 & -a_4 & -a_3 & -a_2 & -a_1 \end{bmatrix} \begin{bmatrix} x_1 \\ x_2 \\ x_3 \\ x_4 \\ x_5 \end{bmatrix} + \begin{bmatrix} c_1 \\ c_2 \\ c_3 \\ c_4 \\ c_5 \end{bmatrix} u \qquad (6.24)$$

where c's are defined as

$$c_o = b_o \quad ; \quad c_i = b_i - \sum_{m=o}^{i-1} a_{i-m}\, c_m$$

and x is given by

$$x = x_1 + c_o u \qquad (6.25)$$

Response (ΔS) due to Perturbation in Reference Input

x and u in equation (6.23) become ΔS and Δe_{ref} respectively during this case. The coefficients of the variables for the operating point of α = 70 and slip = 0.05 are

$a_1 = 157.9$ $\quad b_o = 0$

$a_2 = 9476.9$ $\quad b_1 = 9.47$

$a_3 = 332685.0$ $\quad b_2 = 1458.4$

$a_4 = 7499927.0$ $\quad b_3 = 47823.5$

$a_5 = 11607980$ $\quad b_4 = 113568$

$b_5 = 3868305$

The solution of equation (6.24) is obtained for u = 1 with all initial values set to zero. The computed result (ΔS) is shown in Fig. 6.14.

Response (ΔS) due to Perturbation in ΔT_m

The coefficients in equation (6.23) can be obtained from the closed-loop transfer function (see Fig. 6.5) relating S to T_m and are given by

$a_1 = 157.9$ $\quad b_o = 0.0$

$a_2 = 9476.9$ $\quad b_1 = 0.796$

$a_3 = 332685$ $\quad b_2 = 123.4$

$a_4 = 7499927$ $\quad b_3 = 4521.3$

$a_5 = 11607980$ $\quad b_4 = 141369$

$b_5 = 0$

For a unit step input in ΔT_m, the solution of equation (6.24) is obtained numerically. The variation of ΔS with respect to time, as computed, is given in Fig. 6.15.

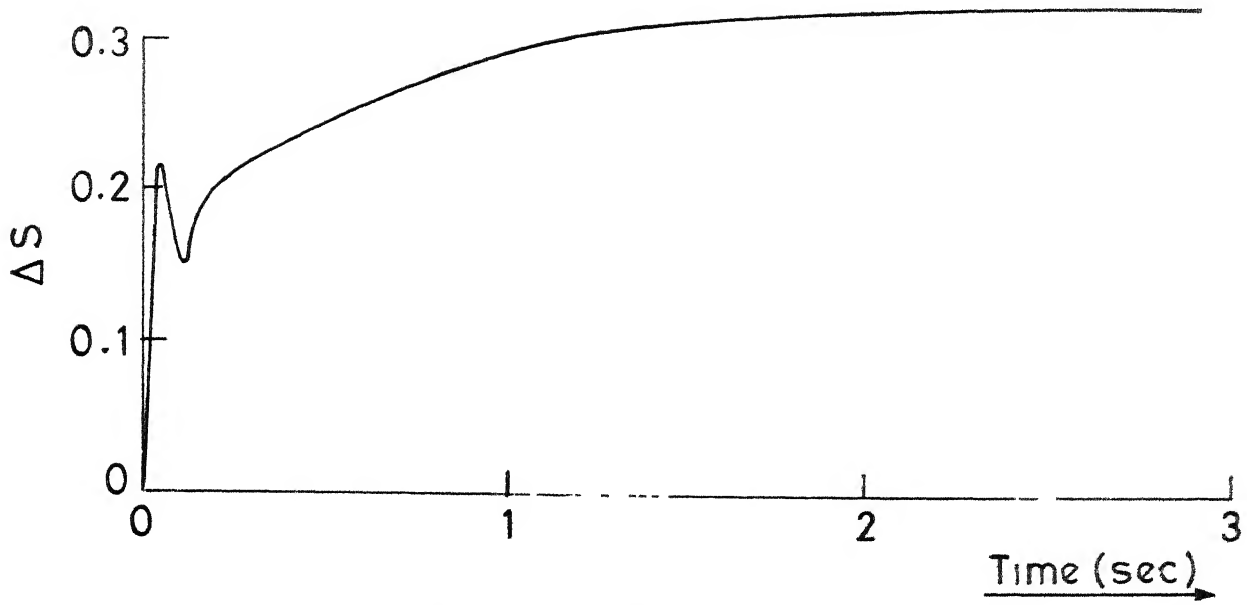

Fig. 6.14 Response due to refrences speed perturbation

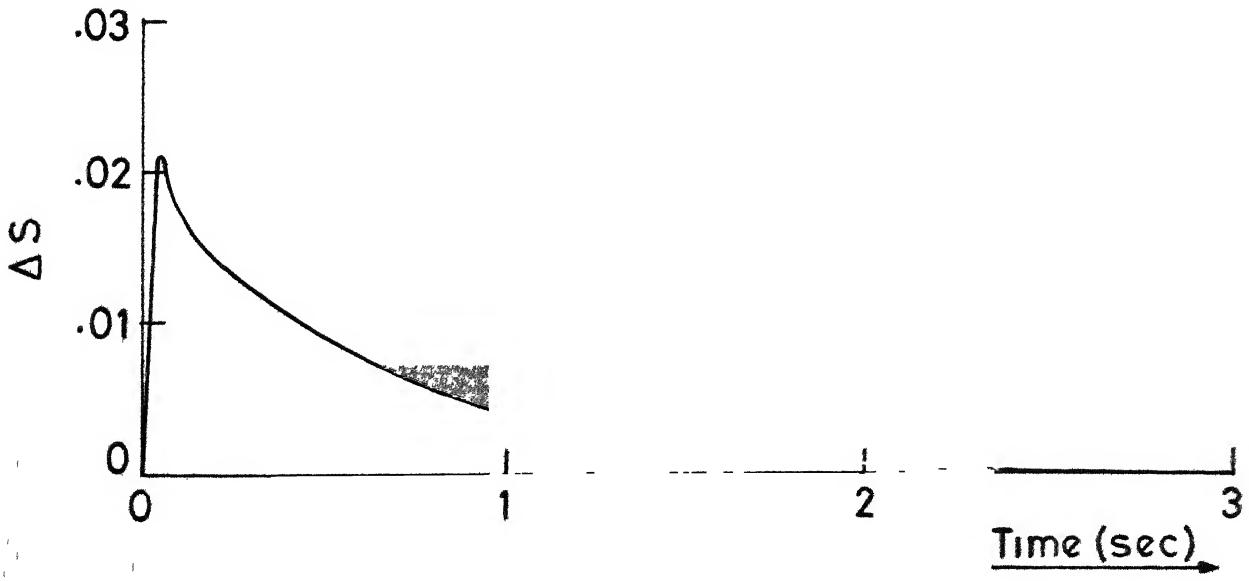

Fig. 6.15 Response due to load perturbation

6.6.3 Discussion

The solution of equation (6.24) is obtained numerically by fourth order Runge-Kutta method. A step size of 0.02 sec. is used for the integration. The computed result (Fig. 6.14) for a disturbance in Δe_{ref} shows that ΔS reaches a steady value of 0.33 in about 2.2 seconds. Comparing with the experimental result given in Fig. 6.12, it can be observed that although the responses are not alike the time needed to reach steady state is nearly same.

The response (ΔS) due to unit step input in ΔT_m, as given in Fig. 6.15, indicates that there is an initial change in slip of 0.02. The system gradually settles down to the initial value of slip in 2.5 seconds. The results of experimental studies (Figs. 6.10 and 6.11) show good correlation with the analytical results. The system could not be operated at the designed value of the controller gain and the operating value had to be reduced. This may be because the dynamics of the triggering circuit is not taken into account when the controller gain is designed.

6.7 CONCLUSIONS

A third order, small signal model of a voltage controlled induction motor drive is developed. It is observed from the eigenvalues of the system that instability may occur near about maximum speed for motors having (R_s/R_r) greater than unity. The

Instability is not observed for induction motors with constant input voltage at rated frequency.

The transfer functions between slip S and small changes in α , T_m and V_m are derived. A closed-loop control system with speed as feedback is designed and developed for the test machine. The response due to load and reference speed perturbations are experimentally observed and analytically verified.

CHAPTER 7

CONCLUSION

7.1 GENERAL

The major aim of this thesis has been to provide a comprehensive analysis of the steady state and transient performance of induction motors with voltage control using thyristors. The application of voltage controlled induction motor drives requires a proper design and selection of the motor for reliable operation and hence, the knowledge of the transient and steady state performance of the drive is of great importance. The earlier approaches to the steady state analysis are based on state space techniques and harmonic equivalent circuits and the limitation of these approaches is either the lack of generality or the computational complexity. Very few articles dealing with the analysis of transient performance of voltage controlled induction motor drives during open-loop and closed loop operations have appeared in literature. This is mainly because of the lack of suitable models for the analysis. This thesis has presented two novel hybrid models of an induction motor. One of which is well suited for the transient and steady state analyses of voltage-controlled induction motor drive under wide range of operating conditions. Specific contributions made in the thesis are reviewed in subsequent sections.

7.2 STEADY STATE ANALYSIS OF THYRISTOR VOLTAGE CONTROLLED DRIVES

The generality of the BVA in the steady state analysis of voltage controlled induction motor drives has been illustrated in Chapters 2 and 3 where the steady state analysis and simulation of a motor with

a) a pair of back-to-back connected thyristors in each line (Chapter 2),

b) delta connected thyristor bank at the open neutral of the stator winding (Chapter 3), and

c) back-to-back connected thyristor-diode pairs in each line (Chapter 3)

have been presented. In the BVA approach, the motor equations are invariant while the different modes of operation, are accounted by altering the forcing voltages. The open circuit condition is simulated by applying an equal but opposite voltage to the open circuited winding so as to force a current zero condition in the winding.

A comparative study of the performance of the drives with different thyristor configurations has also been presented.

7.3 CIRCUIT MODELS OF INDUCTION MOTORS

For easier formulation of thyristor controlled drives, it is necessary to have a three phase circuit model of the machine, which retains the identity of the motor terminals

and yet is computationally simple. Two novel hybrid models of an induction motor have been described, one particularly suitable for stator controlled machines while the other is well suited for rotor controlled machines. Simple, three phase equivalent circuits have been presented which can accomodate any external terminal constraints. The need for the inversion of a time dependent matrix is eliminated in this model. Using one of the hybrid circuit models, the formulation of state equations for different terminal conditions has been described with the application of network theory. The simulation results indicate that the rotor flux linkages referred to a synchronously revolving reference frame are essentially constants during steady state even when the stator current contains large harmonic components. This implies that the constant component of the torque , as per the model presented in Chapter 4, is produced solely by the fundamental component of current during steady state. This fact is of great significance in developing models suitable for the analysis of closed loop systems.

7.4 PREDICTION OF STEADY STATE CHARACTERISTICS

Determination of the steady state characteristics of a voltage controlled induction motor drive generally involves numerical integration or evaluation of state transition matrix over a certain duration. In Chapter 5, a simplified analysis has been described by which the steady state characteristics such as average torque, phase angle ϕ , fundamental

components of stator current and voltage can be obtained accurately by solving three nonlinear algebraic equations by Newton-Raphson method. Computationally, this method is much faster compared to other methods.

Another advantage is that a direct relationship between the motor performance and control variables is available. This is necessary for the analysis and design of closed-loop systems for speed control applications.

7.5 STABILITY ANALYSIS

No work has been reported in the previous literature on the stability aspect of voltage controlled induction motors using thyristors. From eigenvalue analysis, it is observed that the induction motor drive experiences instability during a narrow range of operation close to synchronous speed. From a case study of 9 machines, it is observed that machines with (R_s/R_r) greater than unity show a tendency for instability at near maximum speed when subjected to voltage control using thyristors.

7.6 DYNAMIC ANALYSIS OF THE DRIVE WITH FEEDBACK

Using a linear model of the drive and its associated transfer functions, a closed-loop system with speed feedback has been designed and developed. Dynamic response due to perturbations in load torque and reference speed has been obtained both analytically and experimentally.

7.7 SUGGESTION FOR FUTURE WORK

The following topics are suggested for future work :

1) One of the hybrid models developed in Chapter 4 has been used for the digital simulation of voltage controlled induction motor drives. The same model can be used for the digital simulation of other types of stator controlled machines such as inverter-fed drives.

   Although a model suitable for rotor controlled machines is developed in Chapter 4, it has not been used since it does not come under the purview of this thesis. This model can be used for the digital simulation of rotor controlled machines.

2) A detailed study of the stability aspect of voltage controlled drives may be undertaken to investigate the causes of instability observed in certain category of machines.

3) The study of the closed-loop system presented in Chapter 6 is of preliminary nature. A comprehensive study of the closed-loop system incorporating other types of feedbacks such as current feedback and a detailed analysis using modern control theory can be undertaken.

REFERENCES

1. S.B, Dewan and A. Straughen. Power Semiconductor Circuits, New York: John Wiley & Sons, 1975.

2. M.S. Erlicki, J. Ben Uri and Y. Wallach, "Switching drive of induction motors", Proc. IEE (London), vol. 110, pp. 259-265, August 1963.

3. M. Ramamoorty, Thyristors and their Applications, New Delhi: East West Press, 1977.

4. D.A. Paice, "Induction motor speed control by stator voltage control", IEEE Trans. Power Apparatus and Systems, vol. PAS-87, pp. 585-590, February 1968.

5. B.D. Bedford and R.G. Hoft, Principles of Inverter Circuits, New York: Wiley, 1964.

6. L. Abraham, J. Forster and G. Schliephake, "A.C. motor supply with thyristor converters", IEEE Trans. Industry and General Applications, vol. IGA-2, pp. 334-340, September/October 1966.

7. B. Mokrytzki, "The controlled slip static inverter drive", IEEE Trans. Industry and General Applications, vol. IGA-4, pp. 312-317, May/June 1968.

8. M. Ramamoorty, "Steady-state analysis of inverter driven induction motor using harmonic equivalent circuits", Proceedings of Industry Applications Annual Meeting 1973, (IEEE), pp. 437-440.

9. K.P. Phillips, "Current source inverter for a.c. motor drives", IEEE Trans. Industry Applications, vol. IA-8, pp. 679-683, November/December 1972.

10. B.R. Pelly, Thyristor Phase-Controlled Converters and Cycloconverters, New York: Wiley-Interscience, 1971.

11. W. Shepherd and J. Stanway, "The polyphase induction motor controlled by firing angle adjustment of silicon controlled rectifiers", IEEE International Convention Record, vol. 12, pp. 135-154, 1964.

12. W. Shepherd, "On the analysis of the three-phase induction motor with voltage control by thyristor switching", IEEE Trans. Industry and General Applications, pp. 304-311, May/June 1968.

13. T.J. Takeuchi, Theory of SCR Circuit and Application to Motor Control, Tokyo: Tokyo Electrical Engineering College Press, 1968.

14. T.A. Lipo, "The analysis of induction motors with voltage control by symmetrically triggered thyristors", IEEE Trans. Power Apparatus and Systems, vol. PAS-90, pp. 515-524, March/April 1971.

15. M. Ramamoorty and M.F. Samek, "Steady state analysis of phase controlled induction motor with isolated neutral", IEEE Trans. Industrial Electronics and Control Instrumentation, vol. IECI-23, pp. 178-184, May 1976.

16. R.E. Bedford and V.D. Nene, "Voltage control of three-phase induction motor by thyristor-switching: a time domain analysis using the α- β-o transformation", IEEE Trans. Industry and General Applications, vol. IGA-6, pp. 553-562, November/December 1970.

17. B. Ilango and M. Ramamoorty, "Steady state analysis of thyristor controlled three phase induction motors using state space technique", Annual Meeting of the IEEE Industry Application Society, Milwaukee, Wis. pp. 1165-1172, October 1973.

18. S. Rahman and W. Shepherd, "Thyristor and diode controlled variable voltage drives for 3-phase induction motors", Proc. IEE,(London), vol. 124, pp. 784-790, September 1977.

19. M. Arunachalam, "Solid state speed control of induction motors", Ph.D. Thesis, IIT Kanpur, 1977.

20. E.D. Spooner, "Three-phase three-thyristor voltage control scheme", IEEE Trans. Industry Applications, vol. IA-11, pp. 478-482, September/October 1975.

21. N. Hayashi, "Analysis of induction motors controlled by symmetrically triggered delta-connected thyristors", Electrical Engineering in Japan, vol. 92-B, No.5, pp. 105-115, 1972.

22. W. McMurray, "A comparative study of symmetrical three-phase circuits for phase controlled a.c. motor drives", IEEE Trans. Industry Applications, vol. IA-10, pp.403-411, May/June 1974.

23. H.C. Stanley, "An analysis of induction machines", Trans. American Institute of Electrical Engineers, vol. 57, pp. 751-757, 1938.

24. H.E. Jordan, "Digital computer analysis of induction machines in dynamics systems", IEEE Trans. Power Apparatus and Systems, vol. PAS-86, pp. 722-728, June 1967.

25. I.R. Smith and S. Sriharan, "Transient performance of the induction motor", Proc. IEE (London), vol. 113, pp. 1173-1181, July 1966.

26. P.C. Krause, "Method of multiple reference frame applied to the analysis of symmetrical induction machinery", IEEE Trans. Power Apparatus and Systems, vol. PAS-87, pp. 218-234, January 1968.

27. Y. Saito and K. Miyazawa, "Digital simulation of poly-phase induction motors", Computer Metnods in Applied Mechanics and Engineering, 6 (1975) pp. 249-264.

28. A.K. De Sarkar and G.J. Berg, "Digital simulation of three-phase induction motors", IEEE Trans. Power Apparatus and Systems, vol. PAS-89, pp. 1031-1037, July/August 1970.

29. S.D.T. Robertson and K.M. Hebbar, "A digital model for three phase induction machines", IEEE Trans. Power Apparatus and Systems, vol. PAS-88, pp. 1624-1634, November 1969.

30. R.S. Ramshaw and K.R. Padiyar, "Generalized system model for slipring machines", Proc. IEE (London), vol.120, pp. 647-658, June 1973.

31. K.R. Padiyar and R.S. Ramshaw, "Dynamic analysis of multi-machine power systems", IEEE Summer Meeting and International Symposium on High Power Testing, Portland, Ore, pp. 526-535, July 1971.

32. A.M. Wahl and L.A. Kilgore, "Transient starting torques in induction motors", Trans. American Institute of Electrical Engineers, 59, p. 603, 1940.

33. T.J. Takeuchi, "Starting transient torque of squirrel cage induction motor", ETJ Japan, 6, (3/4), p. 120, 1961.

34. F.M. Hughes and A.S. Aldred, "Transient characteristics and simulation of induction motors", Proc. IEE (London), vol. vol. 111, p. 2041, 1964.

35. R.W. Ager, "Transient overspeeding of induction motors", Trans. American Institute of Electrical Engineers, 60, p. 1030, 1941.

36. E.S. Gifillan and E.L. Kaplan, "Transient torques in squirrel-cage induction motors with special reference to plugging", Trans. American Institute of Electrical Engineers, 60, p. 1200, 1941.

37. P.J. Lawrenson and J.M. Stephenson, "Note on induction-machine performance with a variable-frequency supply", Proc. IEE (London), vol. 113, October 1966.

38. P.C. Krause and C.H. Thomas, "Simulation of symmetrical induction machinery", IEEE Trans.Power Apparatus and Systems, vol. PAS-84, pp. 1038-1053, November 1965.

39. D.W. Novotny and J.H. Wouterse, "Induction machine transfer functions and dynamic response by means of complex time variable", IEEE Trans. Power Apparatus and Systems, vol. PAS-95, pp. 1325-1335, July/August 1976.

40. R. Stern and D.W. Novotny, "A simplified approach to the determination of induction machine dynamic response", IEEE Trans. Power Apparatus and Systems, vol. PAS-97, pp. 1430-1439, July/August 1978.

41. W.L. Kenly and B.K. Bose, "Triac speed control of three-phase induction motor with phase-locked loop regulation", IEEE Trans. Industry Applications, vol. IA-12, pp. 492-498, September/October 1976.

42. W. Shepherd and J. Stanway, "An experimental closed loop drive incorporating a thyristor driven induction motor", IEEE Trans. Industry and General Applications, pp. 559-565, November/December 1967.

43. K.Y.G. Li, "Analysis and operation of an inverter-fed variable-speed induction motor", Proc. IEE (London), vol. 116, pp. 1571-1580, September 1969.

44. K.R. Rao and V.V. Sastry, "Current fed induction motor analysis using boundary value approach", IEEE Trans. Industrial Electronics and Control Instrumentation, vol. IECI-24, pp. 178-182, May 1977.

45. K.R. Rao, "Analysis of inverter-fed asynchronous-machine drives", Ph.D. Thesis, IIT Madras, 1977.

46. N.G. Hingorani, R.E. Crosbie and McConnach, "Steady state simulation of h.v.d.c. converters by digital computers", Proc. IEE (London), vol. 115(5), pp. 703-710, 1968.

47. R. Simard and V. Rajagopalan, "Economical equidistant pulse firing scheme for thyristorized D.C. drives", IEEE Trans. Industrial Electronics and Control Instrumentation, vol. IECI-22, pp. 425-429, 1975.

48. B. Adkins and R.G. Harley, The General Theory of Alternating Current Machines, London: Chapman and Hall, 1975.

49. H.N. Hancock, Matrix Analysis of Electrical Machinery, London: Pergamon Press, 1964.

50. R. L. Morris and J.R. Miller, Designing with TTL Integrated Circuits, Tokyo: McGraw-Hill, Kogakusha Ltd. 1971.

51. J.D. Graeme, G.E. Tobey and L.P. Huelsman, Operational Amplifiers, Tokyo: McGraw-Hill, 1971.

52. D.W. Novotny, Discussion of 28 , IEEE Trans. Power Apparatus and Systems, vol. PAS-89, p. 1037, July/August 1970.

53. G. Krons, Tensors for Circuits, New York: Dover, 1959.

54. J. Millman, "A useful network theorem", Proc. IRE, vol.28, pp. 413-417, September 1940.

55. A.F. Ralston and H.S. Wilf, Mathematical Methods for Digital Computers, New York: Wiley & Sons, Inc., 1960.

56. J.J. D'Azzo and C.H. Houpis, Feedback Control System Analysis and Synthesis, New York: McGraw-Hill Book Co., 1960.

57. G.J. Rogers, "Linearised analysis of induction-motor transients", Proc. IEE (London), vol. 112, pp. 1917-1926, October, 1965.

58. T. Krishnan and B. Ramaswami, "Slip ring induction motor speed control using thyristor inverters", Automatica, vol. 11, pp. 419-424, 1975.

59. N.S. Wani, "Thyristor controllers for slip ring induction motors", Ph.D. thesis, November 1978, IIT Kanpur, India.

60. J.C. Hsu and A.U. Meyer, Modern Control Principles and Applications, New York: McGraw-Hill, 1968.

61. K. Ogata, State Space Analysis of Control Systems, London: Prentice Hall International, 1967.

62. T.J. Takeuchi, "Characteristics of a.c. motors controlled by general periodic voltage", Electrical Engineering in Japan, vol. 90, No.6, pp. 26-37, 1970.

APPENDIX A

BOUNDARY RELATIONSHIP BETWEEN FINAL AND INITIAL VECTORS AT A DISTANCE OF $\pi/3$

Since the voltages v_{as}, v_{bs} and v_{cs} are half wave symmetric

$$v_{as}(\omega t + \pi) = -v_{as} \tag{A.1}$$

$$v_{bs}(\omega t + \pi) = -v_{bs} \tag{A.2}$$

$$v_{cs}(\omega t + \pi) = -v_{cs} \tag{A.3}$$

In addition, these three-phase voltages are displaced by $2\pi/3$ radians. Hence,

$$v_{bs}(\omega t + 2\pi/3) = v_{as}(\omega t) \tag{A.4}$$

$$v_{cs}(\omega t + 2\pi/3) = v_{bs}(\omega t) \tag{A.5}$$

$$v_{as}(\omega t + 2\pi/3) = v_{cs}(\omega t) \tag{A.6}$$

Increasing the arguments of equations (A.4 - A.6) by $\pi/3$, and substituting the results in (A.1 - A.3) yields

$$v_{as}(\omega t + \pi/3) = -v_{bs}(\omega t) \tag{A.7}$$

$$v_{bs}(\omega t + \pi/3) = -v_{cs}(\omega t) \tag{A.8}$$

$$v_{cs}(\omega t + \pi/3) = -v_{as}(\omega t) \tag{A.9}$$

The relationship between d-q and phase variables are

$$v_{as} = \sqrt{2/3}\, v_{ds} \tag{A.10}$$

$$v_{bs} = -1/\sqrt{6}\, v_{ds} - 1/\sqrt{2}\, v_{qs} \tag{A.11}$$

$$v_{cs} = -1/\sqrt{6}\, v_{ds} + 1/\sqrt{2}\, v_{qs} \tag{A.12}$$

Substituting equations (A.10 - A.12) in (A.7 - A.9), we get

$$\begin{bmatrix} v_{ds} \\ v_{qs} \end{bmatrix}_{(\omega t + \pi/3)} = \begin{bmatrix} 1/2 & \sqrt{3}/2 \\ -\sqrt{3}/2 & 1/2 \end{bmatrix} \begin{bmatrix} v_{ds} \\ v_{qs} \end{bmatrix}_{(\omega t)} \tag{A.13}$$

Similar relationship holds good for the variables V_{s1}, V_{s2}, V_{r1} and V_{r2}.

i.e.,

$$\begin{bmatrix} V_{s1} \\ V_{s2} \\ V_{r1} \\ V_{r2} \end{bmatrix}_{(\omega t + \pi/3)} = \begin{bmatrix} 1/2 & \sqrt{3}/2 & 0 & 0 \\ -\sqrt{3}/2 & 1/2 & 0 & 0 \\ 0 & 0 & 1/2 & \sqrt{3}/2 \\ 0 & 0 & -\sqrt{3}/2 & 1/2 \end{bmatrix} \begin{bmatrix} V_{s1} \\ V_{s2} \\ V_{r1} \\ V_{r2} \end{bmatrix}_{(\omega t)} \tag{A.14}$$

APPENDIX B

BOUNDARY RELATIONSHIP BETWEEN THE FINAL AND INITIAL VECTORS AT A DISTANCE OF $2\pi/3$

Three phase symmetry demands that

$$v_{bs}(\omega t + 2\pi/3) = v_{as}(\omega t) \tag{B.1}$$

$$v_{cs}(\omega t + 2\pi/3) = v_{bs}(\omega t) \tag{B.2}$$

$$v_{as}(\omega t + 2\pi/3) = v_{cs}(\omega t) \tag{B.3}$$

The phase voltages are related to the d-q voltages by

$$v_{as} = \sqrt{2/3}\, v_{ds} \tag{B.4}$$

$$v_{bs} = -1/\sqrt{6}\, v_{ds} - 1/\sqrt{2}\, v_{qs} \tag{B.5}$$

$$v_{cs} = -1/\sqrt{6}\, v_{ds} + 1/\sqrt{2}\, v_{qs} \tag{B.6}$$

Substituting equations (B.4 - B.6) in (B.1 - B.3), we get

$$\begin{bmatrix} v_{ds} \\ v_{qs} \end{bmatrix}_{(\omega t + \frac{2\pi}{3})} = \begin{bmatrix} -1/2 & \sqrt{3}/2 \\ -\sqrt{3}/2 & -1/2 \end{bmatrix} \begin{bmatrix} v_{ds} \\ v_{qs} \end{bmatrix}_{(\omega t)} \tag{B.7}$$

Similar relationship holds good for the vector $[\, V_{s1}\ V_{s2}\ V_{r1}\ V_{r2}\,]^T$

$$\begin{bmatrix} V_{s1} \\ V_{s2} \\ V_{r1} \\ V_{r2} \end{bmatrix}_{(\omega t + 2\pi/3)} = \begin{bmatrix} -1/2 & \sqrt{3}/2 & 0 & 0 \\ -\sqrt{3}/2 & -1/2 & 0 & 0 \\ 0 & 0 & -1/2 & \sqrt{3}/2 \\ 0 & 0 & -\sqrt{3}/2 & -1/2 \end{bmatrix} \begin{bmatrix} V_{s1} \\ V_{s2} \\ V_{r1} \\ V_{r2} \end{bmatrix}_{(\omega t)} \tag{B.8}$$

APPENDIX C

ELECTROMAGNETIC TORQUE IN A MOTOR WITH 3-PHASE STATOR AND 2-PHASE ROTOR

The general expression for the electromagnetic torque is

$$T_e = 1/2\, i^T \frac{\partial L}{\partial \theta_r} i \qquad (C.1)$$

Referring to equations (4.1 - 4.4)

$$i^T = [i_s^T \quad i_r^T] \; ; \quad i_s^T = [i_{1a} \; i_{1b} \; i_{1c}] \, ,$$

$$i_r^T = [i_{2\alpha} \quad i_{2\beta}] \; ; \; \frac{\partial L}{\partial \theta_r} = \begin{bmatrix} 0 & N \\ N^T & 0 \end{bmatrix} ,$$

$$N = L_{12} \begin{bmatrix} -\sin\theta_r & \cos\theta_r \\ -\sin(\theta_r - 2\pi/3) & \cos(\theta_r - 2\pi/3) \\ -\sin(\theta_r + 2\pi/3) & \cos(\theta_r + 2\pi/3) \end{bmatrix}$$

Therefore,

$$T_e = \frac{1}{2} [i_s^T \quad i_r^T] \begin{bmatrix} 0 & N \\ N^T & 0 \end{bmatrix} \begin{bmatrix} i_s \\ i_r \end{bmatrix}$$

i.e.

$$T_e = i_s^T N i_r \qquad (C.2)$$

Equations (4.18) and (4.4) are rewritten as

$$i_s = C_1 i_{1dq} \qquad (C.3)$$

$$i_r = \frac{1}{L_2} \{ \psi_r - M^T i_s \} \qquad (C.4)$$

where

$$C_1 = \sqrt{2/3}\begin{bmatrix}\cos\theta_o & \sin\theta_o \\ \cos(\theta_o-2\pi/3) & \sin(\theta_o-2\pi/3) \\ \cos(\theta_o+2\pi/3) & \sin(\theta_o+2\pi/3)\end{bmatrix},\quad i_{1dq}^T = [\,i_{1d} \quad i_{1q}\,]$$

$$M^T = L_{12}\begin{bmatrix}\cos\theta_r & \cos(\theta_r-2\pi/3) & \cos(\theta_r+2\pi/3) \\ \sin\theta_r & \sin(\theta_r-2\pi/3) & \sin(\theta_r+2\pi/3)\end{bmatrix},\quad \psi_r^T = [\psi_{2\alpha} \quad \psi_{2\beta}\,]$$

The relationship between $\alpha-\beta$ and d-q variables is

$$\psi_r = C_2\,\psi_{2dq} \tag{C.5}$$

where

$$C_2 = \begin{bmatrix}\cos(\theta_o-\theta_r) & \sin(\theta_o-\theta_r) \\ -\sin(\theta_o-\theta_r) & \cos(\theta_o-\theta_r)\end{bmatrix},\quad \psi_{2dq}^T = [\,\psi_{2d} \quad \psi_{2q}\,]$$

Substituting equations (C.3 - C.5) in (C.2) and after simplification, we get

$$T_e = \sqrt{3/2}\,\frac{L_{12}}{L_2}\,(i_{1d}\,\psi_{2q} - i_{1q}\,\psi_{2d}) \tag{C.6}$$

APPENDIX D

RELATIONSHIP BETWEEN THE PARAMETERS OF THE HYBRID MODEL AND CONVENTIONAL PASSIVE EQUIVALENT CIRCUIT

Let the two-axis rotor currents in the hybrid model be

$$i_{\alpha}^{r} = I_r \cos(\theta_r - \theta_o) \tag{D.1}$$

and

$$i_{\beta}^{r} = -I_r \sin(\theta_r - \theta_o) \tag{D.2}$$

The stator flux linkage is given by

$$\begin{aligned}\psi_a^s &= (L_1 - L_{11})i_{1a} + L_{12}\cos\theta_r I_r \cos(\theta_r - \theta_o) + \\ &\qquad L_{12}\sin\theta_r I_r \sin(\theta_r - \theta_o) \\ &= (L_1 - L_{11})i_{1a} + L_{12} I_r \cos\theta_o \\ &= (L_1 - L_{11})i_{1a} + L_{12} i_{\alpha}^{r} \\ &= (L_1 - L_{11})i_{1a} + \sqrt{3/2}\, L_{12} i_a^r \end{aligned} \tag{D.3}$$

where i_{α}^{r} and i_a^r are the rotor currents referred to the stator. Referring to the conventional passive equivalent circuit (Fig. D.1(a)), the stator flux linkage is

$$\psi_a^s = L_s i_{1a} + m i_a^r \tag{D.4}$$

where

$$m = X_m/\omega \,, \quad L_s = X_s/\omega = (X_m + X_{sl})/\omega$$

Comparing equations (D.3) and (D.4)

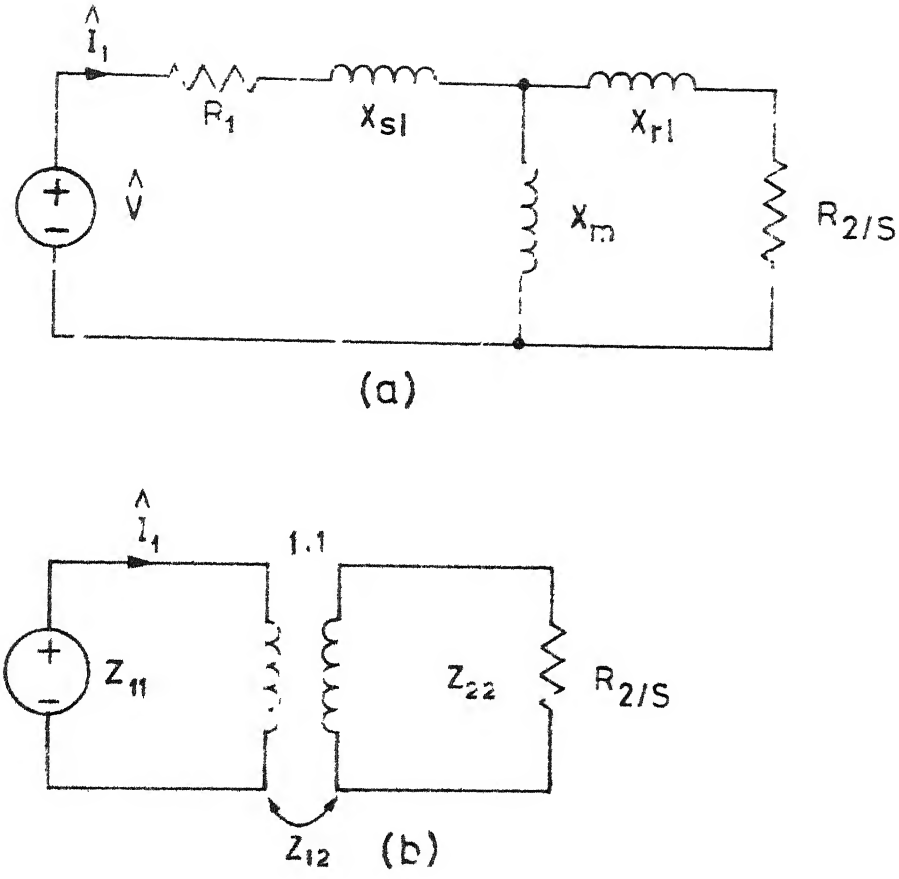

Fig. D.1 Passive equivalent circuits

$$L_{12} = \sqrt{2/3}\, m \tag{D.5}$$

$$L_1 - L_{11} = L_s \tag{D.6}$$

It is possible to prove [28,62] that

$$L_{11} = -\frac{X_m}{3\omega} \tag{D.7}$$

Therefore,

$$L_1 = (\frac{2}{3} X_m + X_{sl})/\omega \tag{D.8}$$

From the definition of L_r (equation 4.4), it is evident that

$$L_2 = X_r/\omega = (X_m + X_{rl})/\omega \tag{D.9}$$

L_1'' in equation (4.11) is defined as

$$L_1'' = L_1 - L_{11} - \frac{3 L_{12}^2}{2L_2}$$

$$= (X_s - X_m^2/X_r)/\omega \tag{D.10}$$

APPENDIX E

TORQUE EXPRESSION FOR A MOTOR WITH 2-PHASE STATOR AND 3-PHASE ROTOR

The general expression for electromagnetic torque is

$$T_e = 1/2\ i^T \frac{\partial L}{\partial \theta_r}\ i \qquad (E.1)$$

Referring to equations (4.22 - 4.26)

$$i^T = [\,i_s^T \quad i_r^T\,],\quad i_s^T = [\,i_{1\alpha} \quad i_{1\beta}\,],\quad i_r^T = [\,i_{2a}\ i_{2b}\ i_{2c}\,]$$

$$\frac{\partial L}{\partial \theta_r} = \begin{bmatrix} 0 & N' \\ N'^T & 0 \end{bmatrix},\quad N' = L'_{12} \begin{bmatrix} -\sin\theta_r & -\sin(\theta_r+2\pi/3) & -\sin(\theta_r-2\pi/3) \\ -\cos\theta_r & -\cos(\theta_r+2\pi/3) & -\cos(\theta_r-2\pi/3) \end{bmatrix}$$

Therefore, torque expression becomes

$$T_e = i_s^T\, N\, i_r \qquad (E.2)$$

The relationship between the phase currents (rotor) and d-q currents is

$$i_r = C_3\, i_{2dq} \qquad (E.3)$$

where

$$C_3 = \sqrt{2/3} \begin{bmatrix} \cos(\theta_o-\theta_r) & \sin(\theta_o-\theta_r) \\ \cos(\theta_o-\theta_r-2\pi/3) & \sin(\theta_o-\theta_r-2\pi/3) \\ \cos(\theta_o-\theta_r+2\pi/3) & \sin(\theta_o-\theta_r+2\pi/3) \end{bmatrix},\quad i_{2dq}^T = [\,i_{2d}\ i_{2q}]$$

Equation (4.27) defining the stator current i_s is rewritten as

$$i_s = \frac{1}{L_1'}\{\psi_s - M^T i_r\} \qquad (E.4)$$

where

$$M^T = L_{12}'\begin{bmatrix} \cos\theta_r & \cos(\theta_r+2\pi/3) & \cos(\theta_r-2\pi/3) \\ -\sin\theta_r & -\sin(\theta_r+2\pi/3) & -\sin(\theta_r-2\pi/3) \end{bmatrix} ;$$

$$\psi_s{}^T = [\psi_{1\alpha}\ \psi_{1\beta}] ,$$

The relationship between α - β and d-q stator flux linkages are

$$\psi_s = C_4\ \psi_{1dq} \qquad (E.5)$$

where

$$C_4 = \begin{bmatrix} \cos\theta_o & \sin\theta_o \\ -\sin\theta_o & \cos\theta_o \end{bmatrix} ; \quad \psi_{1dq}^T = [\psi_{1d}\ \ \psi_{1q}]$$

Substituting equations (E.3 - E.5) in (E.2) we get

$$T_e = \sqrt{3/2}\,\frac{L_{12}'}{L_1'}(\psi_{1d}\, i_{2q} - \psi_{1q}\, i_{2d}) \qquad (E.6)$$

APPENDIX F

DERIVATION OF STATOR CURRENT EXPRESSION

For the purpose of analysis, the half cycle period of the current waveform is divided into six sections as shown in Fig. 5.1. Referring to equations (5.1 - 5.4), the current expressions for each section are derived as follows :

Section 1 $\qquad \alpha \leq \theta_o \leq (60° + \phi)$

The differential equation defining the stator current is

$$R_1 i_{1a} + L_1'' p(i_{1a} + I_{1a}) = V_m \sin \theta_o \qquad (F.1)$$

where

$$\theta_o = \omega t$$

Rearranging the terms and replacing pI_{1a} (as defined in equation (5.2)),

$$L_1'' p i_{1a} + R_1 i_{1a} = E \sin(\theta_o + \theta) \qquad (F.2)$$

where

$$E = (E_q^2 + E_d^2)^{\frac{1}{2}}, \quad E_q = V_m + K \psi_{2d}, \quad E_d = -K \psi_{2q},$$

$$K = \frac{\omega L_{12}}{L_2}, \qquad \theta = \tan^{-1} \frac{E_d}{E_q}$$

Solution of (F.2) with the initial value of $i_{1a} = 0$ at $\theta_o = \alpha$ is

$$i_{1a} = \frac{E}{|Z_1''|} \{\sin(\theta_o + \delta) + C_1 \exp(-\beta(\theta_o - \alpha))\} \qquad (F.3)$$

where

$$Z_1'' = R_1 + J X_1'', \quad \delta = \theta - \rho, \quad \beta = \frac{R_1}{X_1''}, \quad \rho = \tan^{-1}(\frac{1}{\beta})$$

$$X_1'' = \omega L_1'' \quad \text{and} \quad C_1 = -\sin(\alpha + \delta)$$

Section 2 $\quad (60° + \phi) \leq \theta_o \leq (60° + \alpha)$

In this section the current in phase c is zero. The initial value of i_{1a} during this section is the final value of i_{1a} in the previous section.is i.e.,

$$I_2 = \frac{E}{|Z_1''|} \{\sin(\pi/3 + \phi + \delta) + C_1 \exp(-\beta(\pi/3 + \phi - \alpha))\} \qquad (F.4)$$

Differential equation defining i_{1a} is

$$R_1 i_{1a} + L_1'' p i_{1a} = \sqrt{3}/2 \; E \sin(\theta_o + \pi/6 + \theta) \qquad (F.5)$$

On solving this equation with I_2 as initial current, we get

$$i_{1a} = \frac{E}{|Z_1''|} \{\sqrt{3}/2 \sin(\theta_o + \frac{\pi}{6} + \delta) + C_2 \exp(-\beta(\theta_o - \pi/3 - \phi))\} \qquad (F.6)$$

where

$$C_2 = C_1 \exp(-\beta(\pi/3 + \phi - \alpha)) + \sin(\pi/3 + \phi + \delta) - \sqrt{3}/2 \cos(\phi + \delta)$$

Section 3 $\quad (60° + \alpha) \leq \theta_o \leq (120° + \phi)$

In this period all the 3-phases carry current as in Section 1. The differential equation defining i_{1a} is same as (F.2) with an initial current given by

$$I_3 = \frac{E}{|Z_1''|}\{\sqrt{3}/2 \cos(\alpha+\delta) + C_2 \exp(-\beta(\alpha-\phi))\} \qquad (F.7)$$

The solution of i_{1a} is given by

$$i_{1a} = \frac{E}{|Z_1''|}\{\sin(\theta_o+\delta) + C_3 \exp(-\beta(\theta_o - \pi/3 - \alpha) \qquad (F.8)$$

where

$$C_3 = C_2 \exp(-\beta(\alpha-\phi)) + \sqrt{3}/2 \cos(\alpha+\delta) - \sin(\pi/3+\alpha+\delta)$$

Section 4 $\quad (120° + \phi) \leq \theta_o \leq (120° + \alpha)$

Phases a and c are conducting while b is open during this section. The initial values of i_{1a} is obtained from (F.8) by substituting $\theta_o = \frac{2\pi}{3} + \phi$. i.e.,

$$I_4 = \frac{E}{|Z_1''|}\{\sin(2\pi/3+\phi+\delta) + C_3 \exp(-\beta(\pi/3+\phi-\alpha)) \qquad (F.9)$$

The differential equation defining i_{1a} is

$$L_1'' p\, i_{1a} + R_1\, i_{1a} = \sqrt{3}/2E \sin(\theta_o - \pi/6 + \theta) \qquad (F.10)$$

Solution of (F.10) is

$$i_{1a} = \frac{E}{|Z_1''|}\{\sqrt{3}/2 \sin(\theta_o - \pi/6 + \delta) + C_4 \exp(-\beta(\theta_o - 2\pi/3 - \phi))\} \qquad (F.11)$$

where

$$C_4 = C_3 \exp(-\beta(\pi/3+\phi-\alpha)) + \sin(2\pi/3+\phi+\delta) - \sqrt{3}/2 \cos(\phi+\delta)$$

Section 5 $\quad (120° + \alpha) \leq \theta_o \leq (180° + \phi)$

Three phase conduction takes place as in Section 1 and 3.

The initial value of current during this section as obtained from (F.11) is

$$I_5 = \frac{E}{|Z_1''|}\{ \sqrt{3}/2 \cos(\alpha + \delta) + C_4 \exp(-\beta(\alpha - \phi))\} \qquad (F.12)$$

Since the differential equation defining i_{1a} is same as (F.2), solution of i_{1a} is

$$i_{1a} = \frac{E}{|Z_1''|}\{\sin(\theta_o + \delta) + C_5 \exp(-\beta(\theta_o - 2\pi/3 - \alpha))\} \qquad (F.13)$$

where

$$C_5 = C_4 \exp(-\beta(\alpha-\phi)) + \sqrt{3}/2 \cos(\alpha+\delta) - \sin(2\pi/3 + \alpha + \delta)$$

Section 6 $\qquad (180° + \phi) \leq \theta_o \leq (180° + \alpha)$

During this period i_{1a} is zero since a-phase is open.

APPENDIX G

CALCULATION OF FOURIER COMPONENTS OF THE VOLTAGE WAVEFORM

The general form of Fourier series is

$$f(\theta_o) = a_o + \sum_{n=1}^{\infty} (a_n \cos n\theta_o + b_n \sin n\theta_o) \qquad (G.1)$$

where

$$a_o = \frac{1}{2\pi} \int_0^{2\pi} f(\theta_o)\, d\theta_o$$

$$a_n = \frac{1}{\pi} \int_0^{2\pi} f(\theta_o) \cos(n\theta_o) d\theta_o$$

$$b_n = \frac{1}{\pi} \int_0^{2\pi} f(\theta_o) \sin(n\theta_o) d\theta_o$$

The voltage wave shape of Fig. 5.1 has zero time average value so that a_o is zero in (G.1). The fundamental component a_1 is given by

$$a_1 = \frac{2}{\pi} \int_{\alpha}^{(\pi+\alpha)} v_{as} \cos\theta_o\, d\theta_o$$

Let

a_{11} = fundamental components of voltages in Sections 1,3 and 5.

a_{12} = fundamental component of voltage in Section 2

a_{13} = fundamental component of voltage in Section 4

a_{14} = fundamental component of voltage in Section 6

so that

$$a_1 = a_{11} + a_{12} + a_{13} + a_{14}$$

$$a_{11} = \frac{2}{\pi} \int_{\alpha}^{\alpha} V_m \sin\theta_o \cos\theta_o \, d\theta_o \quad \begin{matrix}(\pi/3+\phi)\ (2\pi/3+\phi)\ (\pi+\phi) \\ (\pi/3+\alpha)\ (2\pi/3+\alpha)\end{matrix} = 0 \qquad (G\ 2)$$

$$a_{12} = \frac{2}{\pi 2} \int_{(\pi/3+\phi)}^{(\pi/3+\alpha)} \{\sqrt{3}\, V_m \sin(\theta_o+\pi/6) + E_1 \sin(\theta_o+2\pi/3)\ E_2 \cos(\theta_o+2\pi/3)\} \cos\theta_o \, d\theta_o$$

$$= \frac{1}{8\pi}\{[\cos(2\alpha+2\pi/3)\ \cos(2\phi+2\pi/3)]\ [3\, V_m + E_1\sqrt{3}\, E_2] +$$

$$[\sin(2\alpha+2\pi/3)\ \sin(2\phi+2\pi/3)]\ [\sqrt{3}\, V_m + \sqrt{3}\, E_1 + E_2] +$$

$$2(\alpha\ \ \phi)\ [\sqrt{3}\, V_m + \sqrt{3}\, E_1 + E_2]\} \qquad (G\ 3)$$

$$a_{13} = \frac{2}{\pi 2} \int_{(2\pi/3+\phi)}^{(2\pi/3+\alpha)} \{\sqrt{3}\, V_m \sin(\theta_o\ \pi/6) + E_1 \sin(\theta_o\ 2\pi/3)\ E_2 \cos(\theta_o+2\pi/3)\} \cos\theta_o \, d\theta_o$$

$$= \frac{1}{8\pi}\{[\cos(2\alpha+4\pi/3)\ \ \cos(2\phi+4\pi/3)]\ [-3\, V_m + E_1 + \sqrt{3}\, E_2] +$$

$$[\sin(2\alpha+4\pi/3) - \sin(2\phi+4\pi/3)]\ [\sqrt{3}\, V_m\ \ \sqrt{3}\, E_1 + E_2] +$$

$$2(\alpha-\phi)\ [\sqrt{3}\, V_m\ \ \sqrt{3}\, E_1 + E_2]\}] \qquad (G\ 4)$$

$$a_{14} = \frac{2}{\pi} \int_{(\pi+\phi)}^{(\pi+\alpha)} \{E_1 \sin\theta_o + E_2 \cos\theta_o\} \cos\theta_o \, d\theta_o$$

$$= \frac{1}{2\pi}[[\cos(2\alpha)\ \cos(2\phi)]\, E_1 + E_2\{\sin(2\alpha) - \sin(2\phi) + 2(\alpha-\phi)\}] \qquad (G\ 5)$$

Hence

$$a_1 = a_{11} + a_{12} + a_{13} + a_{14}$$

$$= \frac{3}{4\pi} \{ (\cos 2\alpha \quad \cos 2\phi)(V_m+E_1) + E_2(\sin 2\alpha \sin 2\phi + 2\alpha - 2\phi) \} \qquad (G\ 6)$$

The fundamental Fourier coefficient b_1 is defined as

$$b_1 = \frac{2}{\pi} \int_{\alpha}^{(\pi+\alpha)} V_{as} \sin\theta_o \, d\theta_o$$

$$= b_{11} + b_{12} + b_{13} + b_{14}$$

$$b_{11} = \frac{2}{\pi} \int_{\alpha}^{(\pi/3+\phi)} V_m \sin\theta_o \sin\theta_o \, d\theta_o + \int_{(\pi/3+\phi)}^{(2\pi/3+\phi)} \quad + \int_{(2\pi/3+\phi)}^{(\pi+\phi)} = \frac{V_m}{\pi}\{\pi \quad 3(\alpha \ \phi)\} \qquad (G\ 7)$$

b_{12} to b_{14} can be similarly derived as

$$b_{12} = \frac{1}{8\pi} \{ [\cos(2\alpha+2\pi/3) \ \cos(2\phi+2\pi/3)] [\sqrt{3} V_m \ \sqrt{3} E_1 \quad E_2] +$$

$$[\sin(2\alpha+2\pi/3 \quad \sin(2\phi+2\pi/3)] [3 V_m+E_1-\sqrt{3} E_2] +$$

$$2(\alpha \ \phi) [3 V_m \quad E_1 + \sqrt{3} E_2] \} \qquad (G\ 8)$$

$$b_{13} = \frac{1}{8\pi} \{ [\cos(2\alpha+4\pi/3) - \cos(2\phi+4\pi/3)] [\sqrt{3} V_m+\sqrt{3} E_1 \ E_2] +$$

$$[\sin(2\alpha+4\pi/3) \quad \sin(2\phi+4\pi/3)] [3 V_m+E_1+\sqrt{3} E_2] +$$

$$2(\alpha-\phi) [3 V_m - E_1 \quad \sqrt{3} E_2] \} \qquad (G\ 9)$$

$$b_{14} = \frac{1}{2\pi}\{ E_2[\cos(2\alpha)-\cos(2\phi)] + E_1[\sin(2\alpha)\ \sin(2\phi)\ 2(\alpha-\phi)]\} \qquad (G\ 10)$$

Hence

$$b_1 = \frac{3}{4\pi}\{ E_2[\cos(2\alpha)-\cos(2\phi)] + (V_m+E_1)\ [\sin(2\alpha)\ \sin(2\phi)\ 2(\alpha-\phi)] + \frac{4\pi}{3} V_m \} \qquad (G\ 11)$$

The coefficient a_n may be expressed as

$$a_n = a_{1n} + a_{2n} + a_{3n} + a_{4n} + a_{5n} + a_{6n} \qquad n \neq 1$$

$$a_{1n} = \frac{2}{\pi} \int_{\alpha}^{(\pi/3+\phi)} V_m \sin\theta_o \cos n\theta_o\, d\theta_o$$

On simplifying we get

$$a_{1n} = \frac{V_m}{\pi}\{\frac{\cos(1-n)(\pi/3+\phi) - \cos(1-n)\alpha}{(1-n)} + \frac{\cos(1+n)(\pi/3+\phi) - \cos(1+n)\alpha}{(1+n)}\} \qquad (G\ 12)$$

$$a_{2n} = \frac{2}{\pi 2} \int_{(\pi/3+\phi)}^{(\pi/3+\alpha)} \{\sqrt{3}\, V_m \sin(\theta_o+\pi/6) + E_1 \sin(\theta_o+2\pi/3) \quad E_2 \cos(\theta_o+2\pi/3)\} \cos n\theta_o\, d\theta_o$$

$$= \frac{1}{4\pi}\{[-3 V_m+E_1-\sqrt{3} E_2]\ [\frac{\cos(1-n)(\pi/3+\alpha)-\cos(1-n)(\pi/3+\phi)}{(1-n)} + \frac{\cos(1+n)(\pi/3+\alpha) - \cos(1+n)(\pi/3+\phi)}{(1+n)}] +$$

$$[\sqrt{3}\, V_m+\sqrt{3}E_1+E_2]\ [\frac{\sin(1-n)(\pi/3+\alpha)-\sin(1-n)(\pi/3+\phi)}{(1-n)} + \frac{\sin(1+n)(\pi/3+\alpha) - \sin(1+n)(\pi/3+\phi)}{(1+n)}]\} \qquad (G\ 13)$$

$$a_{3n} = \frac{2}{\pi} \int_{(\pi/3+\alpha)}^{(2\pi/3+\phi)} V_m \sin\theta_o \cos n\theta_o \, d\theta_o$$

$$= \frac{-V_m}{\pi} \left\{ \frac{\cos(1\ n)(2\pi/3+\phi)\ \cos(1\ n)(\pi/3+\alpha)}{(1\ n)} + \right.$$

$$\left. \frac{\cos(1+n)(2\pi/3+\phi)\ \cos(1+n)(\pi/3+\alpha)}{(1+n)} \right\} \qquad \text{(G 14)}$$

$$a_{4n} = \frac{2}{\pi 2} \int_{(2\pi/3+\phi)}^{(2\pi/3+\alpha)} \{ \sqrt{3}\ V_m \sin(\theta_o\ \pi/6) + E_1 \sin(\theta_o\ 2\pi/3)\ E_2 \sin(\theta_o\ 2\pi/3) \} \cos n\theta_o \, d\theta_o$$

$$= \frac{1}{4\pi} \{ [\ 3\ V_m + E_1 + \sqrt{3}\ E_2] \left[\frac{\cos(1\ n)(2\pi/3+\alpha)\ \cos(1\ n)(2\pi/3+\phi)}{(1\ n)} + \right.$$

$$\left. \frac{\cos(1+n)(2\pi/3+\alpha)\ \cos(1+n)(2\pi/3+\phi)}{(1+n)} \right] +$$

$$[\ \sqrt{3}\ V_m - \sqrt{3}\ E_1 + E_2] \left[\frac{\sin(1\ n)(2\pi/3+\alpha)\ \sin(1\ n)(2\pi/3+\phi)}{(1\ n)} + \right.$$

$$\left. \frac{\sin(1+n)(2\pi/3+\alpha)\ \sin(1+n)(2\pi/3+\phi)}{(1+n)} \right] \} \qquad \text{(G 15)}$$

$$a_{5n} = \frac{2}{\pi} \int_{(2\pi/3+\alpha)}^{(\pi+\phi)} V_m \sin\theta_o \cos n\theta_o \, d\theta_o$$

$$= -\frac{V_m}{\pi} \left\{ \frac{\cos(1\ n)(\pi+\phi)\ \cos(1\ n)(2\pi/3+\alpha)}{(1\ n)} + \right.$$

$$\left. \frac{\cos(1+n)(\pi+\phi)\ \cos(1+n)(2\pi/3+\alpha)}{(1+n)} \right\} \qquad \text{(G 16)}$$

$$a_{6n} = \frac{2}{\pi} \int_{(\pi+\phi)}^{(\pi+\alpha)} \{ E_1 \sin \theta_o + E_2 \cos \theta_o \} \cos n\theta_o \, d\theta_o$$

$$= \frac{1}{\pi} \{ E_1 [\frac{\cos(1-n)(\pi+\alpha) \quad \cos(1\ n)(\pi+\phi)}{(1\ n)} +$$

$$\frac{\cos(1+n)(\pi+\alpha) \quad \cos(1+n)(\pi+\phi)}{(1+n)}] +$$

$$E_2 [\frac{\sin(1-n)(\pi+\alpha) \quad \sin(1\ n)(\pi+\phi)}{(1\ n)} +$$

$$\frac{\sin(1+n)(\pi+\alpha) \quad \sin(1+n)(\pi+\phi)}{(1+n)}] \} \qquad \text{(G 17)}$$

Similarly the components of b_n (b_{1n} b_{2n} b_{6n}) can be derived as

$$b_{1n} = \frac{V_m}{\pi} \{ \frac{\sin(1\ n)(\pi/3+\phi) \quad \sin(1\ n)\alpha}{(1\ n)} \quad \frac{\sin(1+n)(\pi/3+\phi) \quad \sin(1+n)\alpha}{(1+n)} \}$$

(G 18)

$$b_{2n} = \frac{1}{4\pi} \{ [3\ V_m\ E_1 + \sqrt{3}\ E_2] [\frac{\sin(1\ n)(\pi/3+\alpha) \quad \sin(1-n)(\pi/3+\phi)}{(1-n)} -$$

$$\frac{\sin(1+n)(\pi/3+\alpha) \quad \sin(1+n)(\pi/3+\phi)}{(1+n)}]$$

$$[\sqrt{3}\ V_m + \sqrt{3}\ E_1 + E_2] [\frac{\cos(1\ n)(\pi/3+\alpha) \quad \cos(1\ n)(\pi/3+\phi)}{(n\ 1)} +$$

$$\frac{\cos(1+n)(\pi/3+\alpha) \quad \cos(1+n)(\pi/3+\phi)}{(1+n)}] \} \qquad \text{(G 19)}$$

$$b_{3n} = \frac{V_m}{\pi} \{ \frac{\sin(1\ n)(2\pi/3+\phi) \quad \sin(1\ n)(\pi/3+\alpha)}{(1\ n)}$$

$$\frac{\sin(1+n)(2\pi/3+\phi) \quad \sin(1+n)(\pi/3+\alpha)}{(1+n)} \} \qquad \text{(G 20)}$$

$$b_{4n} = \frac{1}{4\pi}\{ [3 V_m E_1 \sqrt{3}E_2][\frac{\sin(1-n)(2\pi/3+\alpha)- \sin(1-n)(2\pi/3+\phi)}{(1-n)}$$

$$\frac{\sin(1+n)(2\pi/3+\alpha)- \sin(1+n)(2\pi/3+\phi)}{(1+n)}]+$$

$$[\sqrt{3} V_m+\sqrt{3}E_1 E_2][\frac{\cos(1-n)(2\pi/3+\alpha)- \cos(1-n)(2\pi/3+\phi)}{(n-1)} +$$

$$\frac{\cos(1+n)(2\pi/3+\alpha)- \cos(1+n)(2\pi/3+\phi)}{(1+n)}] \} \qquad \text{(G 21)}$$

$$b_{5n} = \frac{V_m}{\pi}\{\frac{\sin(1-n)(\pi+\phi)- \sin(1-n)(2\pi/3-\alpha)}{(1-n)} -$$

$$\frac{\sin(1+n)(\pi+\phi) \quad \sin(1+n)(2\pi/3+\alpha)}{(1+n)} \qquad \text{(G 22)}$$

$$b_{6n} = \frac{1}{\pi}\{ L_1 [\frac{\sin(1-n)(\pi+\alpha) \quad \sin(1-n)(\pi+\phi)}{(1-n)}$$

$$\frac{\sin(1+n)(\pi+\alpha) \quad \sin(1+n)(\pi+\phi)}{(1+n)}]$$

$$E_2 [\frac{\cos(1-n)(\pi+\alpha) \quad \cos(1-n)(\pi+\phi)}{(n-1)} +$$

$$\frac{\cos(1+n)(\pi+\alpha) \quad \cos(1+n)(\pi+\phi)}{(1+n)}] \} \qquad \text{(G 23)}$$

Hence

$$b_n = b_{1n} + b_{2n} + \quad + b_{6n} \quad n \neq 1 \qquad \text{(G 24)}$$

APPENDIX H

RELATIONSHIP BETWEEN ACTIVE AND PASSIVE EQUIVALENT CIRCUITS DURING STEADY STATE

From the circuit model of Fig 5 2 the current i can be written as (see eqn (5 23))

$$i = \frac{\hat{V} \quad I_J X_1}{Z_1''} \tag{H 1}$$

The rotor flux linkages as defined in Section 4.2.1 of Chapter 4 are

$$L_2 p \psi_{2d} = R_2 \psi_{2d} \quad S \lambda_2 \psi_{2q} + R_2 m i_d \tag{H 2}$$

$$L_2 p \psi_{2q} = S X_2 \psi_{2d} \quad R_2 \psi_{2q} + R_2 m i_q \tag{H 3}$$

where

$m = \sqrt{3/2}\, L_{12}$ (see Appendix D)

Since ψ_{2d} and ψ_{2q} are constants during steady state the terms $p \psi_{2d}$ and $p \psi_{2q}$ can be set equal to zero in (H 2 and H 3) The resulting equations are

$$R_2 \psi_{2d} + S \lambda_2 \psi_{2q} \quad R_2 m i_d \tag{H 4}$$

$$R_2 \psi_{2q} \quad S X_2 \psi_{2d} \quad R_2 m i_q \tag{H 5}$$

Multiplying (H 5) by j and adding to (H 4) we get

$$\psi = \frac{R_2 m}{Z_2} i \tag{H 6}$$

where $R_2 + J S X_2$

The relation hip between I and ψ as given in equation (5 ~~15~~ 22) is

$$I = \frac{m}{L_2 L_1''} \psi \qquad \text{(H 7)}$$

Substituting equation (H 6) in (H 7) we get

$$I = \frac{m^2 R_2}{L_2 L_1'' Z_2} i \qquad \text{(H 8)}$$

Hence equation (H 1) becomes

$$i = \frac{V}{(Z_1 + \frac{\omega\ m^2 R_2}{Z_2 L_2})} \qquad \text{(H 9)}$$

Let u now consider the conventional passive equivalent circuit as shown in Fig D 1 of App D where D 1(a&b) are equivalent

The impedance Z_{11} Z_{22} and Z_{12} are defined as

$$Z_{11} = R_1 + j\omega L_1$$

$$Z_{12} = j\omega m$$

$$Z_{22} = \frac{R_2}{S} + j\omega L_2$$

where

$$L_1 = (X_{sl} + X_m)/\omega \qquad L_2 = (X_{rl} + X_m)/\omega \qquad m = X_m/\omega$$

From Fig D 1(b)

$$\hat{V} = Z_{11} I_1 + Z_{12} I_2 \qquad \text{(H 10)}$$

$$0 = Z_{12} I_1 + Z_{22} I_2 \qquad \text{(H 11)}$$

Eliminating I_2 from equations (H 10 and H 11)

$$V = I_1 (Z_{11} \quad \frac{Z_{12}^2}{Z_{22}})$$

i e

$$\hat{I}_1 = V/Z_T$$

where

$$Z_T = Z_{11} \quad Z_{12}/Z_{22}$$

$$= R_1 + J\omega L_1 \quad \frac{(J\omega m)^2}{R_2/S+J\omega L_2}$$

Rearranging the terms after adding and subtracting a term $(J\omega m)^2/J\omega L_2$ to the right hand side of the equation we get

$$Z_T = R_1 + J\omega (L_1 \quad m^2/L_2) + (J\omega m)^2 \{ \frac{R_2/S}{J\omega L_2 (R_2/S+J\omega L_2)} \}$$

In Appendix D it is proved that $(L_1 \quad m^2/L_2) = L_1$

Therefore

$$Z_T = Z_1 + J\omega m^2 R_2/(L_2 Z_2) \qquad \text{(H 13)}$$

i e

$$I_1 = \frac{V}{Z_1 + J\omega m^2 R_2/(L_2 Z_2)} \qquad \text{(H 14)}$$

Comparing (H 9) and (H 14) it can be seen that $i = \hat{I}_1$

Hence the active circuit given in Fig 5 2 is equivalent to the conventional passive equivalent circuit (Fig D 1) during steady state

APPENDIX I

RELATIONSHIP BETWEEN HARMONIC COMPONENTS OF D Q AXIS CURRENTS AND PHASE CURRENTS

The transformation matrix relating d-q axis and phase currents is

$$\begin{bmatrix} i_d \\ i_q \end{bmatrix} = \sqrt{\frac{2}{3}} \begin{bmatrix} \cos\theta_o & \cos(\theta_o - 2\pi/3) & \cos(\theta_o + 2\pi/3) \\ \sin\theta_o & \sin(\theta_o - 2\pi/3) & \sin(\theta_o + 2\pi/3) \end{bmatrix} \begin{bmatrix} i_a \\ i_b \\ i_c \end{bmatrix} \quad \text{(I 1)}$$

For a nth harmonic phase current the d-axis current can be expressed as

$$i_d(t) = \sqrt{2/3}\, I_n \{ \sin(n\theta_o + \alpha_n) \cos\theta_o + \sin(n(\theta_o - 2\pi/3) + \alpha_n) \cos(\theta_o - 2\pi/3) + \sin(n(\theta_o + 2\pi/3) + \alpha_n) \cos(\theta_o + 2\pi/3) \} \quad \text{(I 2)}$$

where

$I_n = \{a_n^2 + b_n^2\}^{\frac{1}{2}}$ a_n and b_n are Fourier components of phase current

Equation (I 2) after simplification becomes

$$i_d(t) = \sqrt{\frac{2}{3}}\, \frac{1}{2}\, I_n \{ [\sin((n+1)\theta_o + \alpha_n) + \sin((n+1)(\theta_o + 2\pi/3) + \alpha_n) + \sin((n+1)(\theta_o - 2\pi/3) + \alpha_n)] + [\sin((n-1)\theta_o + \alpha_n) + \sin((n-1)(\theta_o + 2\pi/3) + \alpha_n) + \sin((n-1)(\theta_o - 2\pi/3) + \alpha_n)] \} \quad \text{(I 3)}$$

It may be noted from (I 3) that two harmonic components

of phase current contribute a single harmonic component in the d axis current For example 5th and 7th harmonics in phase current contribute to 6th harmonic d axis current 11th and 13th produces 12th harmonic d-axis current and so on The d axis current contain the harmonics of order 6 12 18 and so on Since the phase current harmonics are of 5 7 11 13 17 etc The general expression for i_{dn} in terms of the Fourier components of phase current as obtained from equation (I 3) is

$$i_{dn} = \sqrt{3/2}\,\{(a_{n\ 1} + a_{n+1})^2 + (b_{n\ 1} + b_{n+1})^2\}^{\frac{1}{2}} \qquad \text{(I 4)}$$

Similarly i_{qn} can be derived as

$$i_{qn} = \sqrt{3/2}\,\{(a_{n-1} - a_{n+1})^2 + (b_{n\ 1} \quad b_{n+1})^2\}^{\frac{1}{2}} \qquad \text{(I 5)}$$

where

$n = 6\ 12\ 18$

APPENDIX J

EXPRESSION FOR $\Delta\phi$

The non linear equation defining ϕ (equation (5.3.6) of Chapter 5) can be written as

$$C_{11} \exp(\beta\beta\alpha) + C_{12} \exp(\beta\phi) = 0 \qquad (J\ 1)$$

where

$$C_{11} = -\sqrt{3}/2 \cos(\phi+\delta)(1+\exp(-\beta\pi/3)) - \sin(\phi+\delta) \exp(\beta\pi/3) + \sin(2\pi/3+\phi+\delta) + \sin(\pi/3+\phi+\delta) \exp(-\beta\pi/3)$$

$$C_{12} = \sqrt{3}/ \cos(\alpha+\delta)(1+\exp(\beta\pi/3)) \quad \sin(\alpha+\delta)\exp(-\beta 2\pi/3) \quad \sin(2\pi/3+\alpha+\delta) \quad \sin(\pi/3+\alpha+\delta)\exp(\beta\pi/3)$$

$$\delta = \theta - \rho \quad \theta = \tan^{-1}(E_d/E_q) \quad E_d = K\psi_{2q}$$

$$E_q = V_m + K\psi_{2d} \quad \rho = \tan^{-1}(X'_1/R_1) \quad \beta = R_1/X_1$$

On linearizing equation (J 1) we get

$$\exp(\beta\alpha)(\beta C_{11}\Delta\alpha + \Delta C_{11}) + \exp(\beta\phi)(\beta C_{12}\Delta\phi + \Delta C_{12}) = 0 \qquad (J\ 2)$$

and

$$\Delta C_{11} = C_{22}(\Delta\phi+\Delta\theta) \qquad (J\ 3)$$

$$\Delta C_{12} = C_{33}(\Delta\alpha+\Delta\theta) \qquad (J\ 4)$$

where

$$C_{22} = \sqrt{3}/2 \sin(\phi+\delta)(1+\exp(\beta\pi/3)) - \cos(\phi+\delta) \exp(\beta\pi/3) + \cos(2\pi/3+\phi+\delta) + \cos(\pi/3+\phi+\delta)\exp(\beta\pi/3)$$

$$C_{33} = \sqrt{3}/2 \sin(\alpha+\delta)(1+\exp(\beta\pi/3)) - \cos(\alpha+\delta)\exp(\beta 2\pi/3) - \cos(2\pi/3+\alpha+\delta) \cos(\pi/3+\alpha+\delta)\exp(\beta\pi/3)$$

Substituting (J 3) and (J 4) in (J 2) we get

$$C_4 \Delta\phi = C_5 \Delta\alpha + C_6 \Delta\theta \qquad \text{(J 5)}$$

where

$$C_4 = C_{22} \exp(-\beta(\alpha \phi)) \beta C_{12} \quad C_5 = \beta C_{11} \exp(\beta(\alpha \phi)) C_{33}$$

$$C_6 = C_{33} - C_{22} \exp(\beta (\alpha \phi))$$

The equation defining θ is given by

$$E_q \tan\theta = E_d \qquad \text{(J 6)}$$

On linearizing the above equation we get

$$\Delta\theta = C_7 \Delta\psi_{2d} + C_8 \Delta\psi_{2q} + C_9 \Delta V_m \qquad \text{(J 7)}$$

where

$$C_7 = -\frac{E_d K}{(E_d^2 + E_q^2)} \qquad C_8 = \frac{E_q K}{(E_d^2 + E_q^2)} \qquad C_9 = \frac{E_d}{(E_d^2 + E_q^2)}$$

Eliminating $\Delta\theta$ from equation (J 5) using (J 7)

$$\Delta\phi = g^T \begin{bmatrix} \Delta\psi_{2d} \\ \Delta\psi_{2q} \end{bmatrix} + g_3 \Delta\alpha + g_4 \Delta V_m \qquad \text{(J 8)}$$

where

$$g^T = [g_1 \quad g_2] \qquad g_1 = \frac{C_6 C_7}{C_4} \qquad g_2 = \frac{C_6 C_8}{C_4}$$

$$g_3 = \frac{C_5}{C_4} \quad \text{and} \quad g_4 = \frac{C_6 C_9}{C_4}$$

APPENDIX K

SMALL SIGNAL MODEL OF AN INDUCTION MOTOR WITH SINUSOIDAL EXCITATION

Let the source voltage v be defined by

$$v = V_m \sin(\omega t)$$

so that

$$\hat{v} = j \sqrt{3/2}\, V_m$$

Referring to Fig (5 2) of Chapter 5 current $\hat{i}$ is given by

$$\hat{i} = \frac{j \sqrt{3/2}\, V_m \quad \sqrt{3/2}\, K\, (\psi_{2q} + j\, \psi_{2d})}{Z_1}$$

where

$$Z_1 = R_1 + j\, X_1$$

After simplification we get

$$i_d = \sqrt{3/2}\, [\, K R_1 \psi_{2q} \quad X_1 (V_m + K \psi_{2d})] / |Z_1|^2 \qquad (K\ 1)$$

$$i_q = \sqrt{3/2}\, [\, K X_1 \psi_{2q} + R_1 (V_m + K \psi_{2d})] / |Z_1|^2 \qquad (K\ 2)$$

On linearizing (K 1) and (K 2)

$$\begin{bmatrix} \Delta i_d \\ \Delta i_q \end{bmatrix} = [P] \begin{bmatrix} \Delta \psi_{2d} \\ \Delta \psi_{2q} \end{bmatrix} \qquad (K\ 3)$$

where

$$[P] = \frac{\sqrt{3/2}\,K}{|Z_1'|^2} \begin{bmatrix} X_1 & R_1 \\ R_1 & X_1 \end{bmatrix}$$

The linear dynamical equation of the motor (ref equation 6 5)) is

$$p\,X = A_1\,X + B_1\,Y + C_1\,u \qquad (K\ 4)$$

where

$X^T = [\Delta\psi_{2d}\ \Delta\psi_{2q}\ \Delta S]$ $Y^T = [\Delta i_d\ \Delta i_q]$ $u = \Delta T_m$

and A_1 B_1 and C_1 are defined in equation (6 5)

Substituting (K 3) in (K 4) we get

$$p\,X = A\,X + C_1\,u \qquad (K\ 5)$$

where

$A = A_1 + A_2$ and $A_2 = [B_1\,P \quad 0]$

CURRICULAM VITAE

1 Candidates Name N Prabhakaran

2 Academic Background

Degree	Specialization	University	Year
B Sc (Engg)	Electrical Engineering	Kerala	1966
M Tech	Electrical Machines	I I T Kharagpur	1972

3 Publications

1 Digital simulation of voltage controlled a c motor drives (with Dr V V Sastry) Electrical Machines and Electromechanics No 4 pp 233 253 October 1979

2 'Analysis of a voltage controlled three phase induction motor drive with feedback (with Dr K R Padiyar), Paper to be presented at the International Conference on Electrical Machines to be held at Athens Greece September 1980

A 65960

Date Slip